Nanoscale

REVIEW

View Article Online
View Journal | View Issue

Cite this: *Nanoscale*, 2024, **16**, 21216

Holistic insights into carbon nanotubes and MXenes as a promising route to bio-sensing applications

Nadeem Hussain Solangi, [a] Rama Rao Karri, *[b,c] Nabisab Mujawar Mubarak, *[b,d] Shaukat Ali Mazari*[e] and Bharat Prasad Sharma [f,g]

Essential biosensor use has become increasingly important in drug discovery and recognition, biomedicine, food safety, security, and environmental research. It directly contributed to the development of specialized, reliable diagnostic instruments known as biosensors, which use biological sensing components. Traditional biosensors have poor performance, so scientists need to develop advanced biosensors with promising selectivity, sensitivity, stability, and reusability. These are all parameter modifications associated with the characteristics of the sensing material. Carbon nanotubes (CNTs) and MXenes are promising as targeted sensing agents in advanced functional materials because of their promising chemical and physical properties and limited toxic effects. Based on available data and sensing performance, MXene is better for biosensing applications than CNTs. Because of their large specific surface area (SSA), superior electrical conductivity, and adaptable surface chemistry that facilitates simple functionalization and robust interactions with biomolecules, MXenes are typically regarded as the superior option for biosensors. Additionally, because of their hydrophilic nature, they are more suited to biological settings, which increases their sensitivity and efficacy in identifying biological targets. MXenes are more suitable for biosensing applications due to their versatility and compatibility with aquatic environments, even if CNTs have demonstrated stability and muscular mechanical strength. However, MXenes offer better thermal stability, which is crucial for applications in diverse temperature environments. This study reviews and compares the biosensing capabilities, synthesis methods, unique properties, and toxicity of CNTs and MXenes. Both nanomaterials effectively detect various pollutants in food, biological substances, and human bodies, making them invaluable in environmental monitoring and medical diagnostics. In conclusion, CNTs work better for biosensors that must be strong, flexible, and long-lasting under different conditions. MXenes, on the other hand, work better when chemical flexibility and compatibility with wet environments are essential.

Received 20th July 2024,
Accepted 30th September 2024

DOI: 10.1039/d4nr03008g

rsc.li/nanoscale

1. Introduction

A biosensor is a device that utilizes biological molecules, especially antibodies or enzymes, to identify the existence of chemicals. Although a biosensor was first proposed in 1906, Clark *et al.* produced the first biosensor in 1956, earning Clark the title of "father of biosensors".[1] In 1962, he also exhibited an amperometric enzyme electrode to detect glucose. Currently, biosensors are widely used in various fields, namely, surveillance of the environment, industrial applications, clinical analysis, and medical diagnosis. Fabricating biosensors for precisely and quickly monitoring chemicals or biomolecules that lead to persistent illnesses and negative consequences is a top priority today for early diagnosis, enhancing therapy effectiveness.[2] These instruments were created over

[a]*State Key Laboratory of Chemical Resource Engineering and College of Chemistry, Beijing University of Chemical Technology, P. Box 98, Beisanhuan East Road 15, Beijing 100029, PR China*
[b]*Petroleum and Chemical Engineering, Faculty of Engineering, Universiti Teknologi Brunei, Bandar Seri Begawan, BE1410, Brunei Darussalam. E-mail: kramarao.iitd@gmail.com, mubarak.yaseen@gmail.com*
[c]*Faculty of Engineering, INTI International University, 71800 Nilai, Malaysia*
[d]*University Centre for Research and Development, Chandigarh University, Mohali, Punjab, 140413, India*
[e]*Department of Chemical Engineering, Dawood University of Engineering and Technology, Karachi 74800, Pakistan. E-mail: shaukatmazari@gmail.com*
[f]*Beijing Key Laboratory of Electrochemical Process and Technology of Materials, College of Material Science and Engineering, Beijing University of Chemical Technology, Beijing 100029, China*
[g]*CAS Key Laboratory of Green Process and Engineering, Institute of Process Engineering, Chinese Academy of Sciences, Beijing 100190, China*

many years to monitor critical analytes employing optical, electrochemical (EC), and piezoelectric transducers. Because of their superior efficiency, cheap cost, ease of use, and portability, electrochemical detectors stand out among these for use in clinical diagnostics and for the identification of environmental pollutants.[3] The use of biosensors to accelerate the process of diagnosis and therapy in the wake of the current COVID-19 outbreak has gained importance.[3]

Biosensors are important for finding new drugs, biomedicine, food safety, and environmental studies. They stress the need for better biosensors that are more selective, sensitive, stable, and reusable. CNTs and MXenes, two new 2D materials found to show a potential candidate for biosensing. MXenes are considered better because they have a larger surface area, better electrical conductivity, more flexible surface chemistry, and a hydrophilic nature that makes them better for biological settings. While CNTs are very strong and stable mechanically, MXenes are better at withstanding heat and chemicals, which makes them perfect for biosensing in wet settings. Additionally, CNTs are highly effective in applications that need resilience, adaptability, and robustness, but MXenes are better suited for scenarios that prioritize chemical adaptability and compatibility with moist environments. This article presents a comparative analysis of carbon nanotubes and MXenes regarding their biosensing capabilities and fabrication methods. Both nanomaterials have efficacy for identifying contaminants in food, biological substances, and the human body, making them highly valuable for environmental monitoring and medical diagnostics. This review further examines the efficacy of MXenes over CNTs for various biosensors such as electrochemical biosensors, advanced biosensors, immunosensors, aptasensors, and electrochemiluminescence biosensors.

2. Types of sensors

The sensors, in general, are divided into physical, chemical, thermal, and biological sensors on a large scale or macro level.

2.1. Physical sensors

In the realm of technology, physical sensors are instruments capable of detecting and measuring various physical characteristics, including temperature, pressure, humidity, light, sound, and motion.[4,5] These sensors transform the physical amount into an electrical signal, which can then be transferred, collected, or measured. The usage of physical sensors is widespread throughout various industries, including the automotive and aerospace industries, as well as the healthcare and consumer electronics sectors. The following is a list of the most essential categories of physical sensors, along with the elements that influence their performance. The majority of applications for physical sensors have been found in the field of biomedicine, particularly with the development of microelectromechanical systems technology, which has led to the creation of more accurate and small sensors and innovative measuring technologies.

2.2. Chemical sensors

Chemical sensors are gadgets that identify and quantify the existence of chemical compounds in a sample and their concentration or activity levels. These sensors convert the chemical data into a measurable signal, often an electrical, optical, or mass change. This signal can then be quantified and analyzed.[6–8] Chemical sensors have many uses, including monitoring the environment, controlling industrial processes, providing medical treatment, and functioning as safety systems. Chemical sensors are an essential component of modern technology, as they make it possible to obtain vital information to secure and effectively operate various systems and procedures. These sensors can measure the activities or quantity of chemical species in the gas or liquid phase. Additionally, they are utilized for the monitoring of environmental pollution, the analysis of food and drugs, and the monitoring of assays for organophosphorus chemicals. Additionally, they can be used for diagnostic reasons in healthcare settings.

2.3. Thermal sensors

Thermal sensors are gadgets that can identify and quantify temperature or heat-related alterations in their surrounding environment. Sensors like this are vital for various uses, such as controlling industrial processes, monitoring the environment, medical diagnostics, and consumer electronics.[8,9] They can function according to different principles, transforming thermal energy into an identifiable electrical signal. Examples of temperature sensors include thermocouples, thermistors, and RTDs.

2.4. Biological sensors

Biosensors are analytical instruments that integrate a biological component with a physicochemical detector to quantify

Mr Nadeem Hussain Solangi is a research scholar at the Beijing University of Chemical Technology, PR China. He has published 28 research articles in reputed journals and 3 book chapters. He has published 10 review papers on CNTs and MXenes. His research interests are MXene materials, Layered double hydroxides (LDHs), 2D materials, photocatalysis, energy storage, environmental remediation, and wastewater treatment. He believes in lifelong learning and has a habit of reading the latest research articles regularly.

Dr Rama Rao Karri is a Professor (Sr Asst) in the Faculty of Engineering, Universiti Teknologi Brunei, Brunei Darussalam. He has over 20 years of working experience in academics, industry, and research. As of 20 Jul 2024, he has published 260 research articles in reputed journals, book chapters, and conference proceedings. He is a peer-review member for more than 100 reputed journals and handled 200 articles as an editor. He also has the distinction of being listed in top 2% of the world's most influential scientists in chemical engineering field for 2021, 2022, 2023 & 2024.

the existence or quantity of biological molecules, pathogens, or chemical compounds. Biosensors find extensive applications in healthcare, environmental monitoring, food safety, and biotechnology.

3. Mechanisms and factors that influence the performance of biosensors

3.1. Working mechanisms of biosensors

Biosensors operate through a series of processes in which a biological recognition element interacts with the target analyte, and this interaction is subsequently transformed into a quantifiable signal by a transducer. This procedure enables the identification and measurement of particular chemicals, frequently in real time. Fig. 1 presents a schematic of the working principle of biosensors.

3.2. Factors that influence the performance of biosensors

Several physical and chemical parameters are available to affect the performance of biosensors. The interaction between the sensing material and the sensor massively affects the performance of the biosensor material. Among these characteristics are affinity, which refers to the degree of the power of the association that exists between the biorecognition element and the target biomolecule; particularity, which refers to the capability of the biorecognition component to differentiate the target biomolecule from other similar molecules; and activity, which refers to the functional effectiveness of the biorecognition element in terms of catalysis or recognition.[10,11] The interference, temperature, ionic strength, and pH are environmental factors that impact the sensor's performance in the sample solution. These factors determine the performance of electrochemical biosensors in various environments and uses. Higher temperatures potentially denature receptors or alter the reaction kinetics and pH, affecting binding affinity and sensor response.[12,13] Ionic strength influences the electrostatic forces and screening effects between charged molecules. On the other hand, interference influences the precision and dependability of electrochemical biosensors because it causes undesired signals to be produced by other molecules in the sample solution.[14] The transducer's qualities refer to the characteristics that enable it to transform a biorecognition incident into an electrical signal, which may appear as a current, voltage, or impedance modification. The characteristics of a transducer involve its material, which defines its electrical conductivity and reliability; its structure, which represents the extent of its surface and sensitivities; and its surface enhancement, which includes supplying or covering the transducer with various molecules or substances to improve its biological compatibility and signal transduction.[8,15]

3.3. Parameters for the selection of promising biosensors

The selection of materials for practical or lab scales is associated with their curtained parameters. The parameters that have a viable role in sensor selection are discussed below.

3.3.1. Selectivity of biosensors. The biosensor's selectivity refers to its capacity to discern between the target analyte and other components present in the sample. A highly selective biosensor is crucial for complicated biological samples because it can precisely identify the target molecule without interference from other elements. The ability of a biosensor to identify and quantify only the precise substance it is intended to locate, despite the presence of other substances that are identical, is known as selectivity. This is essential in real-world scenarios wherein the specimen may contain various substances, such as medical testing or environmental monitoring. Elevated selectivity ensures accurate and dependable data from the biosensor and helps prevent errors such as false readings.

For applications in healthcare, biosensors have a high probability of false positives and low selectivity. Since biological specimens are complicated and contain many chemicals, selectivity is essential for developing accurate point-of-care biosensors. Antibodies' binding domains, located on the arms of their "Y" conformational shape, offer specificity.[16] Enzymes are comprised of binding pockets that use distinct hydrogen bonding and electrostatic biorecognition mechanisms to accomplish analyte specificity.[17,18] Peptide nucleic acids can lessen the non-specific electrostatic interactions that hinder or

Dr Nabisab Mujawar Mubarak is an Associate Professor in Universiti Teknologi Brunei, Brunei Darussalam. Dr Mubarak has published more than 380 journal papers and 60 conference proceedings and authored 65 book chapters. His interest areas are carbon nanomaterials, MXenes, CNT production, magnetic biochar, and wastewater treatment using advanced materials. He is a recipient of Curtin Malaysia's Most Productive Research award, Outstanding Faculty of Chemical Engineering award, and Best Scientific Research Award London, and citation by i-Proclaim, Malaysia. He also has the distinction of being listed in the top 2% world's most influential scientists in chemicals and energy since 2021.

Dr Shaukat Ali Mazari is an Associate Professor in the Department of Chemical Engineering at Dawood University, Karachi, Pakistan. He has published 115 research articles in reputed journals, book chapters, and conference proceedings and has an h-index of 34 (Google Scholar citations: 4400+). His research interests are purification and separation processes, biofuels from biomass, electrochemical CO_2 reduction and 2D materials synthesis. He has published 3 Elsevier and Springer books.

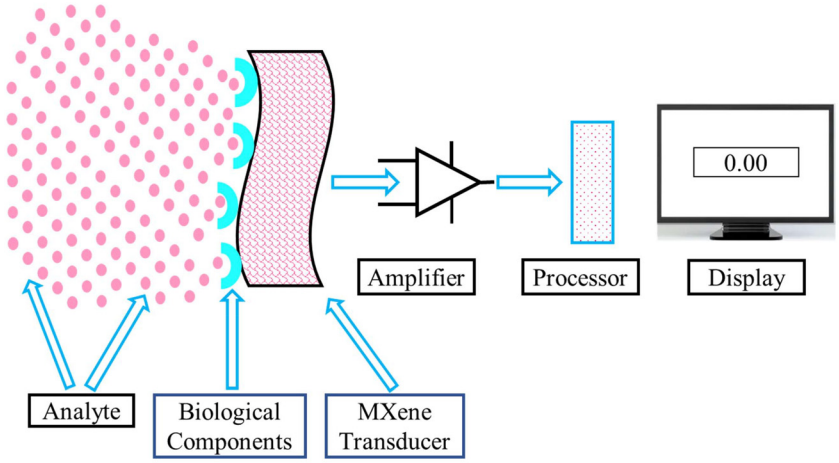

Fig. 1 Schematic working principle of biosensors.

obstruct the selectivity of nucleic acids and aptamer biorecognition elements because of their inherited negative DNA charge.[19,20] Poor selectivity is another drawback of synthetic biorecognition elements like MIPs, although their affordability, stability, and ease of synthesis make them desirable despite this.[21–24] Because of the variety of interactions inside the binding cavity, the non-specific binding of analytes hinders its selectivity. However, boosting the polymer cross-linking quantity may maintain the binding cavity and lessen non-specific binding.[25,26]

3.3.2. Sensitivity of biosensors. The ability of a biosensor to detect even minute quantities of the target material is determined by its sensitivity. Sensitive biosensors are essential for applications such as early illness detection and low-pollution monitoring because they can detect slight variations in the quantity of the material they are monitoring. Good sensitivity guarantees that the biosensor can produce relevant and reliable data when the target material exists in minimal concentrations. Additionally, upper and lower detection limits—representing the highest and lowest sample concentrations—specify the biosensor range.[27–29] The desired range spans from pico- to nanometers.[30,31] The sensitivity of aptamers as biorecognition components is enhanced by their insignificant size, ranging from 1 to 2 nm.[32–34] Because of their steric barrier, conventional nucleic acids have restricted sensitivity.[35,36] Surface design modifications can increase the sensitivity and range of enzyme and MIP biorecognition elements.[37,38]

Mr Bharat Prasad Sharma is a research scholar at the Institute of Process Engineering, Chinese Academy of Sciences. He has published 12 research articles in reputable journals. His research interests are 2D materials, nanocomposites, selective extraction, and wastewater treatment. He is constantly in search of novel ideas in diverse disciplines of chemistry to contribute to interdisciplinary advancements.

3.3.3. Reproducibility of biosensors. The term "reproducibility" describes a sensor's capacity to measure the same analyte repeatedly under the same conditions and yield reliable findings. It shows that the sensor functions steadily and reliably when the same sensor retakes measurements and produces consistent results within a predetermined accuracy range. In other words, when measuring an identical parameter under identical conditions, a sensor exhibiting excellent repeatability will yield almost the same reading each time, independent of differences in the device, operator, or time. This consistency plays a critical role in guaranteeing the validity of biosensor data, particularly in medical diagnostics and research where precise and reproducible results are crucial. Because antibodies and enzymes are susceptible to pH or temperature variations, particularly in low-resource areas, processing and manufacturing work in industry is challenging. Since the clinical market uses many biosensors based on them, their management is necessary to avoid irreproducible outcomes.[39–41] Since aptamers are chemically manufactured, their performance and quality are uniform across batches, ensuring highly reproducible results. Reliability is increased by their stable and precise binding to targets, which reduces variability. Because of their consistency, aptamers are perfect for applications that need a high level of repeatability.[42–44] Because of the strict controls and standardization in their chemical manufacturing procedures, aptamers and molecularly imprinted polymers (MIPs) produce consistent outcomes. Aptamers are designed for particular binding, whereas MIPs are made with exact molds to provide reliable target identification.[45] MIPs are produced economically and straightforwardly in industry, and their minimal variances result in highly repeatable biosensors.[46]

3.3.4. Stability of biosensors. The capability of biosensors to continue operating consistently and accurately over time and in various environmental circumstances is referred to as stability. This covers resistance to deterioration, shifts in sensitivity, and changes in reaction brought on by variables like humidity, temperature swings, or chemical exposure.[9,47,48] A

highly stable biosensor will not require as much recalibration or replacement throughout its working life, making it more dependable and efficient. Stability ensures that the sensor produces consistent data and maintains its performance without noticeably drifting or losing functionality, which is essential for applications requiring long-term monitoring or continuous use.

4. Chemistry and synthesis of CNTs and MXenes

4.1. Chemistry of CNTs and MXenes

Carbon nanotubes are sheets of graphene that have been rolled up into nanosized tubes. These nanotubes, which are composed of sp^2 hybridized carbon atoms organized in a cylindrical pattern at the nanoscale, can be divided into two groups: single-walled carbon nanotubes (SWCNTs) and multi-walled carbon nanotubes (MWCNTs). Comparatively speaking, compared to other nanomaterials, their unique blends of structural, chemical, and electrical characteristics significantly influence the production of electrochemical (EC) biosensors.[49–52] While MWCNTs are formed of several graphene sheets built up into a cylinder-like form with widths ranging from 100 nm, SWNTs are constructed from rolled-up graphene sheets. The Russian doll and parchment designs are two further structural models for MWCNTs. In the parchment design, a single graphene sheet was repeatedly encircled around itself.

In contrast, in the Russian doll design, the carbon tubes each had a smaller width nanotube coiled inside of them.[53,54] Since each carbon atom contains one 2p electron and three $2sp^2$ electrons, CNTs have similar electrical characteristics to those of graphene. However, the chirality or geometrical architecture of CNTs, which gives them metallic and semiconducting electrical behavior, is the only factor influencing their electrical characteristics.[55,56] Because of their biological compatibility and suitability for the identification of biomolecules, many nanomaterials, including CNTs, two-dimensional (2D) materials, and transition metal dichalcogenides, have been used to create EC biosensors.[3] Real-time medical technology is continually developing even though CNT-based biosensors were created in the 2000s.[3] According to the definition, CNTs are pseudo-one-dimensional (1D) allotropes of carbon, distinguished by being made up of a continuous arrangement of carbon atoms arranged into cylinders with either open or closed ends and one or more sheets. Because of their distinct features, CNTs have attracted interest in the medical systems field as one of the potential candidates for medical equipment over the past several years. The outstanding toughness, higher SSA, excellent electrical conductivity, chemical stability under aqueous and nonaqueous conditions, and substantial thermal conductivity of the CNTs makes them suitable choices as biosensors.[57] Due to their shallow detection limit, CNTs are frequently selected as active electrodes for detectors. Enzymes adhere well to CNTs because of their hollow shape. Consequently, CNTs are always utilized to functionalize enzymes to produce enzyme–CNT electrodes or change the surface of electrodes in amperometric CNT-based biosensors.[58]

The general chemical composition of the parent material of MXene is $M_{n+1}AX_n$, and the MXene ($Ti_3C_2T_x$) is created from the parent material by selective chemical or mechanical etching of the A layer.[59,60] The detailed compositions of the MAX phase and MXene are shown in Fig. 2. The availability of

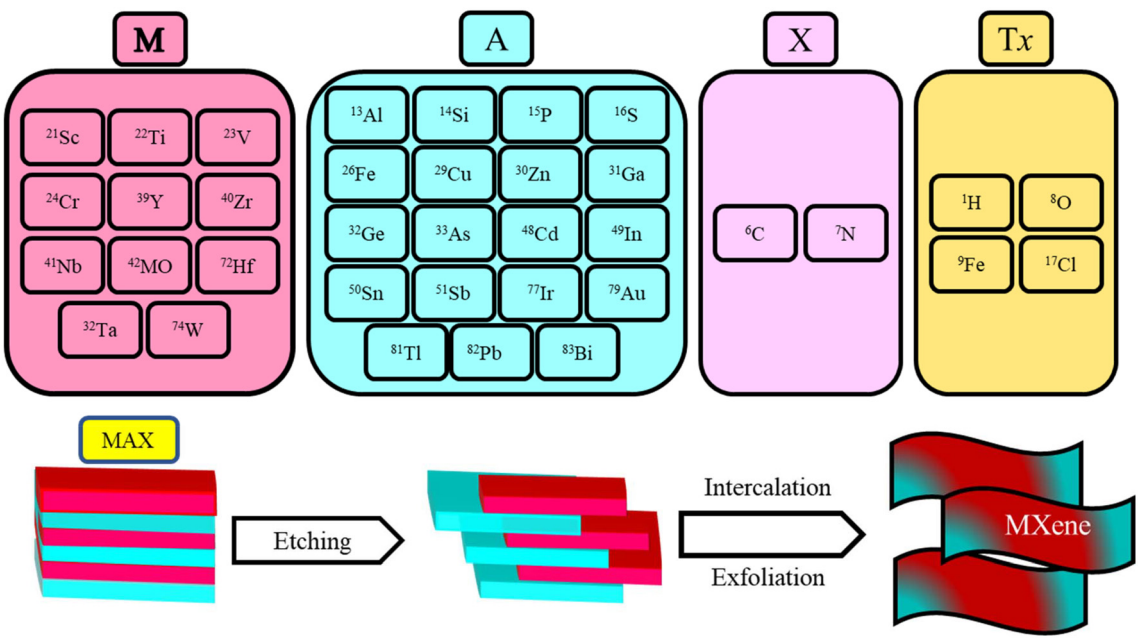

Fig. 2 Composition of MAX and MXene and the synthesis mechanism.

influential functional groups on the surface of MXene makes it an ideal candidate as a biosensor.[61] MXene's parent MAX phases typically exhibit properties resembling those of metals, including strong conductivity and exceptional mechanical stability. They exhibit qualities similar to ceramics, including enhanced resistance to corrosion, excellent toughness, and a lack of density. Additionally, MAX phases are thermally stable. Because of their distinctive properties, MAX phases are helpful in numerous engineering uses, including electrical wiring, high-temperature ceramics, and protective interface coatings. The biosensing performance of pristine CNTs and MXene is always lower; it can be enhanced by introducing active functional groups onto the surface of both advanced nanomaterials and functionalization with polymers. The selective functional groups can be added to the interface of MXene by various chemical treatment techniques that have a viable impact on the performance of the MXene.[62–64] The design and manufacture of EC biosensors make extensive use of MXenes due to their distinctive surface chemical properties, including hydrophilicity, creditable enzyme transferring ability, an abundance of surface functionalities, biological compatibility, outstanding electrocatalytic properties, substantial electron transfer power, ease of surface functionalization and alterations, vast compositional diversity, and substantial SSAs.[65]

4.2. Synthesis techniques for CNTs and MXenes

The finished product's geometry, structure, and morphology depend on the synthesis method. Traditional methods for synthesizing CNTs and MXenes resulted in materials with poor geometry and shape. However, modern methods eliminate all these problems. Many hazardous compounds are used in conventional approaches to create nanomaterials. Advanced synthesis methods, however, are sustainable and beneficial for the environment. In this section, the authors cover the environmentally friendly techniques frequently used to create MXene and CNT nanomaterials. The properties and morphology of nanomaterials are effectively affected by their synthesis routes.[66–68] The synthesis methods, products, advantages, and disadvantages of CNTs and MXenes are given in Table 1.

According to open literature on the CNT development mechanism, several mechanisms may operate when synthesizing CNTs. Both academic and massive industrial applications call for the production of high-quality CNTs. The main disadvantage of currently available nanotubes is their variety in composition. Many factors, including hydrocarbon, deposition time, catalyst, reactor design, gas flow rate, pressure, and temperature, affect the production of CNTs. Although alternative methods have since been proposed, Iijima[75] produced CNTs in 1991 using the arc discharge approach. The chemical vapor deposition (CVD) technique is the best for producing nanotube-based thin films, which are now used in technology and have several applications.[76] A phase change, a chemical process, causes a gas or liquid to decompose and change the composition of a solid surface. There are numerous ways to provide this activation energy *via* CVD. The activation energy in thermal CVD is provided by temperatures exceeding 973 K.[77] The apparatus comprises extreme vacuum, a gas supply, an exhaust, and a deposition chamber. Plasma activates the plasma CVD procedure at 623 K and 1023 K.[78] High-intensity lasers are utilized in laser CVD to initiate pyrolysis on absorbing substrates by generating thermal energy.[79] The UV beams utilized in photolaser CVD have sufficient photon energy to break the interactions in the mixture components during the chemical reaction.

Nanoparticle powders can also be produced using CVD. High deposition rates and 100% pure nanoparticle synthesis are the main advantages of CVD. The material's chemical and mechanical properties, the intensity of the lasers, pressure in the chamber and temperature, the velocity of the buffer gas, and the distance between the backing material and the target all affect how the PLD process produces CNTs. Laser

Table 1 The synthesis techniques, products, advantages, and disadvantages of CNTs and MXenes

Synthesis techniques	Product	Advantages	Disadvantages	Ref.
Laser ablation	CNT	A continuous laser can be used in a high-purity process, allowing great structural control at ambient temperature	It consumes more materials and produces a small output, and after synthesizing the product, purification of the product is required	69
CVD	MWCNT	It is a cost-effective, low-temperature, highly pure, and environmentally friendly method	Process factors should be carefully watched to produce effective SWCNTs because CNTs frequently produce MWCNTs	70
Arc discharge technique	CNT	It is easy and affordable	Since MWCNTs are more common than SWCNTs, process variables must be carefully watched to produce effective SWCNTs	71
Evaporation-induced self-assembly method	g-C_3N_4/Ti_3C_2	This is a time- and money-saving method that is easy to use	It increases the probability that structural order will collapse	72
One-step hydrothermal	MXene/ $NiFe_2O_4$	The manufactured material is affordable, ecologically friendly, and has a significant SSA	The nanomaterial is created using a hydrothermal process, which is unstable at elevated temperatures	73
Thermal reduction	Ti_2C MXene	The resulting composite production method was efficient, environmentally beneficial, and easy to use	Morphological changes caused by thermal treatment vary with temperature	74
In situ growth	Ti_3C_2-MXene/ ZIF-67/CNTs	Cheap to buy, time-saving, and green	There are not many structural flaws in the synthetic material	69

ablation is one of the best ways to create high-quality SWNTs, and purification is a crucial stage of PLD. The mechanics and concepts of this method, which Smalley's group first demonstrated in 1995,[80] are similar to those of an arc discharge process, with the exception that energy is provided by a laser impacting graphite particles containing catalyst materials (often Ni or Co).[81] CO_2 laser beams were virtually always used for ablation. Solangi *et al.*[56] reported SWNTs by pulsed CO_2 laser ablation without further heating the target. They discovered that the average diameter of SWNTs produced by CO_2 lasers increased when the laser power increased.

MXene is a new and innovative member of the group of 2D materials. A relatively secure hydrothermal technique was created by Benjamin *et al.*[82] Additionally, they looked at the effects of temperature, reaction time, and etchant concentration on the creation of $Ti_3C_2T_x$ MXene. Mei *et al.*[74] employed the thermal reduction technique to eliminate the S layers from the Ti_2SC MAX phase to synthesize the 2D Ti_3C MXene as an effective anode material for lithium-ion batteries. This synthetically produced MXene is easily scaled up for industrial purposes and exhibits significant potential as a high-performance anode material for lithium-ion batteries. High-purity MXenes can still be synthesized on a large scale. However, it is still challenging because of the frequent use of hazardous etching chemicals. It would be fantastic if there were a simple, manageable, effective, and environmentally friendly way to make MXenes. Qiu *et al.* successfully used a one-step hydrothermal, eco-friendly, cost-effective technique[73] to manufacture MXene/$NiFe_2O_4$ nanostructures with different MXene (Ti_3C_2) compositions. In the synthesized MXene/$NiFe_2O_4$ composite, the reduction of the grain aggregation due to the enhancement of the MXene concentration. The effectiveness of microwave absorption is increased by the addition of the MXene nanostructure. The results demonstrated that MXene and $NiFe_2O_4$ nanoparticles exhibited superior electromagnetic and microwave absorption properties.

Nanomaterials freely combine predefined components into ordered superstructures that can be applied in various ways during self-assembly. To reduce the system's free energy, self-assembly isolates samples hurriedly assembled into a preset structure.[83] Electrostatic self-assembly is a simple and widely used technique for hetero-composite fabrication. The MXene-based composite was created by Liu *et al.*[72] using an eco-friendly self-assembly method. A Schottky heterojunction was effectively synthesized from a composite of 2D g-C_3N_4 and Ti_3C_2 microsheets, decreasing the recombination of electron–hole pairs and enhancing photogenerated charge separation and migration efficiency. Because of the extensive SSA and active sites on the composite's surface, the current approach produced a modified MXene nanocomposite that had a strong sensing capability. The *in situ* growth method was used by Xu *et al.*[69] to create the MXene-based nanomaterials. This method produced a composite with exceptional thermal, chemical, and mechanical strength. Because of its homogeneous shape, the new material possesses good adsorption and sensing capabilities. This method is economical and safe for the environment. These benefits make it highly likely to become an outstanding practical application for successfully sensing target toxic substances.

5. Functionalization of CNTs and MXenes

The availability of active functional groups on the surface of CNTs and MXenes is responsible for the easy functionalization of nanomaterials with other suitable functional groups. Any nanomaterial's functionalization enhances the mechanical and thermal operating performance, reducing the material's toxicity. In functionalization, scientists add covalent or noncovalent functional groups to the interface of CNTs and MXenes to enhance their biosensing capabilities and stability.

5.1. Functionalization of CNTs

The functionalization process includes attaching molecules or functional groups to the surface of CNTs and changing their chemical and physical characteristics. Because of this change, CNTs have more active sites and may interact with the target analytes more successfully. Because of this, even slight alterations in the surroundings, like the presence of a particular gas or biomolecule, cause discernible changes to the electrical or optical characteristics of the CNTs, enhancing sensitivity. While CNTs have many desirable qualities and benefits, dispersion, triggered by the CNTs' immense surface energy, stands in the way of advancement. Due to their extreme hydrophobicity, CNTs cannot be dispersed in water or typical solvents. To increase their dispersion and other functional qualities, CNTs must be functionalized based on their application.[84] It has become necessary to functionalize CNTs to facilitate the quick manufacture of tiny devices. Across all functionalization strategies, non-covalent and covalent surface changes are the two most frequently utilized techniques. The fundamental benefit of non-covalent functionalization is that the primary structure and characteristics are preserved, making future modification very challenging. Direct covalent functionalization can considerably change the solubility and compatibility of CNTs.[85–87] Thakur *et al.*[88] investigated the impact of functionalization on the properties of CNTs. They found that the functionalized carbon nanotubes (f-CNTs), compared to f-CNTs, had improved sensing capability and working stability and lowered toxicity. The main drawback of covalent functionalization is that it affects the morphology and alters the CNTs' essential mechanical and thermal stability characteristics. Non-covalent functionalization is considered an effective functionalization technique for improving the biological compatibility of CNTs' bio-sensing power without altering the structural characteristics of CNTs. The CNTs can be effectively and easily functionalized through non-covalent van der Waals forces and poly aromatic π–π adsorption stacking.[87,89] Polymers replaced surfactants, but it was observed that they did not significantly increase dispersion. In detection uses, the broad sensitivity of raw CNTs to different

chemicals may lead to poor selectivity. CNTs can react only to specified analytical substances by functionalizing them using specific chemical groups or biological entities (such as enzymes or antibodies). Specifically, identification stems from the CNT-based sensor's ability to differentiate between various chemicals thanks to this selective binding. Additionally, functionalization can increase CNT stability, especially in abrasive environments. For instance, CNTs can be shielded against oxidation, aggregation, and environmental deterioration by adhering to polymer coatings or other stabilizing chemicals. Long-term applications benefit from the enhanced stability of CNT-based sensors, which guarantees steady performance over an extended time. The functionality allows one to adjust the electrical characteristics of CNTs, including bandgap and conductivity. This is especially crucial for electronic detecting devices, which use chemical adsorption or other external stimuli to modify conductivity to identify analytes. Improved sensor efficiency can be achieved by optimizing the kind and density of functional groups to alter the electrical response of CNTs.

Similarly, anionic, cationic, and non-ionized surfactants are all used for the dispersion of SWCNTs; however, these surfactants are typically utilized in extremely small quantities, often less than 5%.[58] Noncovalent functionalization is likewise more heavily influenced by cytotoxic groups. However, these functional groups may constrain the biological applications of such f-CNTs. Sireesha *et al.*[58] reported that the pyrene derivatives introduced as functional groups on most SWCNTs outermost layer enhanced their bio-sensing ability and reduced their toxicity. Liu *et al.*[90] utilized the non-covalent technique *via* grafted copolymers to synthesize functionalized MWCNTs. Due to the lack of carboxyl groups on the grafted interface, this method can only be used with acid-treated MWCNTs, not pure MWCNTs. To enable the dispersion of CNTs in water, water-soluble polyvinyl alcohol is wrapped around the CNTs. Starch was also used to wrap CNTs to create starched nanostructures.[90] Long-chain polymers such as gum arabic were also mechanically adsorbed to disseminate the carbon nanotubes separately in solvents.[91,92] Aromatic polyimides were also utilized as functionalizing polymers to accomplish the non-covalent functionalization of CNTs.[93,94] The functionalization techniques are classified into physical and chemical routes. The chemically functionalized techniques are more effective than physically functionalized techniques because chemical functionalization techniques develop powerful covalent bonds between CNTs and functional groups. Chemical functionalization has some drawbacks, including high prices of chemicals, high environmental pollutant effects, and long purification times.[95,96]

Mallakpour *et al.*[97] utilized the ultrasonic dispersion technique to functionalize the MWCNTs with vitamin B1 to increase the dispersion of CNTs in a poly(ester-imide) matrix. The carboxylic acid moieties on the outermost layer of MWCNTs may interact with vitamin B1's OH group to create ester groups. Through hydrogen bonds, van der Waals interactions, hydrophobic interactions, and electrical interactions, vitamin B1 is expected to communicate with different polar groups on the outermost layer of MWCNTs. Vitamin B1 additionally possesses an aromatic composition. Therefore, by layering negative charges, it might be attached to the graphite surface of MWCNTs. The detailed functionalization procedure of MWCNTs is outlined in Fig. 3.

5.2. Functionalization of MXenes

MXene's ability to sense is greatly improved by functionalization, which alters its surface chemistry and electrical characteristics. MXene's affinity for particular analytes can be adjusted by adding functional groups to its surface, which improves selectivity and sensitivity. These functional groups improve the detection capacities of MXene-based sensors because they increase the number of active sites available for interactions with target molecules. Functionalization can also stabilize MXenes under various conditions, enhancing their robustness and dependability in sensing-related applications.

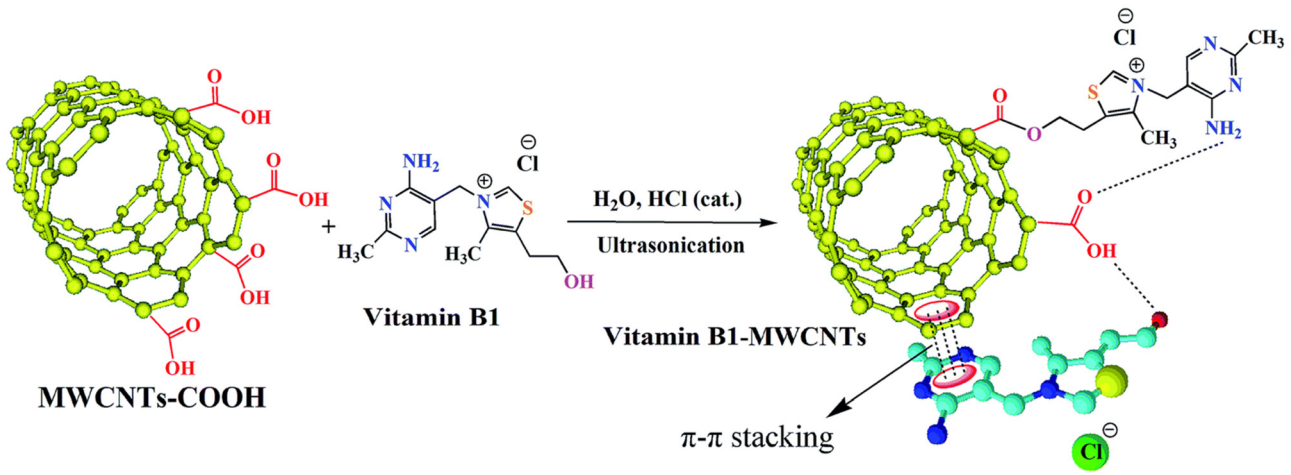

Fig. 3 The functionalization of MWCNTs with vitamin B1.[97]

Functionalization makes MXenes more practical for multiple sensing technologies by allowing them to detect gasses, biomolecules, and other substances. Various synthesis techniques have been used to synthesize single-layer or multilayered MXene. The detailed MXene synthesis techniques are discussed in the next section. Compared to functionalized MXene, non-functionalized MXene quickly precipitated and degraded in water because unfunctionalized MXene possessed limited water dispersibility.[98–101]

Similarly to CNTs, pristine MXene's performance and stability can be enhanced by the functionalization of MXene. The availability of hydroxyl (–OH) and oxygen (–O) active groups on the surface of MXene is responsible for the easy functionalization of MXene with small molecules and polymers. Because MXenes are hydrophilic, their ability to perform can be easily improved by adding suitable functional groups.[102,103] The chemical surface functionalization of MXenes has been extensively researched. Surface modification of MXenes using various small molecules, which are simple to use and reasonably priced, can further improve the performance qualities of MXenes, including mechanical strength, electrical characteristics, and solution stability. Xia *et al.*[104] utilized the small molecules of hexamethylene glycol mono-dodecyl ether ($C_{12}E_6$) on the outermost layer of MXene to form $C_{12}E_6$@Ti_3C_2 nanocomposite. The addition of the small molecule $C_{12}E_8$ to the interface of MXene is responsible for the enhancement of the molecular reaction and increased packing symmetry. He *et al.*[105] reported a diazonium surface chemistry approach for massive amounts of delamination of MXenes. This reduces M–X bonds and extends the interlayer distance by forming an aryl–surface linkage with diazonium and sulfanilic salts. In a recently published article, Solangi *et al.*[2] reported that the MXene sensing performance could be enhanced by changing the chemistry of the MXene parent materials or adding surface functionalities to the outermost layer of MXene. The addition of functional groups to the surface of MXene is responsible for enhancing the biosensing capability, energy storage ability, electron migration characteristics, and band gap (distance between the layers of MXene). The addition of functional groups to the surface of MXene was also responsible for the modification of magnetic characteristics, surface plasmon resonance, and chemical and mechanical stability.[106] Because of the abundance of amino and catechol groups on its backbone, PDA is another promising agent for MXene surface alteration. These groups can interact non-covalently and covalently with both organic and inorganic interfaces. Cobalt has been absorbed into the outermost layer of Ti_3C_2 and CNTs to create a Ti_3C_2@CNT composite. By modifying the PDA, the capacitive ability of Ti_3C_2 was enhanced.[107] Solangi *et al.*[61] reported that the un-functionalized MXene possessed a lower desalination capacity than the functionalized MXene. Because it is functionalized, MXene can attract more salt ions. In a nutshell, the functionalization of nanomaterials in the biosensing sector is responsible for more excellent and more effective sensing of targeted molecules, bacteria, and viruses. Zhang *et al.*[108] utilized the cost-effective and environmentally friendly alkalization–grafting technique to functionalize MXenes with amino groups to enhance the stability and adsorption capacity of MXenes. A graphical representation of the amino-functionalized MXene is shown in Fig. 4.

6. Characteristics of CNTs and MXenes

The characteristics of nanomaterials play an influential role when selecting nanomaterials as biosensors. Nanomaterials with excellent surface morphology, electrical and thermal con-

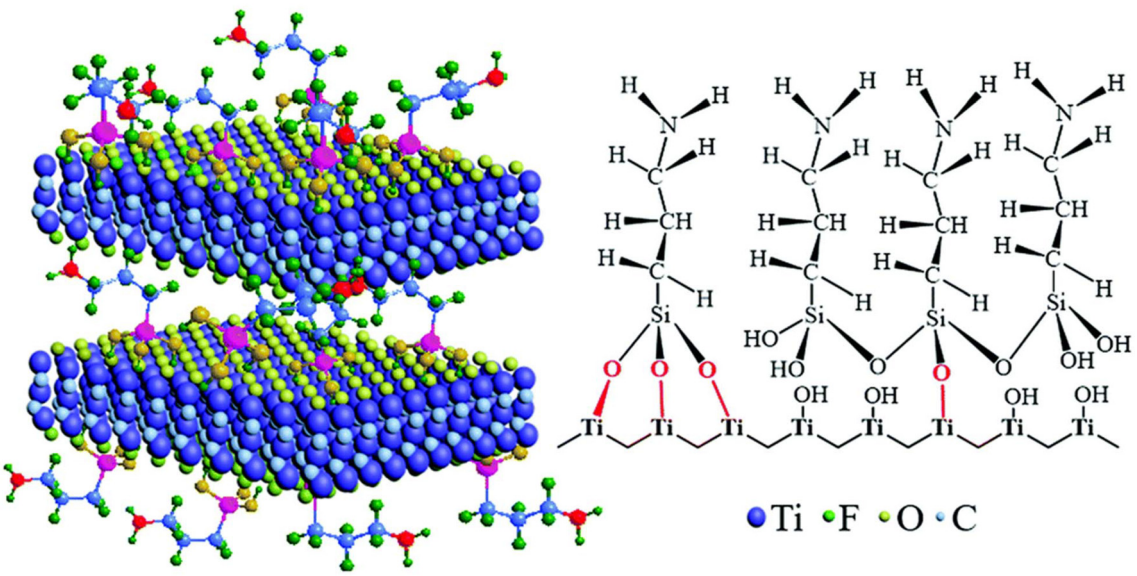

Fig. 4 The alkalization-grafting procedure for producing $Ti_3C_2T_x$ MXene nanosheets with amino functionalities.[108]

Table 2 Comparative analysis of the characteristics of CNTs and MXenes

Characteristics	1D CNTs	2D MXenes	Remarks	Ref.
Electrical conductivity	1×10^6 S cm^{-1}	5×10^3 S cm^{-1}	CNTs have greater electrical conductivity than MXene	109 and 110
Mechanical strength	700 GPa	100 GPa	CNTs' mechanical strength is more significant than MXene's because CNTs face more load than MXene	111 and 112
Specific surface area	225.17 m^2 g^{-1}	112.259 m^2 g^{-1}	The average SSA of CNTs is greater than MXene	113 and 114
Transmittance	56%	70%	The transmittance of CNTs is lower than that of MXene	107
Refractive index	11.2%	41.43%	The refractive index of CNTs is lower than MXene's, so a high refractive index is responsible for MXene's higher biosensing capability	115 and 116
Degradation rate in water	30%	55%	CNT degradation rate is lower than MXene when it interacts with water	117 and 118
Dimension	It has a one-dimensional structure	It has a two-dimensional structure	CNTs possess a one-dimensional and poor porous structure, and MXene has a two-dimensional and better porous structure than CNTs	119 and 120

ductivity, and thermal and mechanical stability suit biosensing nanomaterials. In this section, we discuss the properties of CNTs and MXene-based nanomaterials. A comparative analysis of the characteristics of CNTs and MXenes is given in Table 2.

6.1. Comparison of the electronic characteristics of CNTs and MXenes

The rate at which electrons move through a solid object can be used to evaluate electrical conductivity directly. MXenes exhibit various electrical characteristics, including semi-conductivity, metallicity, and being structurally insulative, due to their adaptable thickness tunability, numerous surface functionalization options, and diverse compositions.[120,121] The atoms of the MXene-based nanosheets determine the electronic characteristics. The electrical properties of MXenes can be enhanced *via* effective surface functionalization.[122,123] The pristine MXene possessed metallic characteristics, and F and I functionality-based MXenes possessed semi-conductive characteristics.[98,124] The MXenes based on Mo and W are bad conductors of electricity.[107] The metallic MXene can be transformed into a semiconductor by altering or functionalizing its outermost layer. The presence of surface functionalities, –O, –OH, and –F, has a substantial impact on the electronic characteristics of MXenes. These functional groups change the conductive properties, band structure, and chemical reactivity of MXenes. Oxygen termination often increases conductivity and maintains the metallic properties of MXenes.[64,125] On the other hand, introducing –F and –OH groups tends to decrease conductivity by causing charge localization or band gaps, potentially transforming MXenes into semiconductors. Consequently, surface functionalization enables the exact adjustment of MXenes' electrical characteristics to suit different purposes.

Mozafari *et al.*[107] reported that Ti_2MnC_2 MXene had dual characteristics because sometimes it behaved like a good conductor and sometimes like a semiconductor. Its strength of conductivity depends on the nature of the surface functional groups. The Ti_2MnC_2 MXene behaves like a semiconductor when its surface comprises –O terminating functional groups. Additionally, the MXenes, including Nb_4C_3, Ti_3C_2, Nb_2C, V_2C, and Ti_2C, containing –OH and –O surface functional groups, behave like good conductors because these functional groups speed up the migration of charges between the respective electrodes. However, Ti_3CO_2 MXene possessed semi-conductive characteristics in the presence of –OH and –O surface functionalities because of the long distance induced by the downshifting of the Fermi level. The Fermi level is reduced in Ti_3CO_2 through more extraordinary electron donations between carbon, oxygen, and titanium atoms. They also reported that the MXenes, such as $TiCO_2$, $ZrCO_2$, $Zr_3C_3O_2$, Hf_2CO_2, and $Hf_3C_2O_2$, had –O functional groups. They behave like bad conductors of electricity, but the same MXenes with –F and –OH functionalities behave like good conductors. An experimental investigation by Chen *et al.*[126] verified the impact of the addition of glycine nanomaterial on the electrical conductivity of Ti_3C_2 MXene. The MXene-based Ti_3C_2/glycine composite material possessed lower electrical conductivity than pristine MXene. This study indicated that in the pristine form, MXene and CNTs possess poor electrical conductivity as compared to their composites. The conductivity of CNTs may be improved by including highly conductive nanomaterials. Incorporating the highly conductive nanomaterials aluminum (Al) and copper (Cu) boosted the conductivity of the pure CNTs by up to 389 and 14 times, respectively.[127] The electrical conductivities of CNTs and MXene thin sheets are 1×10^6 S cm^{-1} and 5×10^3 S cm^{-1}, respectively. These experimental results indicated that CNTs had outstanding electrical conductivity compared to MXenes.

6.2. Comparison of the mechanical characteristics of CNTs and MXenes

The mechanical characteristics of the material are essential for selecting the material as a biosensor. The mechanical characteristics of nanomaterials consist of strength, toughness, elasticity, brittleness, hardness, rigidity, yield stress, and malleability. Strength is the ability of a material to resist deformation or breakdown of nanomaterials when exposed to loads or external forces. Materials used in industrial items must be mechanically strong enough for operation under various

mechanical loads or strains. The mechanical characteristics of MXenes, including strength, flexibility, and toughness, are greatly influenced by surface functional groups. The functional groups –O, –OH, and –F can modify the bonding between MXene layers, affecting the relationships between layers and the material's stiffness. Oxygen termination often increases mechanical strength by facilitating stronger interlayer bonding. Conversely, the presence of –OH or –F groups may inhibit these interactions, resulting in a more flexible but less rigid material.[128,129] In addition, surface groups can cause deformation in the lattice structure, impacting the overall mechanical stability. By modifying these surface groups, MXenes can be tailored for precise mechanical applications, effectively achieving a harmonious equilibrium between flexibility and strength.

A solid material's strength is expressed as pressure, specifically in gigapascals (GPa). The mechanical strengths of CNTs and MXenes were 530–700 GPa and 80–100 GPa, respectively. The power of CNTs to face the load is six times higher than MXenes. Pristine CNTs and MXenes possessed lower mechanical power than MXenes. Hardness, which enables the material to tolerate localized, persistent deformation and scratching, is one of the essential mechanical properties of engineering substances. Several engineering design projects incorporate the concept of hardness. The material's appropriateness and usability are directly impacted by this attribute, making it crucial. MXenes and CNTs have a hardness measured in GPa, the unit of pressure for the hardness scale. In light of mechanical stability, the pristine CNTs possess higher tensile strength than the pristine MXene. The deformation rate under stress from compression is a solid material's malleability. Being able to fold or crush a material into a thin sheet is a common definition of malleability. The mechanical property of a substance's malleability, which alters with temperature, is part of the material's elasticity. The substance gets more pliable as the temperature rises. The material's shape cannot influence its movement.[130] Electrons are very mobile because the substance is highly conductive.

6.3. Comparison of the specific surface area of CNTs and MXenes

The specific surface area (SSA) is a very effective parameter for selecting a material for use as a biosensor. The SSA of nanomaterials can be measured in $m^2\ g^{-1}$. More significantly, the SSA is responsible for an excellent sensing capability. Choosing an appropriate adsorbent after considering its stability and recyclable specific surface area has become more crucial. The relationship between an adsorbent's SSA and its ability to absorb CO_2 is direct. The substantial surface area of carbon nanotubes and MXenes dramatically improves the efficacy of biosensors by offering a more significant number of active sites for the attachment of target molecules, resulting in heightened sensitivity. The enhanced surface area facilitates improved interactions between the sensor and analyte, hence enhancing signal transduction and enabling the detection of even minute quantities of chemicals. The increased electron transmission in CNTs results from their huge contact area, leading to quicker response times. On the other hand, MXenes exhibit strong conductivity and chemical flexibility, which is especially advantageous under wet conditions. Moreover, the substantial SSA of both materials enables functionalization, enhancing the selectivity and overall effectiveness of the biosensor. Employing the adsorbent in powder form or increasing the amount of pores in the solid form can improve the SSA of MXene and CNT adsorbents. CNTs and MXenes had SSAs of 225.17 $m^2\ g^{-1}$ and 39.19 $m^2\ g^{-1}$, respectively.[113] These findings demonstrated the advantages of CNTs over MXenes. These results indicated that CNTs were a better biosensor choice because of the larger SSA.

6.4. Comparison of the optical characteristics of CNTs and MXenes

The optical characteristics of nanomaterials are complex and consist of absorption, refractive index, and transmittance. The optical properties of CNTs and MXenes significantly improve the performance of biosensors by allowing for sensitive detection through changes in optical signals. CNTs possess high optical absorption and fluorescence quenching characteristics, making them well-suited for detecting variations in light signals upon interaction with specific molecules. This enhances the sensitivity of optical biosensors, which include fluorescence or Raman-based sensing devices. MXenes, due to their exceptional surface plasmon resonance and adjustable optical characteristics, augment the sensitivity of biosensors by intensifying the interactions between light and matter. The optical properties of these materials, along with their excellent conductivity, enable accurate and immediate detection of biological and chemical substances, enhancing the overall functionality of optical biosensors. Functionalized CNTs and MXenes possessed much better transmittance than unfunctionalized nanomaterials. In other words, synthesized MXenes possessed an excellent transmittance compared to the parent materials. The parent Ti_3AlC_2 MAX phase of the nanomaterial possessed 30% transmittance, but synthesized or functionalized Ti_3C_2 MXene had 77% transmittance. The refractive index of CNTs is 11.2% and MXenes is 41.33%, so, it can be concluded that MXenes possess better optical characteristics than CNTs. Based on optical factors, MXenes may have a higher biosensing capability than CNTs. Furthermore, in the UV spectrum, the reflectivity increased compared to pure MXenes, whereas in the visible spectrum, the reflectivity and absorption of the –F and OH-functionalized MXenes were reduced.[131] The optical properties of pristine CNTs and MXenes are generally better than those of their composite forms.

6.5. Comparison of the hydrophilicity of CNTs and MXenes

MXene has an excellent hydrophilic nature because of the availability of –OH, –O, and –F functionalities at its surface. Because of the high hydrophilicity of MXene, its degradation rate in water is very high. The addition of excellent surface functionalities on the surface of MXenes is responsible for

their enhanced stability and reduction degradation rate. So, adding functional groups to the surface of CNTs and MXenes reduced their degradation rate in water or the hydrophilicity of CNTs and MXenes.[132,133] The water-attracting properties of CNTs and MXenes increase their optical qualities, enhancing biosensors' effectiveness. Hydrophilic carbon nanotubes can bind to water-based solutions, improving dispersion and enhancing contact with biological molecules. This, in turn, enhances optical signal alterations, such as fluorescence or Raman scattering. Furthermore, the hydrophilic characteristics of MXenes and their adjustable optical properties, such as surface plasmon resonance, amplify the interactions between light and matter in water-based circumstances. The hydrophilic property enables enhanced molecule adsorption and increased biosensor sensitivity, especially in moist or biological environments. The combined hydrophilic features of both materials enhance the precision, velocity, and dependability of optical biosensors in real-time applications. Ji *et al.*[118] enhanced the stability or hydrophilicity of a functionalized MXene with a sialylation reagent (APTES). The synthesized APTES–MXene has excellent stability and degradation resistance in water compared to the pristine MXene. Adding APTES to the MXene reduces its interaction with water, enhancing its stability and degradation in water. In air, the degradation rate of un-functionalized MXene was up to 95% and functionalized MXene was up to 20.8% after 11 days. The outcomes demonstrated the transition from hydrophilic to hydrophobic surface characteristics. MXenes have been modified using two extremely hydrophobic self-assembled monolayers, CPTMS and FOTS, by creating covalent connections between –OH and various outer layer functionalities. Li *et al.*[117] utilized a cost-effective technique to synthesize the CNT/PDMS nanocomposite to enhance the stability and degradation of CNTs in water and the environment. The stability of the synthesized CNT/PDMS nanocomposite is many times greater than that of pristine CNTs, Hence, it can be conlcuded that the stability and environmental degradation rate of CNTs and MXenes can be enhanced by functionalization with very stable functional groups.

6.6. Toxicity of CNTs and MXenes

CNTs and MXenes have toxic effects when these nanomaterials come into contact with the human body through oral inhalation or injection into the skin. When the CNT-based material enters the body in any way, it is responsible for various toxic effects: mutations of DNA, malignant transformation, oxidative stress, interstitial fibrosis, inflammatory responses, and granuloma formation.[134] The toxicity of CNTs may be significantly affected by metal contaminants. Metal ions and other contaminants were introduced into the CNT while manufacturing intoxicated cell membranes. Because of cellular internalization collapse, the length of a CNT enormously affects its toxicity.[135] The toxicity of CNTs is also associated with the diameter. CNTs with large diameters have more toxicity than those with lower diameters. SWCNTs and MWCNTs had varied cytotoxic impacts on cells because of differences in their sizes, structures, and chemical interface characteristics.[136] Pristine CNTs have limited toxic effects compared to functionalized MXenes. The functionalization of pristine CNTs increases their stability and specific surface area. Still, unfortunately, it enhances the toxicity of the CNTs. Pure CNTs are more poisonous than functionalized CNTs and can aggregate more quickly. However, MXene has the opposite impact compared to CNTs because pristine MXene is less toxic than CNTs.[137]

When specific natural dispersants are present, the individual CNTs gather together and become poisonous. It is important to note that cell toxicity is induced by CNT surface functionalization. In the HUVEC cell lines, the SWCNT with –COOH functionalization resulted in more significant toxicity than the SWCNT without functionalization.[134,138] Vasyukova *et al.*[139] revealed that a single MnO_x/Ti_3C_2-SP mixture was biologically compatible *in vivo* and safe after healthy laboratory mice were given intravenous injections at 5, 10, and 20 mg kg^{-1} doses. As a result, following the 30-day surveillance period, all significant health markers were normal and consistent with the control. The target organs were examined and subjected to additional biochemical blood testing, but no adverse activity was detected. MXene has a less severe adverse effect on human health and the environment than CNTs.

The functionalization, coating, or encapsulation of CNTs and MXenes can eliminate the toxic effect of the CNT and MXene-based biosensors. It is vital to apply a mix of methods to minimize the hazardous effects that are caused by biosensing devices. These approaches include surface functionalization, biocompatible materials, safe-by-design principles, controlled discharge systems, stringent evaluation, and appropriate handling of the surroundings. Implementing these methods makes it possible to create biosensors that are not only highly efficient but also safe for use in sensitive applications such as medicine, the environment, and other areas. There is the possibility to prevent direct interactions with biological tissues by enclosing harmful nanoparticles inside biocompatible matrices or nanoparticles. The biologically active detector material can be controlled using encapsulating materials such as liposomes, hydrogels, or biodegradable polymers. This helps to reduce the amount of contact that occurs. Developing biosensors made of materials that degrade in a regulated manner and release byproducts that are not poisonous can help lessen the long-term toxicity of the device. Encapsulating or coating harmful sensing compounds can be accomplished, for instance, by utilizing biodegradable polymers that gradually decompose into non-poisonous monomers. It is possible to lessen the toxicity of nanomaterials by functionalizing their surfaces with biomolecules such as peptides, proteins, or DNA, which are intrinsically friendly. These functional groups can improve the material's interactions with the target analytes, enhancing the sensor's performance while minimizing the risk of damage to the cells or tissues. Detailed *in vitro* and *in vivo* tests should be carried out to determine whether the biosensor materials are harmful. To better understand the potential dangers linked to the materials, these tests ought to include cytotoxicity assays, hemocompatibility tests,

and chronic biocompatibility investigations. The above-discussed methods play a primary role in eliminating the toxic effect of MXene and CNTs to a large extent in biosensing applications.

7. Comparative analysis of CNT- and MXene-based biosensors

The working principle of all developed sensors or detectors is the same. The detecting material may be differ from sensor to sensor. The detecting medium used in the sensor are either enzymes or antibodies which are used to identify the harmful diseases or chemicals in the body, which are called biosensors. In this section, we discuss various kinds of CNTs and MXene based biosensors.

7.1. CNT- and MXene-based electrochemical biosensors

Several traditional techniques, including homogenizing a contaminated food sample in a buffer and isolating bacterial colonies using selective agars, are used to detect harmful bacteria or chemicals in food samples and human bodies.[140] However, the EC biosensor is advanced technology that gives more accurate results for detecting target bacteria and harmful chemicals in food and the human body. The idea behind identifying bacteria with biosensors is to convert biological data into a digital signal by employing physical or chemical methods. The relationship between recognition components (antibodies, enzymes, and viruses) and their biological targets produces these biological data. Recognition components are often immobilized on a transducer surface through covalent forces, adsorption, trapping, cross-linking, encapsulation, or adsorption.[140] The biological activity is converted into an identifiable signal using a variety of transducers, including mass-based, optical, and electrochemical sensors, depending on the signal transduction method.

In contrast to indirect identification techniques, which use a labeled probe to identify the result of biochemical reactions, direct identification devices monitor physical changes caused by the contact of the target analyte directly in real time without needing a label. EC biosensors belong to various transducer kinds. They show promise because of their affordability, speed, sensitivity, usability, high signal-to-noise ratio, flexibility in using identification elements, minimal interaction with food matrices, and instrument simplicity.[141–143] Even at low concentrations in turbid environments, electrochemical biosensors enable sensitive and focused detection of bacterial cells. Generally, biosensors are divided into two classes: direct and indirect identification of systems. In this section, the reviewer provides a comparative analysis of CNTs and MXenes. The performance of CNT- and MXene-based EC biosensors for detecting various target materials is given in Table 3.

7.1.1. CNT-based electrochemical biosensors. EC biosensors were created using small carbon particles in the zero- to three-dimensional (0D–3D) range. With a significant

Table 3 The performance of CNT- and MXene-based EC biosensors for detecting various target materials

Name of biosensor	Synthesis techniques	Measurement techniques	Characterization techniques	Analyte	Response time (S)	Sensitivity ($mA\ mM^{-1}\ cm^{-2}$)	Limit of sensing (μM)	Linear range (μM)	Ref.
GA/uricase/chitosan/SACNT/Pt	PECVD	FDA	SEM	Uric acid	9	518.8	1	100–1000	144
Au/CG/C@MWCNTs/PtNPs/GO_x/Nafion	One-step solvothermal technique	Amperometric technique	SEM, XPS	Glucose	<5	26.5	0.005–13 mM	0.005–13	145
VACNTs/PANI/GO_x	CVD	DVP	FESE, ATR-FTIR, and EIS	Blood plasma	20	620	1.1	0.002–0.426	146
GO_x/MEPCM-CNTs/GCE	Microencapsulating	CV	SEM, EDX, FTIR, and XPS	Glucose	8	5.95	13.11	0.2–4.5	147
AuNP(5)/MWCNT (0.05%)/GCE	Simple coating technique	DPV	—	Bisphenol A	12	0.045	16 nM	0.01–0.07	148
PB-$Ti_3C_2T_x$	Self-assembly technique	DPV	SEM, TEM, DLS, AFM	CTCs	—	—	9 cells per mL	1 to 500	149
PB-$Ti_3C_2T_x$	Self-assembly technique	CV	SEM, TEM, DLS, AFM	H_2O_2	—	—	0.57 μM	1.3×10^1 to 1.3×10^6 cells per mL	149
MXene/Pt/C nanocomposite	Simple coating technique	DPV	SEM, EDX, and TEM	SARS-CoV-2	—	100%	0.4 aM	1 aM to 100 nM	150
MXene-AuPd	Auto reduction	DPV	SEM, XPS, TEM, and XRD	MicroRNA-21	0.5 s	95.32%	0.42 fM	1 fM to 1 nM	151
MXene@Au	Self-reduction method	DPV	—	MRSA	—	94.35%	3.8×10^1 CFU per mL	3.8×10^1 to 3.8×10^7 CFU per mL	152
Au@MXene	Chemical reduction	CV	SEM	AFB1	80	—	2.8 nM.	0.01–50 μM	153

Plasma-enhanced chemical vapor deposition (PECVD), chemical vapor deposition (CVD), cyclic voltammetry (CV), electrochemical impedance spectroscopy (EIS), transmission electron microscopy (TEM), dynamic light scattering (DLS), atomic force microscopy (AFM), dynamic light scattering (DLS), scanning electron microscopy (SEM), methicillin-resistant *Staphylococcus aureus* (MRSA), polyethyleneimine (PEI), aflatoxin B1 (AFB1).

increase in field-effect movement and sensitivity, CNTs have several benefits for the EC detection of foodborne bacterial pathogens.[154] Enormous surface-to-volume carbon nanostructures can capture and discriminate electrical impulses before and after combining biological elements.[155] Quick transmission of electron kinetics from the transducer surface to the EC medium is made possible by carbon's excellent electrical conductivity, which is also a result of other fascinating physics brought on by the delocalized p-electron system.[156] The electrochemical characteristics of carbon nanostructures make efficient electron transmission of EC reactions possible.[157] It has been discovered that carbon nanostructures exhibit biological compatibility and facilitate reactions between an identifiable element and the target proteins.[23,24] The mechanical properties, excellent stability, and simplicity of modification also make the surface functionalization of a carbon nanostructure simple.[158,159] The carbon nanomaterials can be modified to precisely identify biological substances thanks to these unique features.[159]

Applications of the CNTs based biosensors in biomedical studies are increasing such as blood glucose screening. Diabetes, a breakdown in blood sugar management, is a major cause of concern for people worldwide.[160] Major adverse reactions such as lower limb amputations, deafness, kidney failure, neuropathy, and coronary artery disease can result from it. Thus, human health must monitored on the basis of the blood glucose levels in human body. In 2030, it is anticipated that 439 million individuals will be dealing with diabetes.[146] Azimi *et al.*[146] utilized the cost-effective chemical vapor deposition (CVD) method to synthesize a biosensor composed of vertically aligned carbon nanotube arrays (VACNTs) to identify glucose in the human blood plasma. Synthetic CNT-based electrodes are very good at identifying glucose. However, by electrodepositing polyaniline (PANI) and then coupling glucose oxidase (GO_x) to VACNTs, researchers hoped to improve further the stability and detection effectiveness of the synthesized CNTs. The EC behavior of the electrode was examined using cyclic voltammetry (CV) and differential pulse voltammetry (DPV). The low glucose LOD, linear range, and sensitivity were 1.1 μM, 2–426 μM, and 620 mA mM^{-1} cm^{-2}, respectively. The synthesized CNT-based biosensors maintain their stability and glucose detection performance up to 95% after 45 working days. The proposed electrode is a good option for identifying glucose, according to the results obtained from using it to determine glucose in plasma samples. The manufactured electrode is compatible with compact analytical systems. Due to its low working potential, which inhibits the oxidation of other interfering compounds like UA and ascorbic acid, the manufactured biosensor successfully detected glucose when other interfering compounds were present. The findings showed that the electrode would be a good choice for identifying glucose.

Yang *et al.*[144] utilized microfabrication to synthesize a CNT-based biosensor to detect uric acid (UA). The manufacturing process and mechanism of the 3D SACNT array EC biosensor for UA sensing are presented in Fig. 5a. The ordered 3D super-aligned carbon nanotube (SACNT) array of the biosensor's functional electrode is immobilized with uricase using a precipitation and cross-linking process. The artificially created CNT-based EC biosensor had a larger SSA for simple contact with reactants, greater enzyme density, and the ability to preserve the SACNT architecture and high conductivity even after the alteration. The SACNT/Pt working electrode's lateral and top profiles both before and after uricase immobilization not affected in large extent. According to the SEM images in Fig. 5b and c, the outermost layer of the SACNT was spaced out before enzyme immobilization, but the array's interior was oriented vertically. The clusters or ellipsoidal particles coated the SACNT array's surface and interior following enzyme immobilization. The CV response of the synthesized electrochemical sensor in 300 μM UA solution was evaluated at a constant scan rate of 50 mV s^{-1}.

The SACNTs modified with different materials possess a promising response for the sensing of UA and have a pair of redox peaks for oxidation at 0.12 V and reduction at −0.20 V, as shown in Fig. 5d. The lack of uricase on the electrode in use resulted in the absence of any apparent redox peaks being detected for the GA/chitosan/SACNT/Pt electrode. Compared to the behavior of the other two modified electrodes, the electrical responsiveness of the pure electrode was even lower. According to these findings, the GA/uricase/chitosan/SACNT/Pt electrode exhibited remarkable electrocatalytic activity when detecting uric acid. The detection limit of the synthesized electrochemical sensors continuously increases up to 20 mg mL^{-1} of UA. This means 20 mg mL^{-1} of UA is the optimal detection concentration. The enhancement of the scanning rate from 10 to 200 mV s^{-1} is responsible for increasing the oxidation current, as presented in Fig. 5e. The maximum oxidation current observed in all CV profiles exhibited a linear relationship with the scanning rate, as depicted in Fig. 5f. It appears from this that the transfer of electrons at the GA/uricase/chitosan/SACNT/Pt electrode is regulated by surface adsorption. This indicates that the redox process's speed depends on the adsorption rate between the reacting compounds and the active substances located on the outermost layer of the electrically conducting electrode. The peak oxidation current of the active CNT-based electrochemical sensor was observed at 50 mV s^{-1} and 9 s response time at various concentrations of UA solutions varying from 1 μM to 2000 μM as presented in Fig. 5g. The peak oxidation current was enhanced linearly as concentrations of the UA solution increased from 100 μM to 1000 μM up to saturation, which occurred at 1000 μM. The 3D SACNT array uric acid biosensor exhibited a linear response ranging from 100 μM to 1000 μM, with a correlation coefficient of 0.9956.

The synthesized sensor possesses an excellent sensing limit of 1 μM, and the sensitivity is 518.8 μA $(mM\ cm^2)^{-1}$. It is evident from the inset in Fig. 5h that the standard deviation of the highest recorded oxidation currents is 4.2×10^{-7} A. This indicates that the 3D SACNT array biosensor exhibits exceptional reproducibility. As the figure suggests, the amperometric *I–t* curve for the dynamic measurement of UA with the bio-

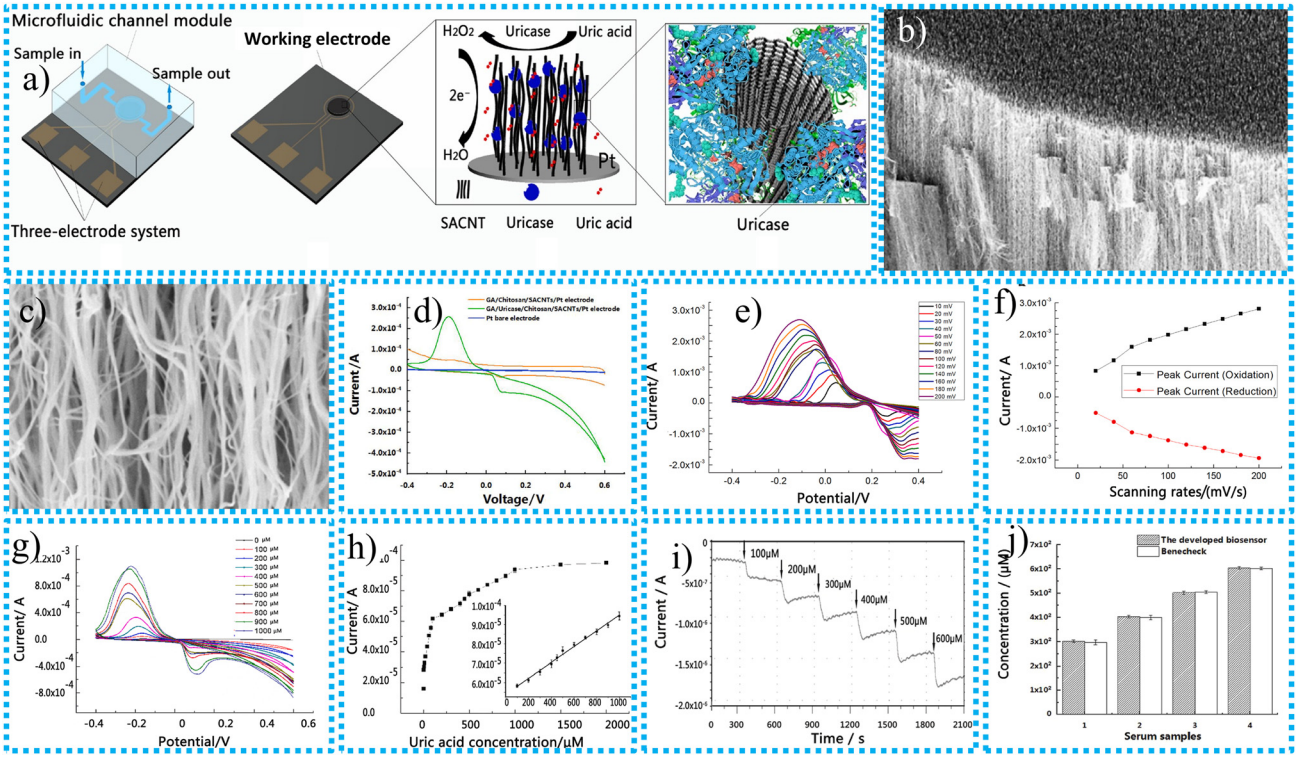

Fig. 5 (a) Synthesis and construction of the 3D SACNT array electrochemical biosensor for UA sensing, SEM image of the SACNT side at (b) 12 000 times magnification, (c) 100 000 times magnification of the SACNT/Pt working electrode before uricase immobilization, (d) CV curves of different electrode materials for biosensors, (e) impact of scanning rate on the redox reaction behaviour for the GA/uricase/chitosan/SACNT/Pt electrode, (f) plot of peak oxidation and reduction currents *versus* scanning rates, (g) CV curves of the GA/uricase/chitosan/SACNT/Pt electrode in 0.01 M PBS at pH = 7.4 containing UA at different concentrations, (h) peak oxidation currents plotted as functions of uric acid concentration, (i) amperometric *I*–*t* curve, (j) determination of uric acid in actual serum samples collected from a human *via* our biosensor compared with the FDA-approved BeneCheck PLUS system (*N* = 4).[144]

sensor is depicted in Fig. 5i. Various concentration gradients of UA, ranging from 0 to 600 μM, were assessed in a solution of PBS with a pH of 7.4. An examination was conducted on the specimens. There is a clear indication that the amplitude of the oxidation current grows in proportion to the increase in the concentration of uric acid. Within 300 s, the amperometric variation of the biosensor occurred in response to a change in the concentration of the uric acid solution. This change happened when the working electrode was refilled with new medium *via* various microchannels. By demonstrating the sensitive and rapid measurement capabilities of the GA/uricase/chitosan/SACNT/Pt biosensor, which enables dynamic uric acid monitoring, this outcome shows the performance of the biosensor. A series of serum samples from human beings in good health injected with uric acid were examined to verify further the practicality of the 3D-structured SACNT array biosensor created for identifying uric acid in bodily fluids. Using the paired *T*-test, shown in Fig. 5j, it was determined that there was no significant difference between the findings obtained using the FDA-approved electrochemical analyzer and the outcomes produced using the other method. The *p*-value was more than 0.05. According to the results, the precision of the biosensor, that is, a 3D-structured SACNT array, is adequate for identifying the presence of uric acid in authentic samples. The low limit of detection (LOD) of UA is 1 μM, and the linear range of detection (LDR) is 100–1000 μM. The response time of the sensing material is very short, up to 9 s. It means the CNT-based EC biosensor developed detects the UA target quickly. The synthesized EC biosensor differs significantly from previous studies because it uses a 3D SACNT array with enzymes immobilized through precipitation and cross-linking. This results in outstanding results, including high sensitivity, a broad identification range, a low detection limit, and a rapid response time. These exceptional results for the synthesized CNT-based EC biosensors are due to their great electrical and optical capabilities, substantial aspect ratio, powerful mechanical properties, good chemical and thermal stability, and excellent chemical resistance.

7.1.2. MXene-based electrochemical biosensors. MXene is an excellent choice for manufacturing EC biosensors because of its outstanding hydrophilicity, high enzyme loading capability, biological compatibility, great electron migration power, and good electrocatalytic characteristics.[65] Su *et al.*[149] utilized the self-assembly technique to deposit Prussian blue (PB) on the surface of $Ti_3C_2T_x$ MXene to synthesize the MXene-based PB-$Ti_3C_2T_x$ biosensor for the identification of circulating

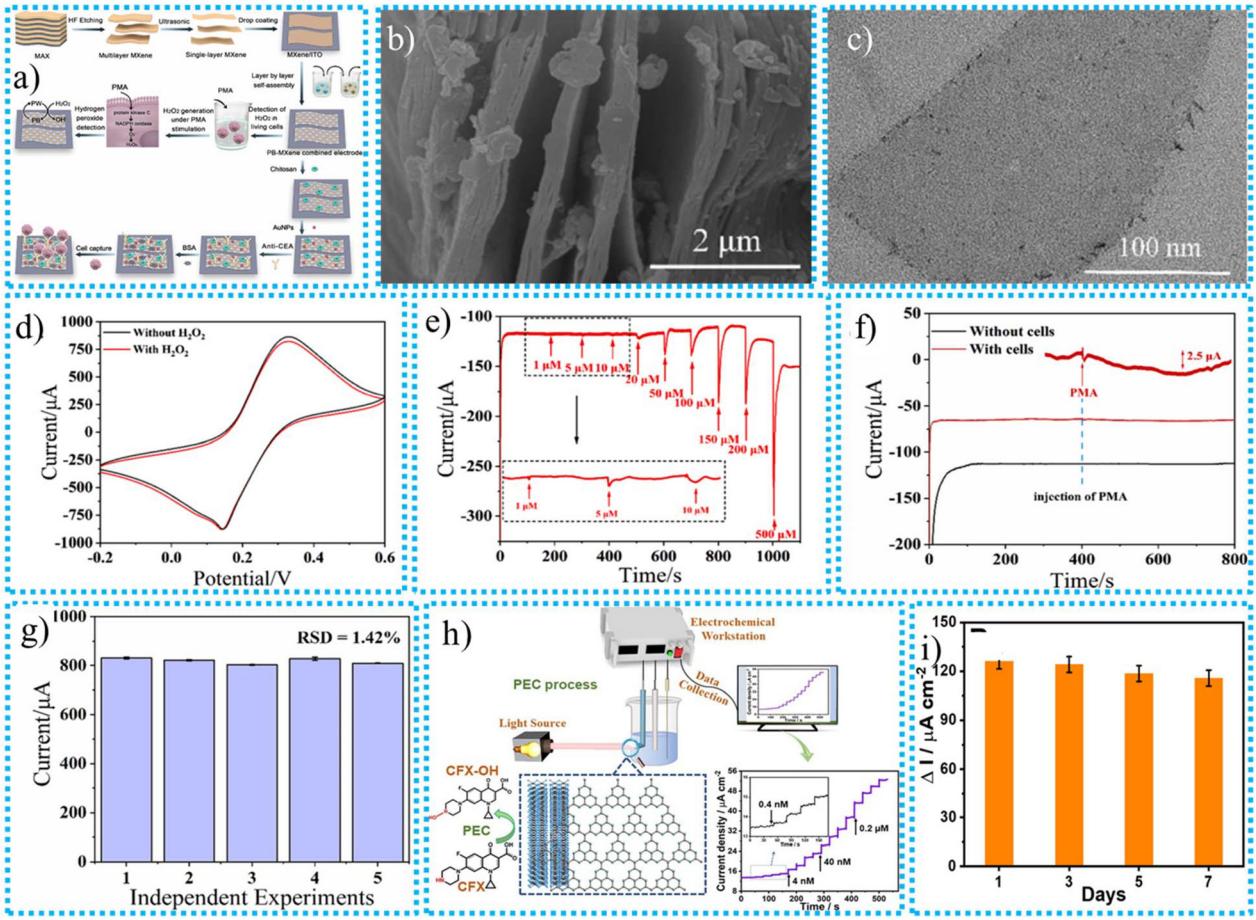

Fig. 6 (a) The synthesis process for the MXene-based PB-MXene biosensor for detecting CTCs, the existence of PB on the layered MXene, (b) SEM image, (c) TEM image, (d) CV curves for the PB-MXene composite electrode in the absence and presence of 1 mM H_2O_2 in 5 mM $[Fe(CN)_6]^{3-}$ solution containing 0.1 M KCl, (e) amperometric *i*–*t* curve of the PB-MXene electrode, (f) amperometric *i*–*t* responses with and without A549 cells under PMA stimulation, (g) reproducibility of 5 independent biosensors in 1.3×10^4 cells per mL of A549 cells,[149] (h) the proposed PEC mechanism at the g-C_3N_4/Ti_3C_2 composite and an *I*–*t* curve selected to explain the stepwise process, choose the best sensing range, and measure the sensing limit, (i) the long-term stability of the proposed PEC sensor.[161]

tumor cells (CTCs). The synthesis process for the PB-MXene biosensor for detecting CTCs is given in Fig. 6a. The existence of PB on the layers of MXene is shown in the SEM and TEM images of MXene-based PB-$Ti_3C_2T_x$ material in Fig. 6b and c. CTCs are crucial prognostic indicators for diagnosing cancer and metastatic disease, and their discovery is an essential step in the metastatic cancer identification process. A very effective electrode modifier for biosensors is PB. The porous nature of PB provides superb efficiency for adsorption. The higher PB catalytic activity is devoted to the existence of iron atoms in it, because iron atoms have higher metal active sites. As a result of its huge pore volume, customizable size, simplicity of synthesis and surface modification, excellent thermal stability, and outstanding biological compatibility, it has attracted increasing amounts of research attention for application in immunosensors and biological imaging, as well as other uses as a therapeutic agent. The addition of PB to the surface of MXene is responsible for excellent electrocatalytic activity and reduced cytotoxicity for the H_2O_2 sensing and living CTC capture.

CV and EIS testing have been used to evaluate the electrochemical performance of the synthesized PB-MXene-based sensor. With 5 mM $K_3[Fe(CN)_6]$ and 0.1 M KCl in the same solution, and the CV curves of various multilayer PB-MXene-based biosensors has been analysed. The combination of redox peak pairs appeared in an obvious way, and it became apparent that the redox peaks of the MXene substance that PB had altered had greatly improved. This can be briefly attributed to the critical part that PB plays in increasing the surface area of MXene and improving the electron transfer process. The enhancement of the MXene layer on the sensor's interface increases the reduction peak current by up to 20 layers sensors with the highest reduction peak current.

The CV curves confirmed the H_2O_2 sensing performance of the PB-MXene-based electrochemical sensor, as presented in Fig. 6d. The electrocatalytic capability of PB is responsible for an upsurge in the reduction peak that occurs when 1 mM H_2O_2 is present, as well as the downward movement of the CV curve compared to the pattern that occurs when H_2O_2 is not

present. In the presence of H_2O_2, PB would perform a catalytic function, enhancing electron transport and accelerating the reduction procedure. The amperometric curve for the simultaneous injection of H_2O_2 into the electrolyte at different concentrations is presented in Fig. 6e. The infusion of H_2O_2 resulted in the gradual appearance of current responses, which could be observed. The synthesized sensor exhibited a meaningful change when PMA was injected into the solution in the presence of the sample with A549 cells, as shown in Fig. 6f. However, in the absence of cells in the electrolyte, an equivalent quantity of PMA was introduced at 400 s, and the amperometric curve exhibited consistent stability. PMA induces the cellular secretion of H_2O_2, which is subsequently recognized by the PB-MXene composite electrode and converted into an electrical current signal. The composite electrode demonstrated the ability to accurately detect a low concentration of H_2O_2 emitted by living cells, exhibiting excellent detection capabilities and heightened sensitivity. The ability of biosensors to be replicated accurately is essential for their future use. The repeatability of biosensors was assessed using an independent test. Five separate sensors were employed to identify A549 cells at a concentration of 1.3×10^4 cells per mL. The electrochemical response data obtained from differential pulse voltammetry (DPV) are displayed in Fig. 6g. The relative standard deviation (RSD) was determined to be 1.42%, indicating excellent reproducibility of the sensor and its suitability for further applications. The synthesized MXene-based PB-MXene biosensor possessed a good LOD, and the outstanding LDRs of H_2O_2 and CTC analytes were 0.57 μM and 9 cells per mL, and 1–500 μM and 1.3×10^1–1.3×10^6 cells per mL, respectively. The results demonstrate the ability to detect A549 cells in the bloodstream of the mouse tumour model, hence confirming the practicality of the biosensor employed for sample detection.

Yuan *et al.*[161] created an MXene and graphene-based g-C_3N_4/Ti_3C_2 hybrid compound for ciprofloxacin (CFX) detection. Different characterization methods looked into the produced nanocomposite's good sensing efficiency. Furthermore, it was demonstrated *via* the analysis of PEC characteristics that using Ti_3C_2 in conjunction with visible light enhanced the efficiency of charged particle immigration and the dissociation of photoinduced electron–hole pairs, illustrating the synergistic activity to support the effectiveness of the photoelectric conversion process. Low intrinsic conductivity is a significant challenge for identifying systems based on g-PEC C_3N_4 since it interferes with electronic communication. Additionally, assessment of the photoelectrochemical (PEC) properties demonstrated that introducing Ti_3C_2 and visible light enhanced the effectiveness of the migration of electrons and the division of photogenerated electron–hole pairs. This synergistic effect contributes to the enhancement of photoelectric efficiency. Numerous methods, such as encapsulating MXene with different materials, have been invented to enhance its photoelectrochemical properties. MXene, in particular, has a remarkable ability to increase performance significantly. The detection limit (3S/N) for g-C_3N_4/Ti_3C_2 was 0.13 nM, and the current density was linearly connected to the concentration of CFX in the range of 0.4 to 1000 nM. The mechanism of the PEC at g-C_3N_4/Ti_3C_2 composite and *I*–*t* curve was selected to explain the stepwise process of the detection of CFX, choose the best sensing range, and measure the lower sensing limit as presented in Fig. 6h.

Additionally, the PEC sensor exhibited enduring stability, commendable repeatability, and selectivity. Ultimately, the identification of actual commercial samples was assessed to verify the feasibility of practical uses. Therefore, the g-C_3N_4/Ti_3C_2 photoelectrocatalyst offers a novel approach for detecting CFX with exceptional selectivity and sensitivity. DPV analysis was used to investigate the stability and reproducibility of the g-C_3N_4/Ti_3C_2 composite in NaH_2PO_4 solution containing 50 μM of CFX. Upon refrigeration at a temperature of 4 °C for seven days, the designed current response exhibited 91.7% retention of its initial activity, as depicted in Fig. 6i. This confirms the exceptional stability of the PEC sensor. In addition, when compared with a set of electrodes modified with g-C_3N_4/Ti_3C_2, the suggested sensor demonstrated an RSD of 1.8%, indicating a certain level of reproducibility.

Bolourinezhad *et al.*[150] synthesized the MXene-based $Ti_3C_2T_x$ and carbon platinum (Pt/C) EC biosensor probe to identify SARS-CoV-2. The traditional RT-PCR technique is used to determine SARS-CoV-2; it is time-consuming and requires high capital investment. However, the EC biosensing technique is cost-effective and time-saving, giving accurate results within the shortest period. The LOD and quantification of SARS-CoV-2 by the MXene-based biosensor were 0.4 aM and 60 copies per mL. The sensitivity and specificity of the sensor used to identify COVID-19 were also evaluated for 192 clinical specimen patients using the RT-PCR technique compared to other respiratory tract viral infections. The results showed 100% accuracy and sensitivity and 97.87% specificity. It was discovered that the biosensor could function in various serum, saliva, and nasopharynx matrices. A medical use requiring the precise, sensitive, and speedy diagnosis of COVID-19 may be feasible using the resulting biosensor.

7.2. Advanced biosensors

Several traditional biosensors are available on the market for the detection of toxic bacteria and to identify the availability of various harmful chemicals in water, food, and the human body to save the environment and human beings. The traditional biosensor has several disadvantages, including low response time, low limit of detection, and minimized reusability and stability. However, these disadvantages have been overcome by advanced biosensors developed from the advanced CNT and MXene nanomaterials. In this section, we compare the sensing limit, the linear detection range, and the sensitivity of the CNT- and MXene-based advanced biosensors. The performance of CNT- and MXene-based advanced biosensors is given in Table 4.

7.2.1. CNT-based advanced biosensors. Zamzami *et al.*[162] utilized a cost-effective and environmentally friendly physical deposition technique to deposit SWCNTs on the interface of

Table 4 The synthesis routes to CNT- and MXene-based biosensors and their sensing performances

Name of biosensor	Synthesis techniques	Sensing techniques	Characterization techniques	Biomarker	Response time (S)	Sensitivity (mA mM^{-1} cm^{-2})	Limit of sensing (μM)	Linear range (μM)	Ref.
CNT-FET	Simple deposition technique	—	XPS, SEM	SARS-CoV-2 spike protein	120–180	91.18%	4.12 fg mL^{-1}	0.1–5.0 pg mL^{-1}	162
LQC@CNTs	Simple coating technique	DPL	XRD, HRTEM, and XPS	OPs	50	—	1.054×10^{-13} M	10^{-12}–10^{-6} M	163
MWCNTs/paper	Vacuum filtration technique	Chemoresistive	FESEM, TEM, and XRD	Cholesterol	30	96.8	0.0032	0.001–75	164
CNT/MoS_2	Simple deposition technique	—	SEM, XRD, and XPS	Prostate cancer	17	—	10^{-13} μg μL^{-1}	10^{-13} to 10^{-4} μg μL^{-1}.	165
HRP/SWCNT	Simple mixing technique	Amperometric and wireless modes	SEM	H_2O_2	120	184	0.3	—	166
MXene-$Ti_3C_2T_x$/Pt@Au/GCE	Drop coating technique	DPV	SEM, TEM, and EDS	H_2O_2	—	4.54	0.00085	0.5–1200	167
Ti_3C_2-PLL-GO_x	—	CV	TEM, SEM, EDS, FTIR, XRD and AFM	Glucose	—	—	2.6 μM	0.02–1.1	168
Chit/ChO_x/$Ti_3C_2T_x$ nanocomposite	Continuous self-assembly process	CV	SEM, XRD	Cholesterol	35	132.66	0.11 nM	0.3–4.5 nM	169
Nb_2C/AChE	Simple mixing	AM	TEM, SEM, HRTEM, SAED and DLS	Phosmet	60	80.35	0.046 ng mL^{-1}	200×10^{-12}–1×10^{-6} M	170
Lac/Au/MXene/GCE	Mixing and coating method	AM	XRD, SEM, and EDX	Catechol	—	0.05 mA μM^{-1}	0.05 mM	0.05–0.15 mM	171

Oxygen evolution reaction (OER), 1-pyrene butanoic acid succinimidyl ester (PBASE), organophosphorus pesticides (OPs).

the SiO_2 substrate to synthesize the carbon nanotube field-effect transistor (CNT-FET)-based biosensor for the identification of SARS-CoV-2 S1. The biosensor was created *via* CNT printing, and anti-SARS-CoV-2 S1 was immobilized on a Si/SiO_2 interface. Employing the linker PBASE and a non-covalent interaction, the SARS-CoV-2 S1 antigen was immobilized on the CNT interface between the S and D channel region. Using an authorized SARS-CoV-2 S1 antibody, the power supply of the CNT-FET biosensor was examined. The newly created CNT-FET immunosensor can identify the SARS-CoV-2 S1 antigen by observing alterations in the source–drain current (I_{DS}). The interaction between the antigen and the binding site is demonstrated by a modification in the electrical signal, as depicted in Fig. 7a. A strong relationship exists between I_{DS} and the source gate voltage (V_{GS}) for the bare carbon nanotube field-effect transistor surface. The graph explicitly presents the data obtained at a constant voltage of −1.5 V. The data show a significant rise in I_{DS} when the gate voltage changes from positive to negative, indicating that the device displays typical features of a p-type field-effect transistor. Including a linker molecule (PBASE) was essential for establishing a connection between the antibody and the CNT surface. The electrical behaviour of the CNT-FET biosensor was altered after treatment with 2 mM PBASE, providing evidence of the effective alteration of the CNT surface. The reaction time, detection limit, and range of the CNT-FET biosensor have been examined by gradually raising the amounts of the SARS-CoV-2 S1 antigen. Once the source–drain current was stabilized using a buffer solution, higher levels of antigens were introduced at intervals of 50 s, and the immediate reaction was documented. Fig. 7b demonstrates that each concentration resulted in a unique spike and saturation in the I_{DS} signal. As shown in Fig. 7c, a calibration curve was developed to examine the relationship between the concentration of SARS-CoV-2 S1 antigen and the normalized sensor response ($\Delta I/I_o$). According to the results, the CNT-FET biosensor can detect antigen concentrations between 0.1 and 5000 fg mL^{-1}. After reaching a concentration of 100 fg mL^{-1}, the sensing response starts to become saturated, and there are only slight increases in I_{DS} after this point. Based on the sensor's dose-dependent response, the LOD was calculated within the linear region of the curve. As shown in Fig. 7d, a calibration curve was developed to examine the relationship between the concentration of SARS-CoV-2 S1 antigen and the normalized sensor response. According to the findings, the CNT-FET biosensor can detect antigen concentrations between 0.1 and 5000 fg mL^{-1}. After reaching a concentration of 100 fg mL^{-1}, the sensing response starts to become saturated, and there are only slight increases in I_{DS} after this point. Based on the sensor's dose-dependent response, the LOD was calculated within the linear region of the curve. As shown in Fig. 7e, the attached anti-SARS-CoV-2 S1 antibodies could identify the target antigen with high specificity. Still, it was unable to identify non-specific antigens. Unlike non-specific antigens, the SARS-CoV-2 S1 antigen's attachment to its specific antibody resulted in a substantially more significant alteration to the I_{DS} signal. Higher electron

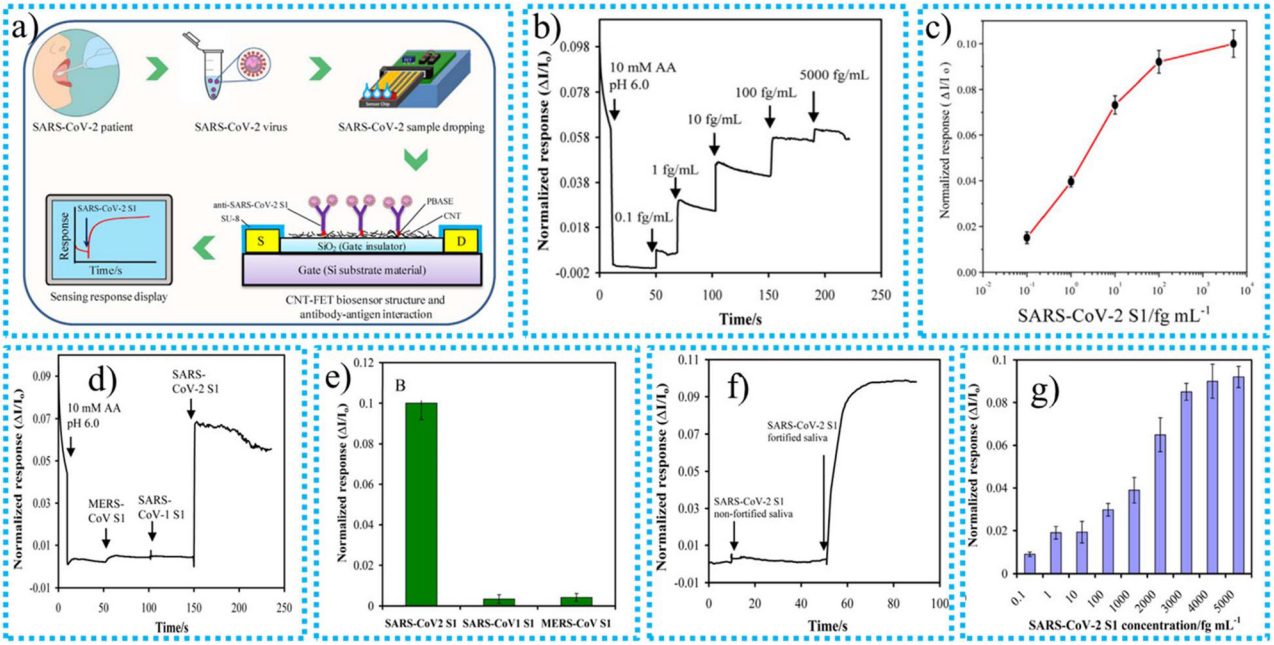

Fig. 7 (a) A modification to the electrical signal demonstrates the interaction between the antigen and the binding site, (b) real-time sensor response characteristics after the addition of increasing concentrations of target material, (c) calibration curve after normalizing the biosensor response *versus* applied concentration of target SARS-CoV-2 S1 antigen, (d) real-time biosensor response for a selectivity test with the target sensing material, (e) normalized real-time biosensor response of target SARS-CoV-2 S1 and non-target SARS-CoV-2 S1 and MERS-CoV S1 antigens, (f) normalized real-time biosensor response *vs.* time properties after the addition of SARS-CoV-2 S1 non-fortified and fortified saliva, (g) normalized real-time biosensor response *vs.* SARS-CoV-2 S1 antigen.[162]

transport properties were seen on the surface of the carbon nanotube when unique antigen–antibody pairs were present. On the other hand, the normalized biosensor reaction was lowered by 8 to 9.5% when non-specific pairs were present. The fact that the biosensor has such a high sensitivity for the target antigen is demonstrated by this. The real-time bio response of the developed biosensor *vs.* time and concentration of the sample is presented in Fig. 7f and g. These findings show that the synthesized sensor possesses an effective real-time response. The synthesized CNT-based biosensor possessed LOD and LDR values of up to 4.12 fg mL^{-1} and 0.1 fg mL^{-1} to 5.0 pg mL^{-1} within the response time of 120–180 s. After five working cycles, the CNT-FET biosensor's reusability demonstrated less than a 10% drop in sensor performance; the system's renewal phase performed admirably. The synthesized CNT-FET biosensor possesses a significant sensitivity of up to 91.18%. Reusability of the biosensor is determined by the CNT-FET produced materials. The CNT-FET biosensor was electrically characterized after each procedure under dry conditions at room temperature. Before the treatment, following CNT surface alteration by PBASE and after antibody immobilization, the semiconductor characteristics of the biosensor were characterized. There was no gate current leakage found.

Li *et al.*[163] utilized a simple coating technique to deposit $Al_{42}Cu_{40}Fe_{16}$ on the interface of MWCNT–COOH to synthesize the CNT-based biosensor for identifying organophosphorus pesticides (OPs). The expansion of agriculture has led to the extensive use of OP compounds as potent pesticides. However, when pesticides are used more frequently, their negative impacts on humanity and the environment are more readily apparent. Pesticide misuse results in trace buildup in the natural world and causes irreparable harm to the soil and water sources. Organophosphorus pesticides have the potential to kill people when consumed in high enough doses.[5] Therefore, developing an accurate and sensitive method for detecting pesticides containing organophosphorus is essential. The LOD and LDR values of the synthesized CNT-based biosensor for sensing OPs were 1.054×10^{-13} M and 10^{-12} M to 10^{-6} M. Due to the composite material's interactions, the OP sensing biosensor exhibits outstanding electrochemical properties and long-term stability for the measurement of acephatemet. According to the DPV experiment, adding LQC@CNT nanocomposite to the electrode interface improved the AChE biosensor's efficiency. The quantities of modified material have an immediate effect on the created system's conductivity. With a specific number of components present, the response current grew with volume and peaked at 5 L. The current sensitivity is reduced as the material volume increases beyond 5 L. These events might result from materials being coated too thickly, preventing electron transfer. Therefore, the bare electrode was modified using 5 L of LQC@CNTs. When combined with the porous QC surface, the significant surface area of the MWCNT–COOH coating produces a sensor with increased catalytic activity. This is because the high surface area enables more active sites to be utilized for catalytic processes. Because of the conductive nature of MWCNTs, the elec-

trical conductivity of the sensor is enhanced, and the biocompatibility of the sensor is preserved, which provides it with the capability to be utilized in biological applications.

Veeralingam *et al.*[164] utilized the vacuum filtration approach to deposit MWCNTs on the outermost interface of the paper substrate to synthesize CNT-based biosensors for effectively sensing cholesterol. A constant vacuum pressure of 50 kPa was maintained during the filtration procedure. The MWCNT solution was applied to the paper substrate using a 500 μL pipette. The limited price of paper substrates has impeded the efficiency of paper-based sensors due to a lack of suitable device fabrication procedures. They are tackling this problem in this work. Both the immunological and neurological systems of humans contain cholesterol. The release of bile juice and steroid hormones, including estrogen, progesterone, and androgens, depends on it as a crucial metabolic component. After regularly consuming saturated fats, human body cells gradually become unable to clear excess cholesterol. Therefore, cholesterol builds up in the artery walls, leading to serious conditions such as cerebral venous thrombosis and sudden myocardial infarction. A healthy human's saliva typically contains 5–46 μM of cholesterol, whereas the normal cholesterol range in blood samples is 1–5.2 mM. Therefore, there is an increasing need for quick, accurate, and user-friendly analytical tools to find cholesterol in biological fluids. The characterization techniques show that the MWCNTs are smooth and uniform on the surface of the paper substrate with a diameter of 15–20 nm. When the synthesized CNT-based biosensor is applied for cholesterol sensing, it shows impressive results. It shows an excellent LOD and LDR up to 3.2 nM and 0.0010–75 μM, respectively. Poor recycling is the main issue with paper-based sensors. The wax line thickness and heater temperature are essential for the paper-based sensors' recycling capability. The deposition process for wax and MWCNTs on the surface of the paper substrate for the synthesis of the MWCNT/paper-based biosensor is shown in Fig. 8. The manufactured biosensor exhibited remarkable reproducibility and stability and excellent sensitivity for identifying cholesterol, with just a small amount of interference from other chemicals. Its efficacy can be attributed to manipulating electrical characteristics through the electrostatic gating effect and direct electron transfer between MWCNTs and cholesterol, which is made possible by the bioconjugation of cholesterol oxidase (ChO_x). The issues that are linked to the use of hard substrates and procedures that are based on liquid electrolytes are eradicated with this approach. The fact that the sensor was able to measure cholesterol levels in saliva accurately is more evidence that it has the potential to be a paper-based biosensor that is inexpensive, interference-free, and disposable for use in point-of-care diagnostic assessments. Recently, Wei *et al.*[165] synthesized the CNT-based CNTs/MoS_2 biosensor for sensing serum prostate-specific antigen (PSA) by the mixed acid oxidation technique. One of the malignancies with the greatest prevalence in males is prostate cancer (PCa), which also happens to be the cancer that kills the most people worldwide. For mortality to be reduced, early diagnosis is crucial. Prostate cancer is frequently diagnosed *via* rectal examination, tissue biopsy, and PSA testing. PSA is a popular indicator for the identification of PCa. The biosensor built with synthetic CNTs demonstrates that the PSA LOD is 10–13 g L^{-1}, and the LDR ranges from 10^{-13} to 10^{-4} g L^{-1}. Additionally, the device displayed improved stability and a quick response. In recognizing both β-actin and PSA, the synthesized CNTs/MoS_2 field-effect transistor with a heterogeneous structure outperformed the conventional MoS_2 FET. This enhancement is likely attributed to the fact that the floating MoS_2 nanofilm has been physically separated from the SiO_2 dielectric layer, decreasing the impact of scattering and improving performance. Likewise, the hanging nanofilm demonstrates a larger surface area for biological analytes, offering greater opportunities for antibody binding and leading to a greater response from the sensor. Amino-functionalized CNTs on MoS_2 also provide more sites for immobilizing proteins, enhancing the accumulation of charge carriers in the MoS_2 channel and further enhancing the detection rate of the biosensor. The synthesized CNT-based advanced biosensors possessed an excellent low limit for detecting harmful biomarkers that were poisonous to humans and might be in the human body, water, or food. The advanced biosensor has tremendous advantages over traditional techniques because of excellent LOD and stability.

7.2.2. MXene-based advanced biosensors. The performance of traditional biosensors is limited. It can be improved by synthesizing advanced biosensors based on MXene. MXene's outstanding characteristics are valuable for selecting MXene to synthesize MXene-based biosensors. The MXene surface can quickly transfer electrons between enzymes, the anode, and the cathode. This property of MXene makes it an ideal candidate for advanced biosensors. In this section, the reviewer discusses the performance of MXene-based biosensors.

Wang *et al.*[167] utilized the drop coating technique to synthesize the MXene-$Ti_3C_2T_x$Au@Pt biosensor for effectively sensing inosine monophosphate (IMP) from meat flavoring. IMP was regarded as a crucial element of meat flavoring and a crucial marker for assessing the overall quality of meat-based goods. Numerous animal meat items have had their quality evaluated by measuring the amount of IMP in muscle tissue. It is widely acknowledged as a vital sign for identifying the umami flavor of meat. So, for the analysis of the quality of meat, it is necessary to develop a cost-effective and short response time biosensor for the determination of IMP quantities to identify the quality of meat. The synthesized MXene-based biosensor possessed LOD and LRD values up to 0.00085 μM and 0.5–1200 μM, respectively. Advantages of this MXene based biosensor are rapid IMP detection, high sensitivity, and posess wide range. A detector with potential for future uses was constructed for the technique presented in this study, which might be used to evaluate the quality of meat.

Wu *et al.*[168] created the Ti_3C_2-PLL-GO_x enzymatic catalyst to separate the hazardous intermediate H_2O_2 produced during the oxidation of glucose; the method for making the MXene-

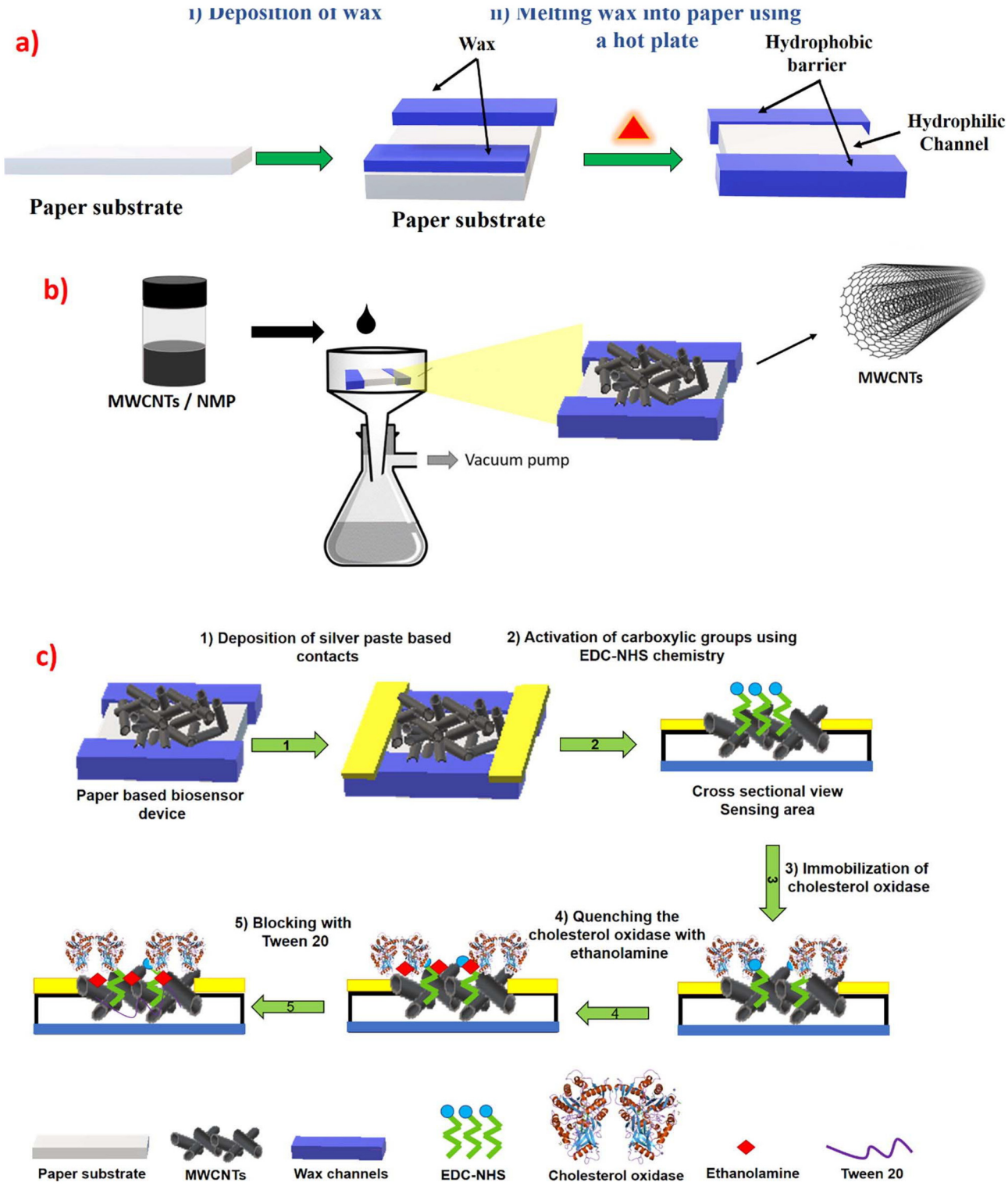

Fig. 8 (a) Hydrophobic and hydrophilic pathways formed by the implantation of wax in the paper substrate. (b) MWCNTs are deposited on paper using a vacuum filtration process. (c) The covalent immobilization of ChO_x over the made-from-paper chemoresistive biosensor is demonstrated step by step.[164]

based biosensor and the mechanism for the degradation of the intended pollutants are shown in Fig. 9. The Ti_3C_2 MXene-based biosensor with a glucose detection limit of 2.6 M was created using the Ti_3C_2-PLL-GO_x biosensor and then painted on the outer half of the outermost layer of the glassy carbon electrode. The Ti_3C_2/GO_x/PLL biosensor with excellent catalytic

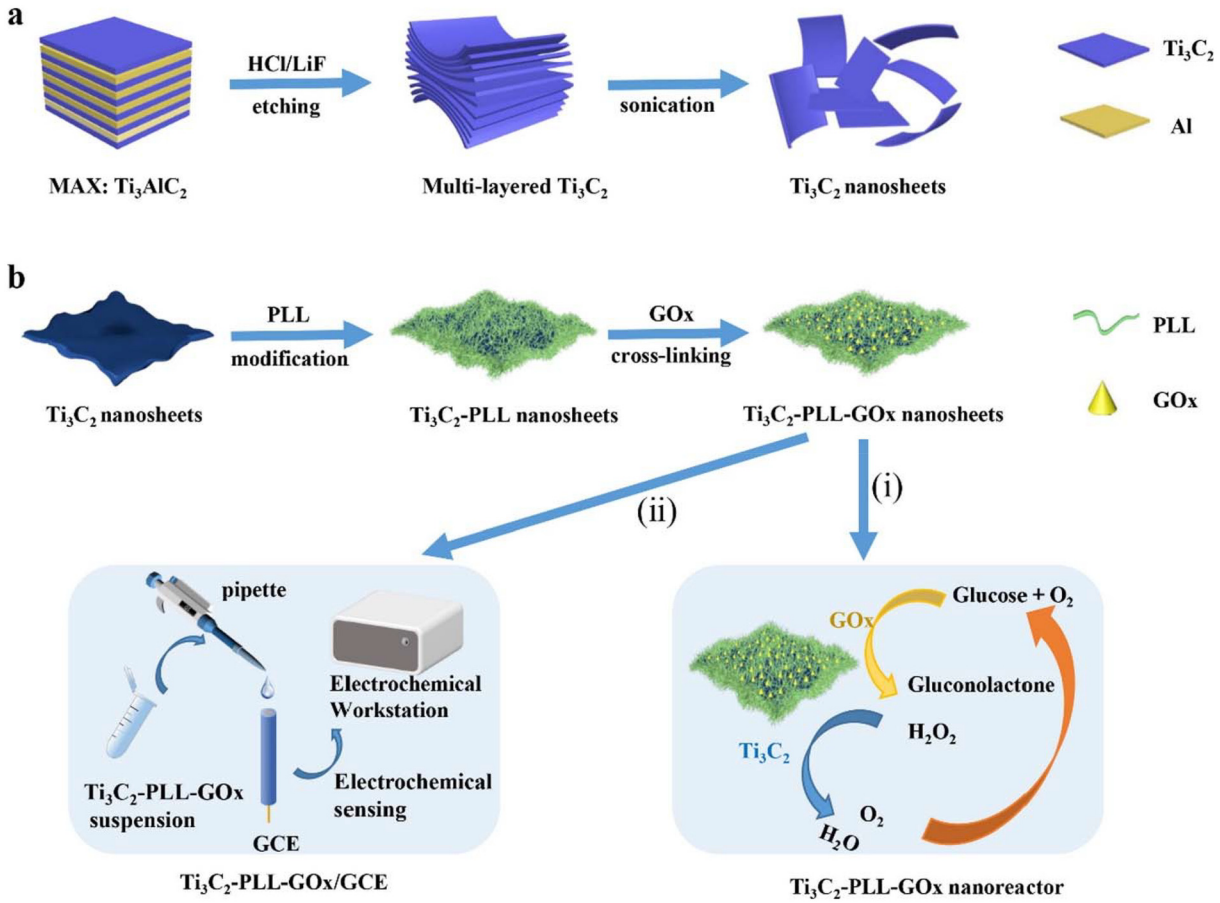

Fig. 9 The synthesis procedure and glucose detection mechanism of the Ti_3C_2-PLL-GO_x bio-sensor, (a) synthesizing process and (b) detection mechanism.[168]

activity was impregnated on the glassy carbon electrodes to construct the newly created glucose biosensor with an LOD of 2.6 μM. The hazardous intermediate product H_2O_2, made during the enzymatic oxidation of glucose, typically restricts the GO_x function in functional applications of biological glucose detection. Ti_3C_2 MXene, which is well-known for its exceptional electrical conductivity, serves as the electrode material for the Ti_3C_2-PLL-GO_x-based biosensor, which makes use of an electrochemical detection mechanism that is exceptionally effective. It is possible to functionalize the surface of Ti_2C_2 by using PLL, which not only improves the biological suitability of the material but also provides a solid foundation for the immobilization of GO_x. When glucose is available, GO_x can catalyze its oxidation, which results in the production of H_2O_2. The Ti_2C_2 electrode then proceeds to identify H_2O_2 through an electrochemical reaction, which generates a current related to glucose concentration. Because of the excellent electrical conductivity of Ti_2C_2, the reliable enzyme immobilization afforded by PLL, and the particular enzymatic activity of GO_x, this arrangement can achieve glucose detection that is both sensitive and selective. This investigation not only enhances the technology of GO_x but also presents a broad and practical approach for preparing and stabilizing different enzymes loaded onto MXenes with a high enzyme concentration and uniform enzyme distribution. This opens up potential applications in electrochemical devices, biosensing, and biofuel cells.

Xia *et al.*[169] reported that the MXene-based Chit/ChO_x/$Ti_3C_2T_x$/GCE biosensor was synthesized using a cost-effective and environment-friendly one-step dip-coating approach for cholesterol sensing. Cholesterol is hazardous for human beings because it is the cause of serious diseases. In large quantities, it is present in lipids and fats. When it comes to the oxidation of cholesterol, adding $Fe(CN)_6$ facilitates the transfer of electrons from the specimen to the modified electrode. Under ideal conditions, the biosensor's differential pulse voltage response revealed a good correlation with the amount of cholesterol ranging from 0.3 to 4.5 nM, with a low limit of detection of 0.11 nM and a high sensitivity of 132.66 A nM^{-1} cm^{-2}. Furthermore, the biosensor has been used to detect cholesterol in natural materials with reasonable specificity and strength, and the outcomes show that the biosensor has a remarkable degree of practical applicability. The Chit/ChO_x/$Ti_3C_2T_x$/GCE electrode-based biosensor uses an electrochemical identification technique in addition to enzymatic oxidation to identify cholesterol. The oxidation of cholesterol is

catalyzed by ChO_x, which results in the byproduct H_2O_2. A detectable current results from the electrochemical oxidation of this H_2O_2 at the GCE's exterior, facilitated by the highly conductive $Ti_3C_2T_x$ nanomaterial. The chit matrix stabilizes the enzyme that acts on the electrode. Sensitive identification is made possible by the resulting current being proportional to the cholesterol levels. The Chit/ChO_x/$Ti_3C_2T_x$/GCE-based biosensor demonstrated outstanding stability, maintaining 98.2% of its initial positive current response.

Furthermore, the repeatability of the biosensor was verified by measuring cholesterol at a concentration of 3 nM using five different sensors from different manufacturers. The results demonstrated that the relative standard deviation among the sensors was equal to or lower than 4.5%, which indicated a good reproducibility level. Fig. 10 illustrates the method for producing Chit/ChO_x/$Ti_3C_2T_x$/GCE and the detection of cholesterol using the created nanocomposite.

Chandran *et al.*[171] synthesized the Lac/Au/MXene/GCE biosensor to identify catechol using a mixing and coating method. Numerous phenolic substances, such as genistein and catechol, are often utilized in factories and are persistent organic contaminants in the environment. Therefore, catechol must be in the wastewater when it is discharged. The characterization techniques include XRD, SEM, and EDX to evaluate the internal structure and sensing performance of MXene-based nanomaterials. The synthesized biosensor has an excellent LOD, LRD, and sensitivity of 0.05 mM, 0.05–0.15 mM, and 0.05 mA μM^{-1}, respectively.

Additionally, it demonstrated outstanding reliability, reproducibility, and robustness. To reduce environmental contamination, the MXene-based biosensor is an excellent tool for identifying catechols in industrial wastewater and bodies of water. The synthesis route for any material has a viable impact on the characteristics of the synthesized nanomaterial. Every synthesis route yields nanomaterials with unique characteristics and structures. The traditional or extensively used method to synthesize MXene is the HF-etching process. The most significant drawbacks of this technique are that it generates low-quality MXene and pollutes the environment by releasing a large quantity of HF into the atmosphere, which is dangerous to human beings. For example, because of the excess consumption of HF acid, the F functionality on the uppermost layer of MXenes is susceptible to releasing HF during hydrolysis operations. The harmful effects of HF would significantly lower the production rate of enzyme synthesis. Their vulnerability to oxidation at ambient temperature or during the OER process significantly impairs the reliability and effectiveness of HF-etched MXenes in the biological sensing process. The HF-etching process limits the biomedical applications of MXene. Therefore, stable, biodegradable MXene nanocomposites require production processes that are reliable, strong, and fluorine-free.

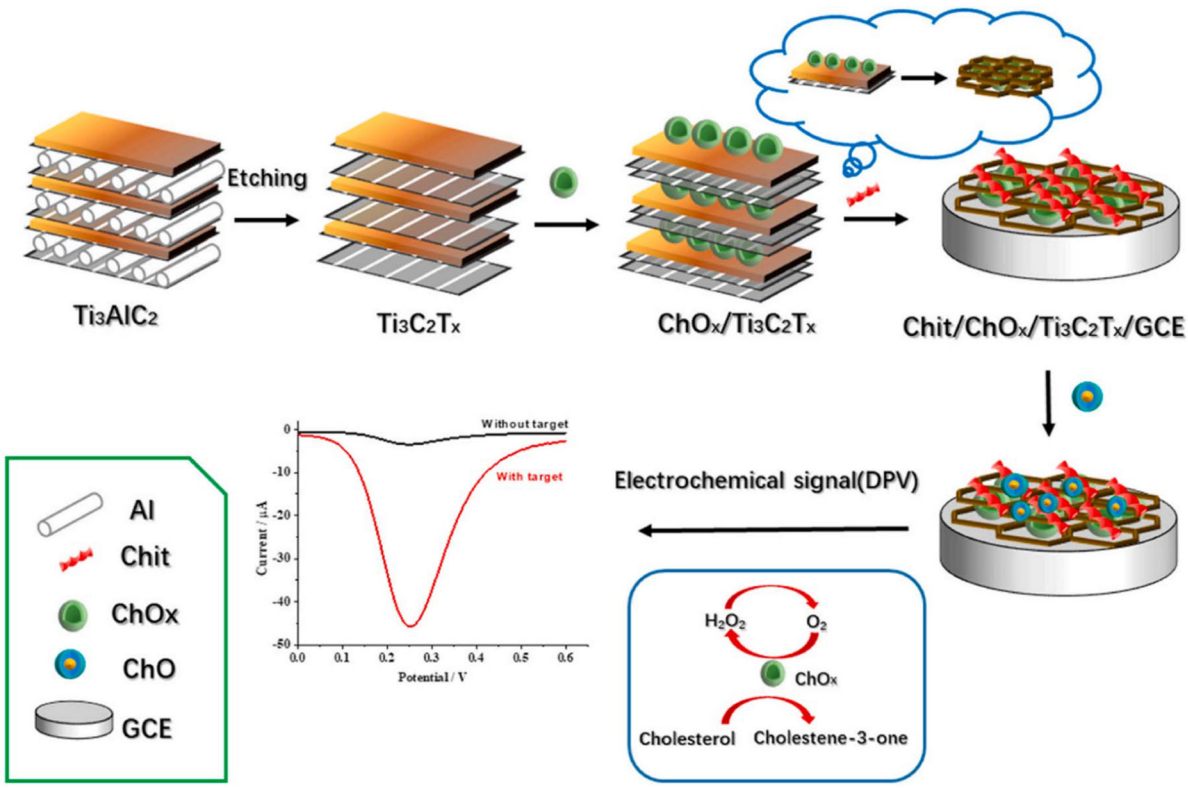

Fig. 10 The production method for Chit/ChO_x/$Ti_3C_2T_x$/GCE and the detection of cholesterol using the created biosensor.[169]

Song *et al.*[172] utilized the cost-effective E-etching approach to synthesize niobium carbide (Nb_2CT_x) MXene to address this issue. The synthesis process for Nb_2CT_x MXene through the E-etching approach and the influence of the inhibition of enzymes on the ability of a biosensor based on Nb_2CT_x/AChE to identify phosmet is given in Fig. 11. This method extensively improves the electrical and thermal conductivity, biosensing capacity, and biological compatibility of the MXene compared to HF etching. The synthesized MXene possessed an excellent LOD for phosmet sensing of up to 0.046 ng mL^{-1}. The manufactured MXene-based biosensor outperforms its HF-etched counterpart, showing that fluoride-free MXene can improve the biosensor's enzyme function and the transmission of electrons. The results demonstrate the potential of HF-free MXene for creating biosensors with outstanding efficiency, including ultrahigh sensitivity selectivity. HF-free MXene is anticipated to have tremendous potential for expansion into many other biological disciplines as a stable and biologically compatible nanoplatform. The Nb_2CT_x/AChE-based biosensor measures the effects of a pesticide called phosmet on the enzyme AChE. AChE usually breaks down acetylthiocholine into a different molecule that can be sensed as an electrical signal. Phosmet decreases the electrical signal because it prevents AChE from functioning correctly when it is present. The signal gets weaker the more phosmet there is in the environment. A unique substance in the sensor, Nb_2CT_x, helps to intensify this signal, which facilitates the detection of even minute levels of phosmet. The evaluation of a biosensor's sensitivity and accuracy in detecting phosmet on fruits, such as apples; the biosensor's selectivity was shown by testing it with various interfering substances, none of which had an impact on the activity of the enzyme. The sensor demonstrated dependable and precise identification when phosmet was applied to apple specimens, showing recovery rates of 98.05%, 105.57%, and 107.77% at various phosmet doses. These outcomes show how well the biosensor works to identify low concentrations of phosmet in actual samples, demonstrating both its efficacy and repeatability. The Nb_2CT_x nanoplatforms that have been E-etched exhibit markedly greater sensitivity than the ones that have been HF-etched. The heightened sensitivity is a result of the release of HF by HF-etched Nb_2CT_x, which hampers the action of AChE, resulting in diminished electroactivity of choline and impaired electron transfer.

On the other hand, E-etched Nb_2CT_x overcomes this problem, leading to improved efficiency. This enhances the efficiency of the E-etched Nb_2CT_x-based biosensor for real-time and on-site detection. The E-etched variant of Nb_2CT_x exhibits significant enhancements in enzyme activity and electron transfer compared to its conventional HF-etched counterpart. Consequently, the resulting biosensor has exceptional sensitivity, selectivity, and resistance to interference. Additionally, it demonstrates outstanding recovery rates in natural specimens and possesses a meagre limit of quantification up to 0.046 ng mL^{-1}. This research is noteworthy for its utilization of an MXene that does not contain fluoride for biosensing; this gives the chance to open up avenues for further biomedical applications such as photothermal therapy and photoacoustic imaging.

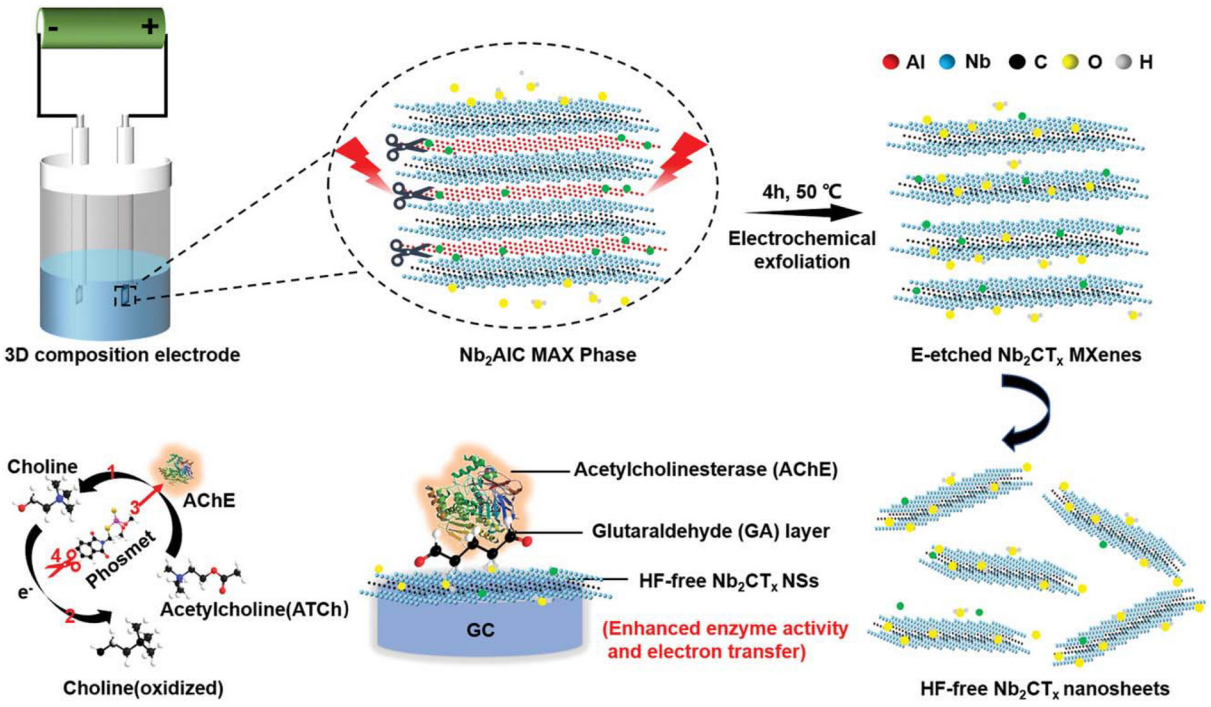

Fig. 11 The synthesis process for Nb_2CT_x MXene through an E-etching approach and the influence of the inhibition of enzymes on the ability of a biosensor based on Nb_2CT_x/AChE to identify phosmet.[172]

7.3. CNT- and MXene-based immunosensors and aptasensors

Immunosensors and aptasensors are special classes of biosensors. Various biosensing applications have substantially used electrochemical immunosensors (ECIs) in the last ten years. The use of enzyme-free systems with immunosensors and aptasensors in recent biosensor advances has attracted much interest. In the past several decades, there has been a lot of interest in developing immunosensors and aptasensors, which has resulted in the creation of reliable and responsive sensing systems for identifying biomarkers before the start of a disease. In this section, we discuss the CNT- and MXene-based immunosensors and aptasensors for detecting antibodies or toxic chemicals in the human body. Immunosensors use antibodies to detect a chosen target in a specimen of mixtures. Humans are significantly affected by several unanticipated protein-based disorders. Conventional methods do not sense such illnesses. For such diseases, scientists must create efficient sensors capable of identifying illnesses at the protein level. Numerous methods and techniques have been developed, such as the enzyme-linked immunosorbent assay (ELISA), photoelectrochemical immunoassay, and capacitance immunoassay.[173] To identify and detect numerous specific diseases, including cancer, pathogens, proteins, peptides, bacteria, viruses, and live cells, as well as to track numerous additional environmental contaminants, several RNA and DNA electrochemical aptasensors have been created. The performance and synthesis routes to CNT- and MXene-based immunosensors and aptasensors are discussed in Table 5.

7.3.1. CNT-based immunosensors and aptasensors. Kumar *et al.*[174] utilized the chemical reduction technique to synthesize the CNT-based CS-CNT-Pd nanocomposite for effectively sensing zearalenone (ZEN). The synthesis procedure for the CNT-based CSCNT-Pd-based immunosensor is shown in Fig. 12a. Among countless mycotoxins, ZEN is the most prevalent pollutant in cattle food and feed supplies. Secondary metabolites can be harmful to both animals and people. Because most human food is made from crops, including corn, maize, wheat, and milk, many nations have established optimum regulatory limits (ORLs) for ZEN in crops and food products. ZEN pollution exposes living things to several grave threats; as a result, it must be regulated and its damaging effects worldwide prevented. The synthesized immunosensor gives excellent results compared to traditional sensing techniques.

The surface of a CNT-based nanocomposite is also functionalized with –COOH functional groups. Functionalization speeds up the oxidation process of the CNT nanocomposite. This causes flaws to form, allowing for an increase in the amount of metal nanoparticles loaded with a finer dispersion. The finer dispersion resulting from this functionalization procedure encourages the dispersion of CNTs in catalytic ink. The pores and metallic particles in the CS-CNT-Pd composite were utilized as a sensor platform to immobilize antibodies. This enabled the nanocomposite to provide active sites, enhancing the catalytic activity and electron transfer mechanisms. Changes in peak electrical currents and peak-to-peak separation values were observed at each stage of the fabrication process, as shown in Fig. 12b. These changes indicated that the electron transfer rate was subject to alterations as the screen-printed carbon electrodes (SPCEs) underwent more and more modifications. It was discovered that a concentration of 2.0 mg mL^{-1} of the nanocomposite resulted in the best results for drop-casting. The time the antigen was allowed to incubate was the most significant aspect that influenced the sensor's performance. Following a series of tests that lasted anywhere from 15 min to 16 h, the best incubation duration was determined to be 3 h, as shown in Fig. 12c. This was because the sensor response became stable at that point. Additionally, the antibody concentration (ZEN-MAb) was an important thing to consider. After conducting tests with concentrations ranging from 1/250 to 1/3000, it was discovered that the sensor response reached a plateau at a concentration of 1/2500, which resulted in this concentration being the most suitable for subsequent investigations. The investigation shows that the immunosensor's response stabilizes when the amount of antibody approaches 1/2500. So, for the following experiments, 1/2500 was the best antibody amount, as shown in Fig. 12d. The immunosensor's resistance (R_{ct}) values rose in direct proportion to the ZEN concentration. A calibration curve was constructed by plotting these values against the amount of ZEN. The regression coefficient was 0.98, indicating a very accurate linear relationship between 0.25 and 4.0 ng mL^{-1} ZEN. It was established that the sensor had a 0.25 ng mL^{-1} LOD, as shown in Fig. 12e.

The immunosensor's response, as determined by EIS, remained relatively constant when subjected to non-specific analytes, as illustrated in Fig. 12f. The histogram of the responses revealed that the variation in the electrochemical impedance spectroscopy response (Δ_{ratio}) for the non-specific analytes was below 10% compared to the response found for ZEN. This slight modification affirms that the immunosensor exhibits a high level of selectivity and is predominantly sensitive to ZEN while experiencing minimal disruption from other chemicals. The replicability of the designed immunosensor to identify ZEN was then tested. The experiment involved applying three groups of ten separate electrodes to test ZEN at three distinct concentrations: 0.5 ng mL^{-1}, 4 ng mL^{-1}, and 16 ng mL^{-1}, as shown in Fig. 12g. The test settings were kept the same for all three concentrations. The results demonstrated that the sensor reactions in four separate trials were uniform, with minimal fluctuation, as seen by a standard deviation of 2.1%. The sensors were held at a temperature of 4 °C for 20 days, after which they were tested to assess their ability to detect a concentration of 2 ng mL^{-1} of ZEN, as shown in Fig. 12h. The results indicated that the sensors exhibited consistent reactions, with just a marginal rise in impedance. This shows that the immunosensors exhibit robust long-term stability, augmenting their viability for practical applications in real-world environments. The CNT-based ECIs possessed outstanding LRD and LOD values of 0.25 to 16 ng mL^{-1} and 0.25

Table 5 The performance and synthesis routes to CNT- and MXene-based immunosensors and aptasensors

Names of biosensor immunosensors & aptasensor	Synthesis techniques	Sensing techniques	Characterization techniques	Biomarker	Limit of sensing (μM)	Linear range (μM)	Remarks	Ref.
CS-CNT-Pd immunosensors	Chemical reduction technique	Impedimetric method	TEM, EDX, and XRD	ZEN	0.25 ng mL^{-1}	0.05–16 ng mL^{-1}	Introducing –COOH functional groups on the interface of synthesized CNT-based immunosensors may generate flaws on the biosensor's surface. Still, the main objective of functionalization is to enhance their stability and sensing performance	174
AuNPs/ERGO@CNT immunosensors	One-step electrochemical co-reduction method	EIS	SEM and EDS	P-gp protein	0.13 ng mL^{-1}	0.01–500 ng mL^{-1}	This quick identification method aids in a clinical study on serum P-gp and resistance to drug development in different illnesses. It provides a scientific foundation for POC diagnosis technology and personalized medicine	175
CNT-FET immunosensors	Thermal evaporation	FET	AFM, RS, XPS, FE-SEM, SEM	Antibody	0.06 μg mL^{-1}	0.01–1000 μg mL^{-1}	According to the results, the antibody response efficiency of the suggested immunosensor was satisfactory, depending on the storage time and stability of the CNT-FET immunosensor. Consequently, the CNT-FET immunosensor nanomaterials exhibited outstanding reliability, remaining intact after exposure to ambient conditions for up to 120 days	176
In_2S_3/MoS_2@Fe-CNT aptasensor	Hydrothermal technique	EIS	SEM, TEMHR, EDX, XRD, RS, XPS,	*S. aureus*	2 CFU per mL	10–1 × 10^7 CFU per mL	The designed PFC-driven self-sustaining aptasensor showed superior selectivity, outstanding repeatability, solid stability, acceptable recycling, and tremendous practicality potential for *S. aureus* detection	177
CNTs/PVA/CP	Facile solvothermal method	DPV	XRD, TEM, FT-IR, and SEM	Cortisol	0.032 ng mL^{-1}	0.1–100 ng mL^{-1}	Cortisol, a hormone generated by the adrenal cortex in response to stress, is an indicator of stress and is essential for many physiological functions, including regulating blood pressure and blood sugar levels, metabolism in many organs, and other functions of the body	178
Ag@Ti_3C_2 immunosensor	One-pot direct reduction technique	DPV	SEM, HRTEM, FTIR and SEM	NSE	0.05 pg mL^{-1}	0.0001–1500 ng mL^{-1}	The physical appearance of the synthesized MXene-based nanocomposite was dark gold because of the reduction of AgNPs at the interface of MXene nanosheets. A viable framework for quantitative NSE identification, the proposed immunosensor demonstrates exceptional biosensing properties	179
AuNPs/ MXene@PAMAM immunosensor	Simple stirring technique	DPV	TEM, HRTEM and TEM-EDS	cTnT	0.069 ng mL^{-1}	0.1–1000 ng mL^{-1}	The developed MXene-based immunosensor's excellent structural and functional advantages influenced such ideal results	2

Table 5 *(Contd.)*

Names of biosensor immunosensors & aptasensor	Synthesis techniques	Sensing techniques	Characterization techniques	Biomarker	Limit of sensing (μM)	Linear range (μM)	Remarks	Ref.
e ZnO-MX/Ag_2S immunosensors	Sonochemical technique	EIS	SEM, SAED and TEM	Ancient silk	1.51 pg mL^{-1}	0.005–50 ng mL^{-1}	The immunosensor demonstrated remarkable specificity, stability, and reproducibility, especially for quantitatively identifying archaeological artefacts. Particularly promising photoactive nanomaterials for vis/NIR PEC immunosensors include ZnO-MX/Ag_2S nanocomposites	180
L-Cys/AuNPs/MXene immunosensor	Simple coating technique	CV	SEM, EDX, and TEM	Cortisol	0.54 ng mL^{-1}	5–180 ng mL^{-1}	This immunosensor offers great repeatability and stability during 6 weeks or longer of storage. In conclusion, this technique provides satisfactory results for successfully detecting cortisol in synthetic sweat	181
Aptamer-CGQDs/FL-V_2CT_x aptasensor	Simple mixing techniques	DPV	FTIR, TEM, EDS, and XPS	PSA	0.03 ng mL^{-1}	0.1 to 20 ng mL^{-1}	According to the findings, the aptasensor can accurately measure PSA in the serum of men with prostate cancer. It might be used to identify clinical human serum specimens	182
Ti_3C_2-AgBrNC nanocomposites	The simple wet chemical technique	EIS	FTIR, XPS, and TEM	Enrofloxacin	5.97×10^{-13} mol L^{-1}	1.0×10^{-12} to 1.0×10^{-6} mol L^{-1}	This investigation indicated that the pristine MXene had a lower sensing capacity than the MXene-based composite	183

EIS: electrochemical impedance spectroscopy, RS: Raman spectra, XPS: X-ray photoelectron spectroscopy.

ng mL^{-1}, respectively. With practical applications and good results in recovery obtained, the newly developed biocompatible CSCNT-Pd-based immunosensor has much potential for use in the food sector. An experiment was conducted to assess the efficacy of the immunosensor in detecting ZEN in actual maize samples. The corn samples were artificially contaminated with ZEN at doses of 2, 8, and 16 μg kg^{-1}. The immunosensor exhibited favorable recovery rates, ranging from 86.5% to 98.6%, suggesting its effective detection of ZEN in maize samples, making it appropriate for practical use.

Lu *et al.*[175] studied the one-step electrochemical co-reduction technique to synthesize CNT-based AuNPs/ERGO@CNT immunosensors to detect P-glycoprotein (P-gp) from tumour cells and blood–brain barrier-related cells. P-gp concentrations are strongly connected with multi-drug susceptibility, which frequently signals the onset of malignant development in treating the disease with drugs. P-gp expression levels can be significantly expressed naturally or acquired after chronic drug therapy. Monitoring P-gp expression is crucial for individualized medication in diagnosing and managing diseases. Additionally, by immobilizing antigens on the electrode for P-gp identification, a very sensitive competitive LOD of 0.13 ng mL^{-1} was obtained for an EC immunosensor based on CNTs synthesized for P-gp quantification. The devised technique can fulfil the criteria for detecting P-gp concentrations in healthy or pathological circumstances due to its linearity, limit of detection, and specificity. Additionally, the findings of this EC immunosensor are consistent with ELISA. It can identify the presence of P-gp in diluted serum. This quick identification method aids in the clinical study of serum P-gp and resistance to drug development in different illnesses. It provides a scientific foundation for POC diagnosis technology and personalized medicine. There is little research on the immediate identification of P-gp in serum *via* electrochemistry. The produced AuNPs/ERGO@CNT modifications exhibited a synergistic effect, resulting in improved electrochemical characteristics of the electrode. When these materials are mixed, their distinct characteristics combine in a way that elevates the overall efficiency of the composite to a greater degree than it would be if they were utilized separately. For instance, AuNPs coated on ERGO/CNT can benefit from the vast surface area and conductive network that ERGO and the CNTs supply. This results in improved sensitivity as well as improved electron transmission. Furthermore, by stabilizing the AuNPs and preventing their aggregation, ERGO maintains their vast surface area and functions as an efficient catalytic. In the meantime, CNTs offer structural support and further improve conductivity. The immunosensor can quickly, accurately, and specifically identify the P-gp protein in diluted human serum. This method's linear range and detection limit are appropriate for clinical use, and its results are equivalent to those of ELISA, making it a promising tool for monitoring the progression of diseases.

Rabbani *et al.*[176] synthesized the carbon nanotube field-effect transistor (CNT-FET) immunosensor for the effective and selective sensing of C-reactive protein (CRP). Belonging to the pentraxin family, CRP is produced in the liver as an indi-

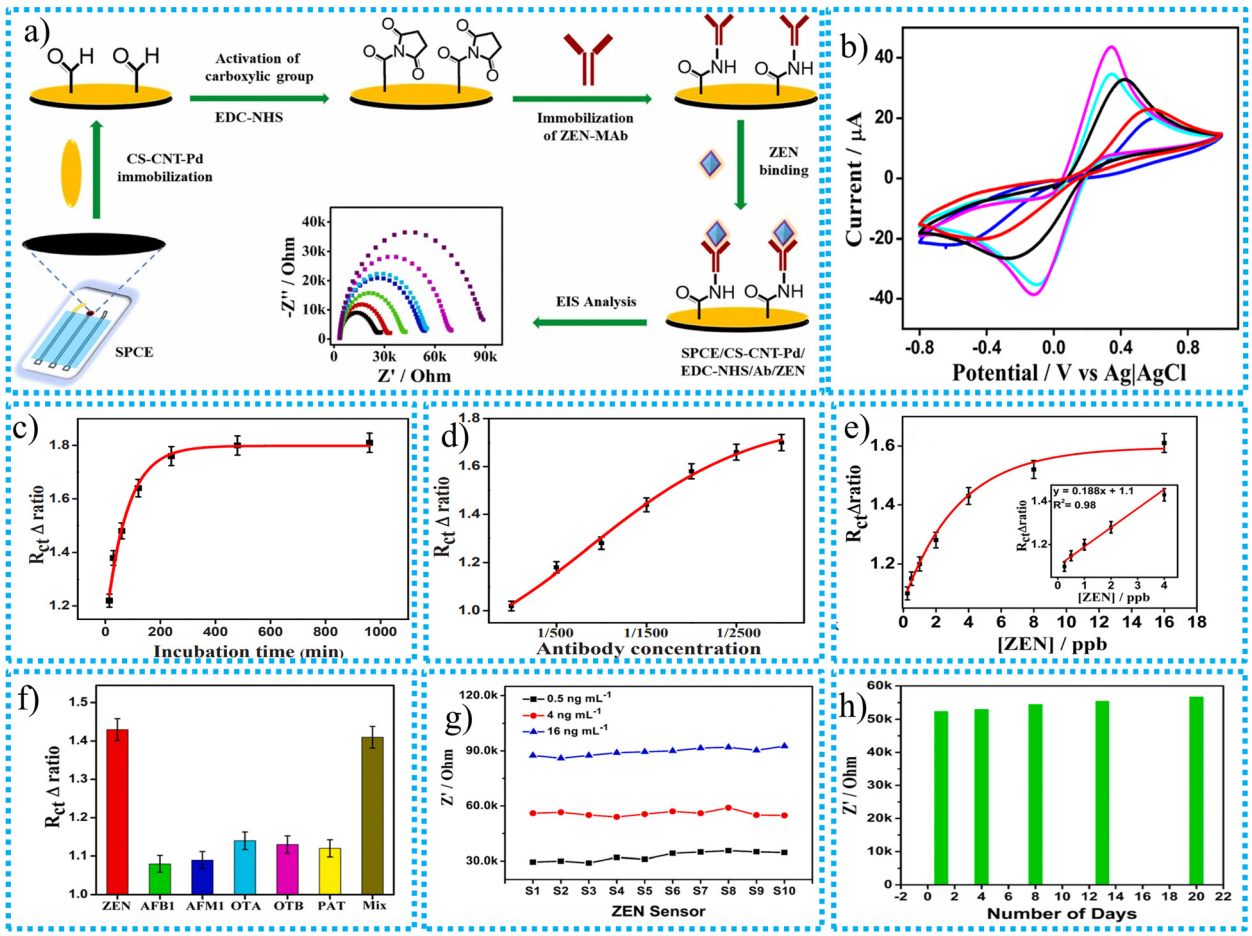

Fig. 12 (a) The CNT-based CSCNT-Pd-based immunosensor synthesis procedure, (b) CV curves for the impact of modification on the SPCE electrode, (c) electrochemical impedimetric responses (Δ_{ratio}) of the SPCE/CS-CNT-Pd/ZEN-MAb modified electrode after incubation with 4 ng mL^{-1} of ZEN at different incubation time intervals, (d) impedimetric responses of the SPCE/CS-CNT-Pd/ZEN-MAb modified electrode to varying concentrations of antibody (ZEN-MAb), (e) the calibration curve of the ZEN immunosensor based on the change in R_{ct}, (f) electrochemical impedimetric responses of the fabricated immunosensor, (g) impedance responses of ten independent immunosensor sets towards ZEN detection, (h) impedance responses of the ZEN immunosensor for 20 days under ambient conditions toward the detection of 2.0 ng mL^{-1} of ZEN.[174]

cator of inflammation brought on by injury and infection. The CNT-based biosensor possessed a dynamic detection range of 0.01–1000 µg mL^{-1} and the LOD of the target CRR was 0.06 µg mL^{-1}. It gives outstanding results within 120–180 s. It is an affordable, effective immunosensor for identifying coronary heart disease. The sensing procedure for CRP antibodies by the CNT-FET immunosensor in blood samples is presented in Fig. 13a.

The CNT-FET immunosensor's characterization involves testing its reaction time, detection range, and limit of detection by employing escalating quantities of CRP antigen. At the beginning, a volume of 1 µL of PBS was used to stabilize the sensor signal for 12 s. Following stabilization, the CRP antigen was incrementally added, with each drop of 1 µL injected at intervals of 10 s. The immunosensor's real-time response was observed, with each subsequent concentration being introduced once the I_{ds} signal had reached a stable state, as shown in Fig. 13b. The process involves developing a calibration curve for identifying C-reactive protein (CRP) utilizing a carbon nanotube field-effect transistor (CNT-FET) immunosensor in a solution of 0.01× phosphate-buffered saline (PBS). The sensor's response was tested at various CRP concentrations on a semi-logarithmic scale, as shown in Fig. 13c. The results demonstrated that $\Delta I/I_o$ grew in direct proportion to the CRP concentration. This can be attributed to negatively charged CRP molecules accumulating within the Debye length.

Nevertheless, when the CRP concentrations reach incredibly high levels (5000 µg mL^{-1}), there is no additional increase in $\Delta I/I_o$. This is most likely because the binding sites on the CNT surface become saturated. The sensor exhibited a linear detection range for CRP from 0.01 to 1000 µg mL^{-1}. The sensor was initially subjected to undiluted serum obtained from a healthy individual. The I_{ds} signal remained unchanged, suggesting that the serum had low or undetectable levels of CRP. To evaluate the specificity of the sensor, it was subsequently subjected to real-time testing using four non-specific antigens (Hb, HSA, hTF, and α1-AG), commonly found proteins in serum, as presented in Fig. 13d. Each antigen was administered in a volume

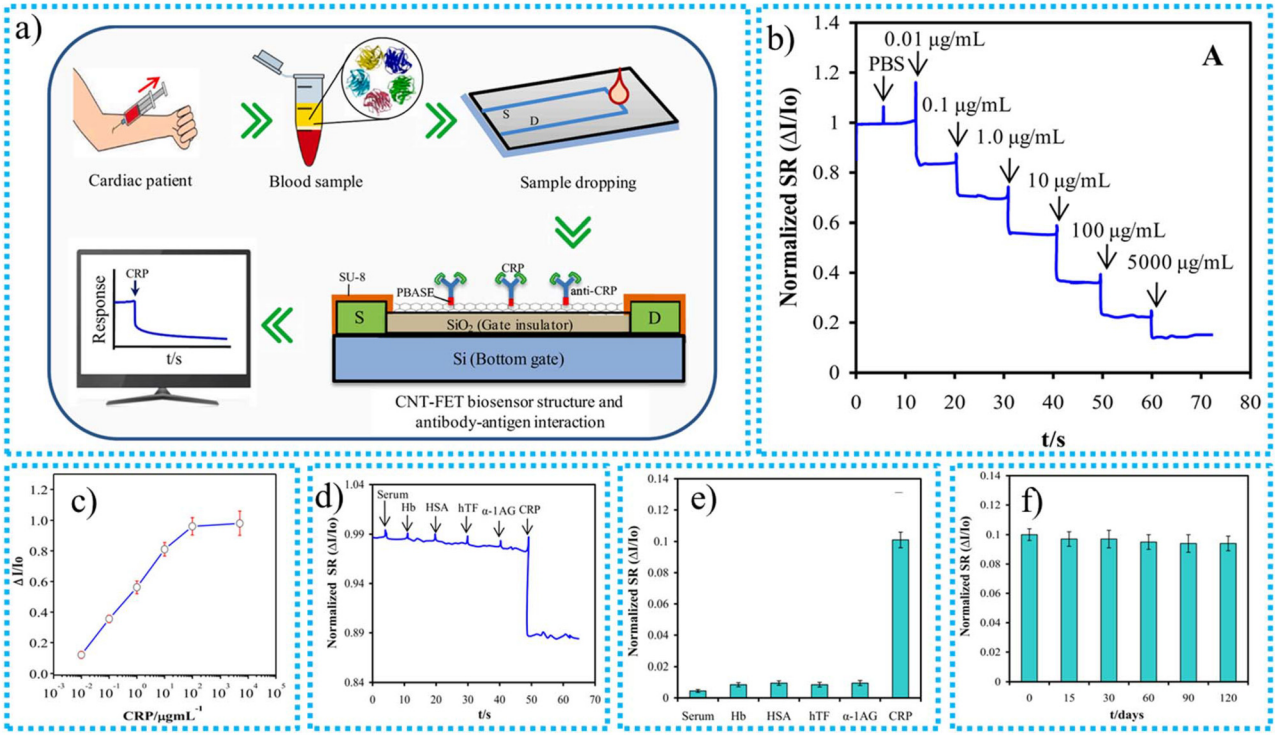

Fig. 13 (a) The sensing procedure for CRP antibodies by the CNT-FET immunosensor in a blood sample, (b) real-time detection response properties after the addition of increasing concentrations of CRP antigen, (c) calibration curve of spiked CRP in human serum detected by the CNT-FET immunosensor, (d) real-time testing for the selectivity of the immunosensor, (e) quantitative comparison of $\Delta I/I_o$ with the injection of target CRP and non-target antigens, (f) storage stability of the immunosensor.[176]

of 1 μL at a concentration of 0.1 μg mL^{-1}. The findings indicated that these obstructive proteins did not impact the sensor's I_{ds} signal, confirming the sensor's exceptional specificity for CRP. The CNT-FET immunosensor demonstrated a robust reaction to CRP at a concentration of 0.1 μg mL^{-1} while displaying little reaction to non-specific proteins such as Hb, HSA, hTF, and α1-AG, as shown in Fig. 13e. This illustrates the sensor's exceptional selectivity for CRP. The sensor is also appropriate for utilization in human serum samples, indicating its suitability for medical applications. The time-dependent storage stability of the CNT-FET immunosensor was assessed by storing the sensor at room temperature and conducting tests on CRP antigen binding for 120 days. The sensitivity remained consistent at 97% of the initial level for the first 30 days, progressively declining but still maintaining 94% of the original reaction after 120 days, as shown in Fig. 13f. This demonstrates that the sensor's performance remains consistent over time, exhibiting no notable decline and affirming its appropriateness for real-world use due to its exceptional stability. The developed immunosensor offers several major advantages, including a rapid response time of 2–3 min, excellent sensitivity with repeatability (2.1% RSD), and stability over the long term with a minimal 6% decline in response over 120 days. The immunosensor is an extra cost-effective and scalable option for clinical applications compared to enzyme-linked immune-sorbent assay (ELISA). The new device's exceptional stability in ambient circumstances makes it a suitable detection system for practical uses. The instrument's wide analytical range, limited nonspecific binding, rapid response, and low sample needs make it a highly beneficial tool for various applications.

Li *et al.*[177] synthesized the In_2S_3/MoS_2@Fe-CNT aptasensor for sensing *Staphylococcus aureus* (*S. aureus*). The most frequent pathogen associated with human blood infections is *S. aureus*, a member of the Gram-positive bacterial group. *S. aureus* can parasitize the bodies of humans and animals, wastewater, air, and other environmental sources to cause serious illnesses. Therefore, preserving human health and achieving accurate ecological surveillance depends on accurately and sensitively identifying *S. aureus*. The ongoing investigation can address this issue. The synthesized CNT-based aptasensor possessed an excellent LOD and the LRD of *S. aureus* was 2 CFU per mL and 0.1×10^7 CFU per mL. The designed PFC-driven self-sustaining aptasensor showed superior selectivity, outstanding repeatability, solid stability, acceptable recycling, and tremendous potential practicality for *S. aureus* detection. The synthesis process for the In_2S_3/MoS_2@Fe-CNT nanocomposite aptasensor is shown in Fig. 14a. The gradual alteration of the electrode surface substantially affects the electrochemical characteristics of the produced photoelectrochemical aptasensor, as demonstrated in Fig. 14b. The progressive decline in open circuit potential

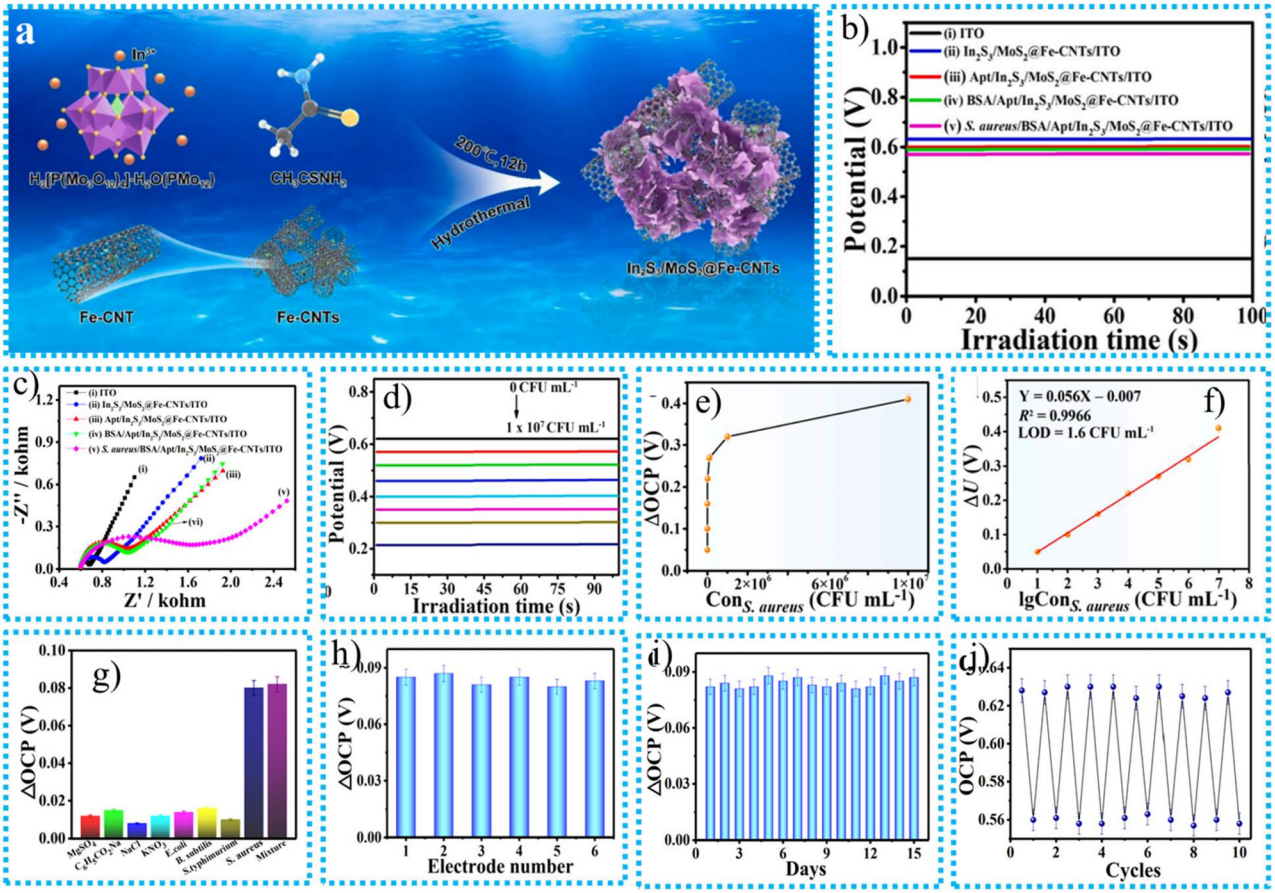

Fig. 14 (a) The synthesis process for the In_2S_3/MoS_2@Fe-CNT nanocomposite aptasensor, (b) OCP–time curves of the photocathodic aptasensor based on In_2S_3/MoS_2@Fe-CNTs for the sensing of *S. aureus* (10 CFU per mL), (c) EIS Nyquist plots, (d) OCP–time curves for the self-powered PFC system for the detection of *S. aureus* at different concentrations, (e) dependence of ΔOCP on the *S. aureus* concentration, (f) the corresponding calibration curves between ΔOCP and *S. aureus* concentration, (g) selectivity, (h) reproducibility, (i) stability, and (j) regenerability of the proposed PFC aptasensor for the analysis of *S. aureus* (10 CFU per mL).[177]

values, along with the concomitant rise in charge transfer resistance exhibited in the EIS Nyquist plots, validate the effective encapsulation of the aptamer and the subsequent binding of *S. aureus*, as shown in Fig. 14c. The continuous fluctuations in both open circuit potential and charge transfer resistance seen throughout every alteration step highlight the effectiveness of the sensor's construction, suggesting its potential for accurate and selective detection of *S. aureus*. The PFC aptasensor exhibited exceptional sensitivity, as evidenced by the OCP–time curves associated with different concentrations of *S. aureus*. The LOD of 1.6 CFU per mL, over a wide linear range of 10^{-1} to 10^{7} CFU per mL, demonstrates the sensor's capacity to detect deficient levels of *S. aureus*, as shown in Fig. 14d–f. The strong correlation between the change in open circuit potential and the logarithm of *S. aureus* concentration provides additional evidence of the sensor's precision and dependability for quantitative evaluation. This makes it a promising instrument for the early and sensitive identification of pathogens. The aptasensor, which operates without external power, demonstrates outstanding selectivity, repeatability, stability, and regeneration qualities. The device can specifically identify *S. aureus* while minimizing interference from other chemicals, ensuring its accuracy. The sensor exhibits consistent findings over several tests, hence proving its reliability. Despite being used 15 times in a row, the sensor maintains its stability and can be refreshed and recycled with only a minor decrease in efficiency. The aptasensor possesses these characteristics, making it a highly viable option for practical use in detecting *S. aureus*. The detailed selectivity, reproducibility, stability, and regenerability of the synthesized In_2S_3/MoS_2@Fe-CNTs aptasensor are presented in Fig. 14g–j. The extreme LOD of the In_2S_3/MoS_2@Fe-CNTs/ITO-based self-powered PFC aptasensor can be attributed to several important reasons. These include the Schottky heterojunction's ability to exchange and separate charges in an effective manner, the dual-photoelectrode system's ability to improve photoelectric conversion, and the structural characteristics of the heterojunction that offer a large number of locations for aptamer adhesion. The sensor's efficiency is greatly improved due to these elements working together. Su *et al.*[178] utilized the facile solvothermal technique

to synthesize the CNT-based CNTs/PU aptasensor for sensing stress biomarkers. Cortisol, a hormone generated by the adrenal cortex in response to stress, is an indicator of stress and is essential for many physiological functions, including regulating blood pressure and blood sugar levels, metabolism in many organs, and other functions of the body. The LOD of cortisol is 0.032 ng mL^{-1}, whereas the synthesized CNT-based had an outstanding LRD of 0.1–100 ng mL^{-1}. In the meantime, under circumstances involving deformation due to force, the sensor demonstrated outstanding precision for cortisol identification. This adaptable and simple sweat cortisol aptasensor has a lot of promise for handling and tracking quantitative stress.

7.3.2. MXene-based immunosensors and aptasensors. Kalkal *et al.*[179] utilized a one-pot direct reduction technique to decorate the surface of Ti_3C_2-MXene with silver nanoparticles (AgNPs) to synthesize the MXene-based Ag@Ti_3C_2 immunosensor for the detection of the target neuron-specific enolase (NSE). NSE is believed to be a useful biomarker for tracking the effectiveness of treatments, the course of diseases, determining the extent of tumors, and early identification. In this section, we summarize the sensing power of pure MXene and MXene-based synthetic materials. According to a study, virgin MXene has a lower detection limit for the target sample than MXene-based composites. The synthesized MXene-based immunosensor exhibited LOD and LRD values up to 0.05 ng mL^{-1} and 0.0001–1500 ng mL^{-1}. The response time for synthesizing the MXene-based immunosensor is 12 min. The NSE sensing mechanism of the MXene-based immunosensor is shown in Fig. 15a. Fluorescence spectroscopy was employed to assess the efficacy of two distinct fluorescent immunosensing systems: anti-NSE/amino-GQDs/Ag@Ti_3C_2-MXene and anti-NSE/amino-GQDs/Ti_3C_2-MXene. These systems were specifically constructed to identify various amounts of NSE antigens. The protein-functionalized amino-GQDs exhibit a boost in fluorescence intensity when the quantity of NSE rises. This is attributed to the creation of an antigen–antibody complex, which hinders energy transfer to the MXene components. The calibration curve plots demonstrate that the anti-NSE/amino-GQDs/Ag@Ti_3C_2-MXene platform has a linear effect over a wider range (0.0001–1500 ng mL^{-1}) in comparison with the anti-NSE/amino-GQDs/Ti_3C_2-MXene platform (1–1000 ng mL^{-1}). The detailed electrochemical performance of the anti-NSE/amino-GQDs/Ti_3C_2-MXene fluorescent biosensor toward detecting selective NSE species is presented in Fig. 15b–e. The physical appearance of the synthesized MXene-based nano-

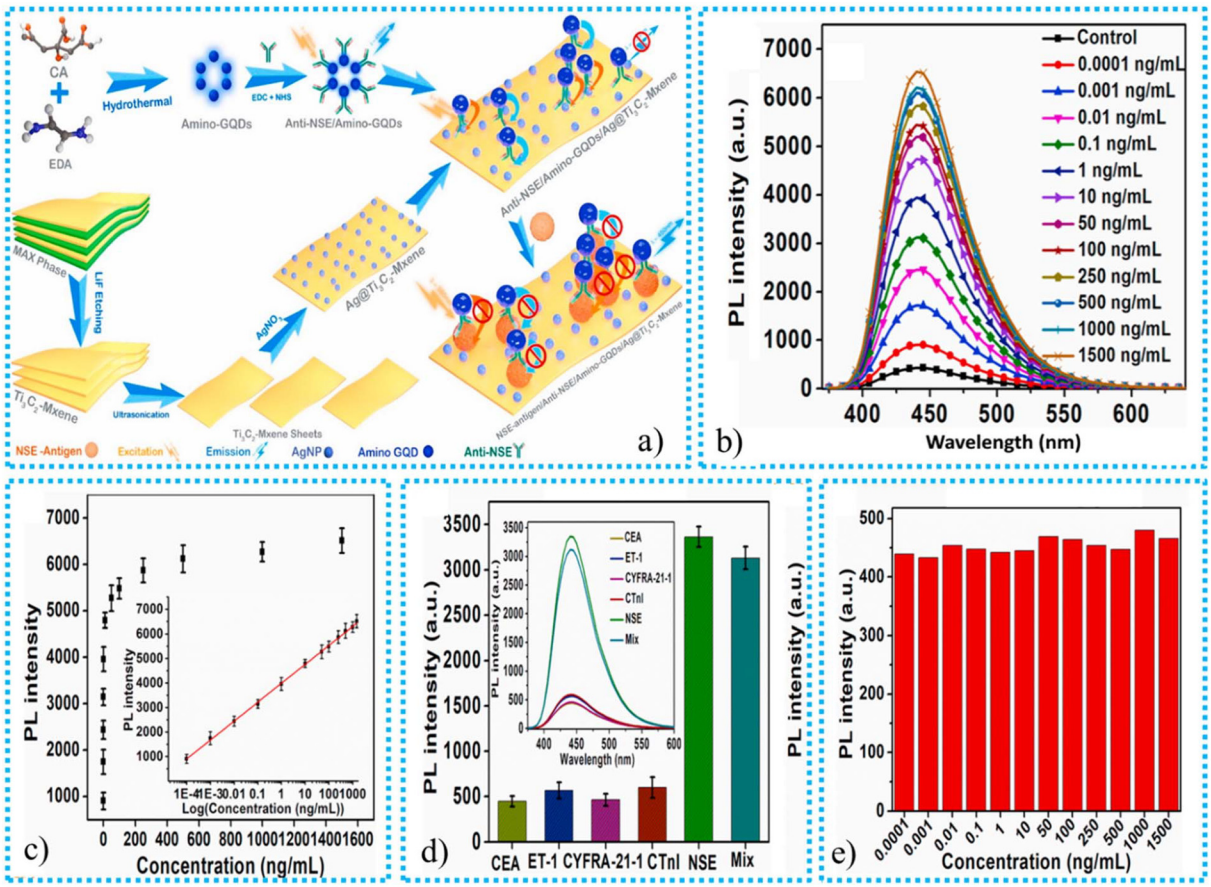

Fig. 15 (a) The NSE sensing mechanism for the MXene-based immunosensor, (b) analytical performance of the MXene-based fluorescent biosensor, (c) the graph of recovered fluorescence *vs.* different NSE concentrations, in the range of 0.0001–1500 ng mL^{-1}, (d) selectivity of the biosensors, (e) control experiment for the amino-GQDs/Ag@Ti_3C_2-MXene immunoelectrode.[179]

composite was dark gold because of the reduction of AgNPs at the interface of MXene nanosheets.

Furthermore, blood specimens have shown exceptional biosensing abilities with a fluorescence recovery rate of roughly 98%. The biosensor based on Ag@Ti_3C_2-MXene exhibits more than double the sensitivity of conventional graphene and AuNP systems. In addition, it shows a superior identification range and a smaller limit of identification in comparison with both bare Ti_3C_2-MXene and graphene. The biosensor has high efficacy when used with serum samples, with a recovery rate of around 98% for spiked NSE.

In summary, this immunosensor demonstrates significant promise for correctly identifying NSE and has the potential to be developed into a compact, portable apparatus for point-of-care diagnostics. As a viable framework for quantitative NSE identification, the proposed immunosensor demonstrates exceptional biosensing properties. More work should be put into combining this perspective platform with microfluidics and flexible electronics to create miniature point-of-care apparatus.

Using self-adsorption, Liu *et al.*[2] synthesized the AuNPs/MXene@PAMAM immunosensor to detect human cardiac troponin T (cTnT). The designed immunosensor was electrochemically active enough to detect the intended analyte. The structured biosensor exhibited a good dynamic detection target of up to 0.1–1000 ng mL^{-1}, and the LOD was 0.069 ng mL^{-1}. When identifying the desired analyte, the sample had exceptional sensitivity and stability. Analyses of its dependability, validity, and effectiveness using serum samples were used to illustrate its importance in the biomedical field. The developed MXene-based immunosensor's excellent structural and functional advantages influenced such ideal results. The work mentioned above increases the use of MXenes in industries related to biosensors by providing a reliable and viable substitute. Laochai *et al.*[181] synthesized the MXene-based L-Cys/AuNPs/MXene immunosensor for sensing cortisol in sweat. Because cortisol inhibits the electron flow mechanism, cortisol's electrochemical identification depends on reducing the oxidation current towards the antigen–antibody binding contact. The synthesized immunosensor utilizes the synergistic properties of MXene's enormous surface area, electrical conductivity, and the biological compatibility and functionalization capacities of PAMAM dendrimers and AuNPs to detect human cardiac cTnT. The PAMAM dendrimers attached to the MXene interface offer many active sites where anti-cTnT antibodies can be immobilized. Upon introducing a sample containing cTnT, the cTnT molecules selectively attach to these antibodies, forming an antigen–antibody complex. The association event results in an alteration of the sensor's electrical or optical signal. This alteration is then recognized and linked to the amount of cTnT in the specimen. The addition of gold nanoparticles improves the sensor's ability to detect and its reliability by aiding in electron transfer and amplifying the signal. This makes the AuNPs/MXene@PAMAM immunosensor an extremely efficient platform for quickly and accurately detecting cTnT, a crucial biomarker for myocardial infarction. This immunosensor provides outstanding sensitivity, a LRD of 5–180 ng mL^{-1}, a LOD of 0.54 ng mL^{-1}, and has a minimal interference impact. Additionally, this immunosensor offers great repeatability and stability during storage for 6 weeks or longer. In conclusion, this technique provides satisfactory results for successfully detecting cortisol in synthetic sweat. Therefore, incorporating this platform into a wristband might work well as a wearable electrochemical sensor for cortisol in sweat.

Zhou *et al.*[180] utilized the sonochemical technique to synthesize a MXene-based ZnO-MX/Ag_2S immunosensor for sensing ancient silk. A naturally occurring polymer with poor durability and rapid degradation is silk fibroin (SF). Most identified fabrics for this silk were ashed, marginalized, mineralized, or carbonized, making it difficult to recognize correctly. Analytical methods used in the past have a tough time analyzing historical silk microtraces. Because of the recent discovery of countless textile artefacts on the Silk Road, it is extremely hard to detect minute remnants of silk. The chances and difficulties outlined above demonstrate the importance of developing exact and delicate detection algorithms to detect SF. To overcome the issue of accurate SF detection, current research provides an effective and rapid-response immunosensor. In this investigation, researchers compare the sensing performance of ZnO-MX/Ag_2S-based and ZnO-M-X-based immunosensors for sensing SF. The immunosensor, which is based on MXene and consists of ZnO and Ag_2S nanoparticles, can detect ancient silk by utilizing the distinctive characteristics of its components. MXene functions as a highly conductive base with a substantial surface area, facilitating effective electron transport and offering several sites of activity for binding ZnO and Ag_2S nanoparticles. The sensor's sensitivity is increased by the presence of ZnONPs, which possess exceptional photocatalytic capabilities and exhibit a robust interaction with silk proteins. Ag_2S plays a role in the detection process by either reducing the fluorescence or enhancing the signal. The sensor undergoes a detectable alteration in its optical or electrical signal when it comes into contact with ancient silk due to the particular interconnections between the silk proteins and the functionalized ZnO-MX/Ag_2S surface. This alteration is directly linked to the existence and amount of silk proteins, which enables the precise and reliable identification of ancient silk objects. Additionally, they found that the response of the ZnO-MX/Ag_2S-based immunosensor was 6.8 times greater than the ZnO-M-X-based immunosensor under visible light. The synthesized MXene-based immunosensor possessed good LOD and LRD values up to 1.51 ng mL^{-1} and 0.005–50 ng mL^{-1} for sensing *Bombyx mori* silk traces. The immunosensor also demonstrated remarkable specificity, stability, and reproducibility, especially for quantitatively identifying archaeological artefacts. Particularly promising photoactive nanomaterials for vis/NIR PEC immunosensors include ZnO-MX/Ag_2S nanocomposites. Furthermore, this approach provides a workable way to investigate the origins and circulation of ancient silk.

The development procedure for the ZnO-MX/Ag_2S nanomaterial and the development procedure for the PEC immunosensor are schematically given in Fig. 16a. Zhu *et al.*[182] syn-

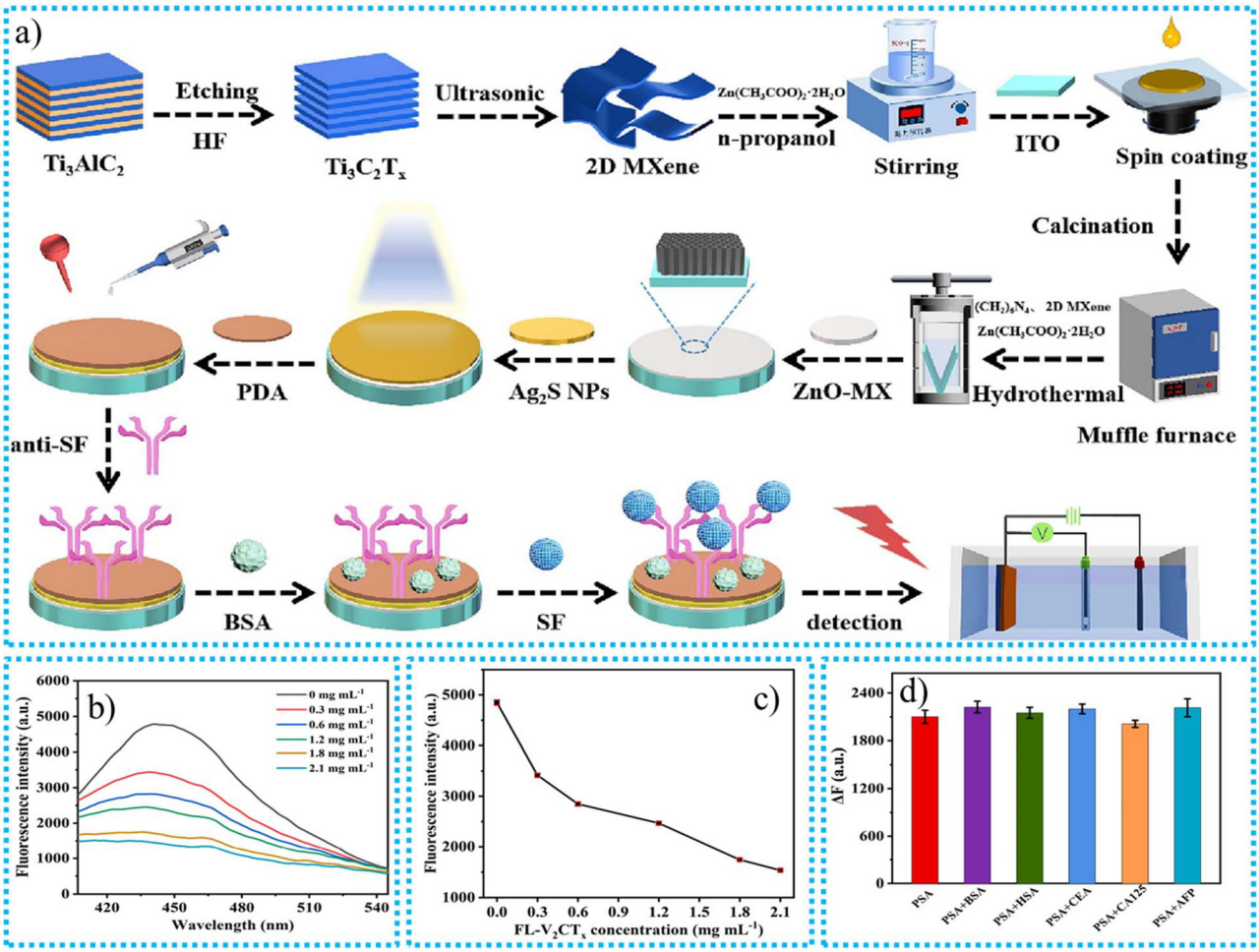

Fig. 16 (a) The ZnO-MX/Ag_2S nanomaterial development procedure and the PEC immunosensor development procedure,[180] (b) fluorescence emission spectra, (c) fluorescence intensity of aptamer-CGQDs with FL-V_2CT_x concentrations, (d) ΔF of the aptasensor for PSA in the presence of 3-fold BSA, HSA, CEA, CA125, and AFP, respectively. Conditions: PSA concentration was 15 ng mL^{-1}.[182]

thesized the MXene-based CGQDs-FL-V_2CT_x aptasensor to identify prostate-specific antigens (PSA) in human blood. The availability of higher concentrations of PSA in human blood is responsible for early-stage prostate cancer. Prostate cancer may be indicated by human blood PSA concentrations higher than 4 ng mL^{-1}. Traditional techniques have a higher response time and poor PSA detection performance. However, the currently developed MXene-based aptasensor is an effective device for detecting PSA in human blood. The LOD and LRD for the MXene-based aptasensor are 0.03 ng mL^{-1} and 0.1 to 20 ng mL^{-1}, respectively. The aptasensor, which utilizes MXene-based CGQDs-FL-V_2CT_x, can detect PSA in human blood using a unique combination of components. MXene serves as a highly responsive platform, while CGQDs produce light emissions. An aptamer, composed of DNA or RNA, is engineered to adhere to PSA selectively. PSA in the bloodstream interacts with the aptamer, leading to a modification of the light emission of the CGQDs. The sensor detects this alteration, indicating the existence of PSA. Furthermore, despite higher concentrations of these alternative proteins, they did not impede the identification of PSA, as depicted in Fig. 16d. This verifies that the aptasensor exhibits a high level of selectivity towards PSA. In the study, the FL-V_2CT_x dosage was optimized by investigating its impact on the fluorescence emission spectra of aptamer–CGQDs. The consequent fluorescence intensity was examined and presented in Fig. 16b and c. Jiang *et al.*[183] utilized a simple wet chemical technique to synthesize the MXene-based Ti_3C_2-AgBrNC aptasensor for sensing enrofloxacin. The LOD and LRD values of enrofloxacin for the MXene-based aptasensor were 5.97×10^{-13} mol L^{-1} and 1.0×10^{-12} to 1.0×10^{-6} mol L^{-1}. Their investigation indicated that the pristine MXene had a lower sensing capacity than the MXene-based composite.

7.4. CNT- and MXene-based electrochemiluminescence biosensors

The existence and cytotoxicity of neurotoxins can be detected and measured using electrochemiluminescence (ECL) assays based on an ECL signal. It combines the detection of optical luminescence with electrochemistry. When an electrical

charge is applied to an electrode, its outermost layer is activated. Therefore, electron transfer occurs between molecules, and the light emitted is measured. In this section, we discuss the CNT- and MXene-based ECL biosensors for identifying toxic nanomaterials in the human body to diagnose disease before it reaches a critical level. The performances of CNT and MXene ECL biosensors are given in Table 6.

7.4.1. CNT-based electrochemiluminescence biosensors. Wang *et al.*[184] utilized a simple decoration technique to synthesize MWCNT/graphene/chitosan electrochemiluminescent materials by decorating electrodes with CNTs to identify glucose in human blood. Glucose is a vital chemical for life processes and a significant portion of animal and plant polysaccharides. As a result, its accurate and sensitive identification is crucial in numerous sectors. In medical practice, the level of blood glucose is fundamental since it can indicate diabetes mellitus, which is a significant risk indicator for innumerable illnesses such as kidney stones, cardiovascular disease, and blindness. The availability of AuNPs on the electrode interface is responsible for generating the different active sites on the electrode surface to enhance their detection capacity and reduce the detection time to give fast and accurate results. The LRD and LOD values of the CNT-based ECL sensor are 0.1–5000 μM and 64 nM. The performance of the synthesized CNT ECL sensor is better than that of pristine CNTs. The sensor's repeatability was validated by assessing its response to glucose, which demonstrated consistent outcomes with minimal deviations among different sensors, with an RSD of 2.7%. The sensor exhibited robust selectivity by accurately detecting glucose, even in the presence of other chemicals, with no disruption. Furthermore, the sensor demonstrated commendable long-term stability, retaining a significant portion of its efficacy even after being held for 20 days. This indicates that it can be confidently employed for remote applications. A cloth-based sensor, which has undergone specific cathodic alterations, demonstrates outstanding results in detecting glucose. The sensor with these alterations exhibited a significantly improved detection limit compared to an identical sensor without them, with a higher limit of 31 μM. This enhanced sensor provides superior sensitivity to conventional glucose sensors and necessitates uncomplicated and cost-effective manufacturing techniques. Overall, it is notable for its exceptional detection sensitivity and efficiency. The ECL sensor, composed of MWCNTs, graphene, and chitosan, can detect glucose. Coating MWCNTs, graphene, and chitosan onto the electrodes achieves this. The electrode's surface area can conduct better thanks to these materials. The presence of glucose causes a reaction at the electrode surface that starts an electrochemiluminescence process that emits light. The brightness of this light is directly related to the amount of glucose present, enabling the sensor to precisely determine glucose levels in human blood. Lastly, it is shown that the C-BP-ECL sensor can accurately and reliably identify glucose in human blood specimens. Potential uses for this brand-new, susceptible sensor include food analysis, environmental monitoring, and clinical diagnostics.

Jiao *et al.*[185] utilized a simple coating technique to synthesize CNT-based ox-MWCNTs-IGQDs for effectively sensing 5-fluorouracil (5-FU) in serum. 5-FU, a potent chemotherapy drug of the fluoropyrimidine class and the third most prevalent chemotherapy agent, is frequently employed in treating solid tumors, such as head, neck, and gastrointestinal tumors. The body may react negatively to this medication if used excessively, and known side effects include sudden myocardial infarction, cardiac failure, or arrhythmia. There are no minor issues in life. These adverse effects and potential risks remind us to exercise greater caution when using these medications in clinical settings. 5-FU is a double-edged sword with benefits and drawbacks, making moderate use crucial. The detection of it is equally vital. Using EIS to assess modifications to electrode resistance at the surface during sensor construction is booming. The two main advantages of the synthesized CNT-based ECL sensor are its large SSA and minimized toxicity. The sensor's stability is crucial for practical applications. The sensor's signal strength escalated in direct proportion to the level of 5-FU detected. After undergoing five testing cycles, the signal exhibited minimal change, with a variance of only approximately 2.2%, as shown in Fig. 17a. This demonstrates the exceptional stability of the sensor developed in this investigation.

The amount of each PdAg NS acceptor, 5-FU covering antigen, and antibody significantly impacted the efficiency of the ECL immunosensor. To enhance these conditions, tests were carried out. It was discovered that the signal level reached its highest point at a value of 0.5 mg mL^{-1} while the amount of PdAg NSs ranged from 0.2 mg mL^{-1} to 0.8 mg mL^{-1}. Nevertheless, when the concentration exceeded 0.5 mg mL^{-1}, the signal intensity significantly decreased due to the pronounced inhibitory effect of the higher level of PdAg NSs on the luminescence properties of the donor material. The synthesized CNT-based ox-MWCNT-IGQD electrochemiluminescent sensor possessed outstanding sensitivity with a LOD of 0.17 pg mL^{-1} and broad LRD from 0.0005 to 500 ng mL^{-1}. The synthesized CNT-based ECL sensor possessed excellent reusability and stability. The synthesis of the CNT-based ECL sensor and the sensing mechanism of 5-FU are shown in Fig. 17.

Huang *et al.*[194] increased the sensing power of the synthesized CNT-based ECL by coating DNA on the surface of synthesized electrodes. This investigation indicated that the pure indium tin oxide (ITO) electrode possessed a poor sensing performance compared to the CNT-based electrodes. The proposed method differs from other studies that reported employing carbon nanotubes (CNTs) to raise ECL, allowing for the planning of ECL improvement through a biological recognition mechanism. The system, which consists of single-walled carbon nanotubes and single-stranded DNA, can be modified to identify and measure different small amounts of substances of interest. Initially, it was demonstrated to identify single-stranded DNA and subsequently employed to identify Hg^{2+} and human α-thrombin by substituting the ssDNA probe for particular probes designed for these targets. The system

Table 6 The performance of CNT and MXene ECL biosensors

Names of CNT and MXene-based ECL biosensors	Synthesis techniques	Sensing techniques	Characterization techniques	Biomarker	Limit of sensing (μM)	Linear range (μM)	Remarks	Ref.
MWCNTs/graphene/chitosan	Simple coating technique	EIS	TEM, SEM	Glucose	64 nM	0.1–5000 μM	The availability of AuNPs on the interface of the electrode is responsible for generating the different active sites on the surface of the electrode to enhance their detection capacity and reduce detection time to give fast and accurate results	184
ox-MWCNT-IGQD	Simple coating technique	EIS	TEM, IR, and HRTEM	5-FU	0.17 pg mL^{-1}	0.0005 to 500 ng mL^{-1}.	The two main advantages of the synthesized CNT-based ECL sensor are its large SSA and minimized toxicity	185
3D graphene/Cu_2O-MWCNT/RuSiNP	Loading technique	EIS	TEM, SEM, XRD, and EDX	Thrombin	1.3×10^{-12} M	5×10^{-15}–5×10^{-11} M	The photocatalytic substance Cu_2O was added to a cyclic catalytic mechanism to increase the ECL quantity. Additionally, electron transmission was accelerated using 3D graphene and MWCNTs, which increased the ECL intensity even more	186
Ru/CNT/graphene	Depositing technique	DPA	SEM, TEM, and EDX	Dopamine	1.9 nM	50–500 M	The synthesized CNT-based equipment accomplished optical ECL analysis of multiplex specimens employing a smartphone as the detector	187
MWCNTs-Cys-AuNPs	Amide bonding	CV	TEM and FESEM	Diphenhydramine hydrochloride	6.7×10^{-9} M	2×10^{-8}–7.5×10^{-4} M	Adding AuNPs to the CNTs is responsible for the sensing enhancement of the AuNP-based CNT ECL biosensor	188
MoS_2 QDs-MXene	Self-reduction techniques	Faraday cage-mode sensing system	FTIR and EDS	miRNA-135b	10 fM	30 fM to 20 nM	A system for miRNA collection and a detecting surface was provided by the Au NPs@biomimetic lipid layer in the meantime. Clinically detecting miRNA-135b in exosomes in patients with stomach tumor effusion using the ECL biosensor has yielded promising results	189
IL-MXene/GPE	Simple mixing and drop-casting technique	CV	SEM	DA	702 nM	10 μM–2000 μM	Researchers believe that this architecture will make it possible to create MXene-based sensors that are robust and commercially feasible without sacrificing any fundamental characteristics	190
Au_{SA}/MXene	Simple mixing technique	CV	SEM, FTIR, and TEM	MiRNA-187	15.6 fM	40 fM–20 nM	Single gold atoms were bound by $Ti_3C_2T_x$ MXene vacancy flaws, avoiding the visualization of active catalytic sites. Titanium dioxide found on the nanosheets made from MXene might also accelerate the movement of electrons	191
Zr-TCBPE/MXene	Depositing technique	EIS	SEM, EDX, TEM, and XPS	miRNA-141	16.2 aM	100 aM–1 nM	The MXene-based synthesized ECL biosensor possessed excellent sensing power and gave an urgent response compared to the traditional techniques	192
Ti_3C_2-Ru	Coating method		XRD, SEM, and TEM	$Ru(bpy)_3^{2+}$	0.13 μM	0.5–100 μM	The pristine MXene possessed lower stability and sensing performance than the synthesized MXene-based composite	193

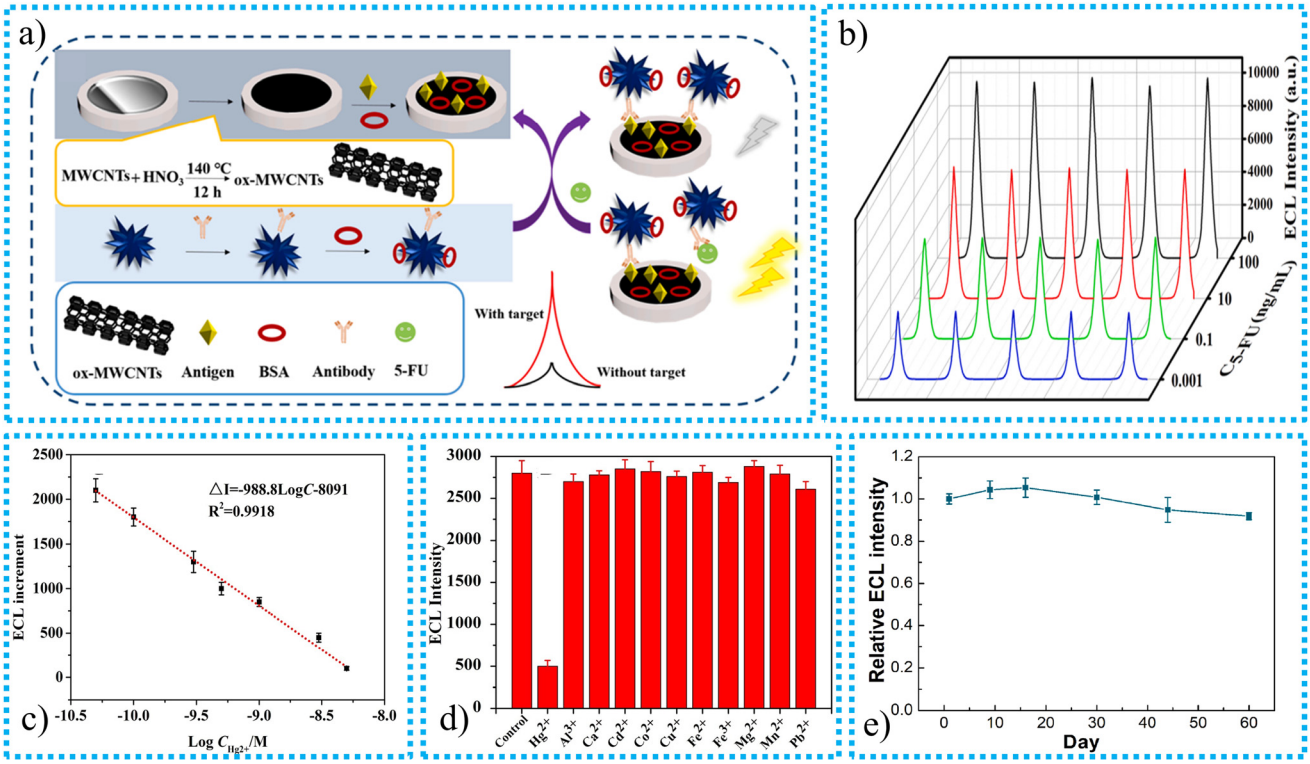

Fig. 17 The synthesis mechanism for the CNT-based ECL sensor and the sensing mechanism for 5-FU, 5-cycle scan peaks of the immunosensor at various concentrations of analyte,[185] calibration graph of detection with ECL increments, (c) selectivity analysis,[194] (d) stability of the SEES using the Ru/CNT/graphene electrode over two months of storage.[187]

exhibited a robust and consistent reaction to Hg^{2+} ions, displaying excellent specificity compared to other metal ions. It could identify levels as low as 22 pM, as shown in Fig. 17b and c. The signal of the system dropped as the level of thrombin increased, enabling identification down to 13 fM. The device exhibited remarkable selectivity towards other proteins. It is established that DNA formation with CNTs permits quantitative testing of many target kinds, such as nucleic acids, Hg^{2+}, and thrombin, in place of capturing probe sequences. Du *et al.*[187] synthesized a CNT/graphene-based ECL sensor modified by a plastic sticker with 24 holes on ruthenium for the sensing of dopamine. The newly created equipment accomplished optical ECL analysis of multiplex specimens employing a smartphone as the detector. The optical DA identification exhibits strong linearity in the 10^3–10 M and 50–500 M ranges. There is a correlation between the outside potential, pH values, and ECL intensity on SEES. The intensity is enhanced as the potential is enhanced from 13 to 17 V because of the quicker oxidation of $Ru(phen)^{2+}$ and TEA. However, the intensity decreases at 18 V, most likely because of water electrolysis and the presence of water. For the purpose of conducting additional experiments, 17 V was selected. The intensity is at its peak at a pH of 5.5. This is due to the fact that higher pH levels diminish intensity because OH^- competes with TEA, which in turn makes the reaction efficient. It was determined that a pH of 5.5 would be the most suitable. The signal-to-noise ratio is 3, and the LOD is 1.9 nM. The ECL system also demonstrates outstanding long-term stability by comparing the ECL response to its original signal after 60 days of storage in an ambient environment, as shown in Fig. 17d.

7.4.2. MXene-based electrochemiluminescence biosensors. Guo *et al.*[189] synthesized a MXene-based ECL sensor by combining MoS_2 QDs–MXene and Au NPs@biomimetic material to sense miRNA-135b. One million people worldwide die yearly from gastric cancer (GC), one of the most prevalent cancers. Over 70% of GC patients have advanced disease when they are diagnosed. The increased mortality of GC is primarily due to delayed identification. Endoscopic inspection and histological biopsy, which are invasive, time-consuming, and expensive, have traditionally been the only options for GC diagnosis. Exosome evaluation, which can be divided into two primary classifications, surface analysis of proteins and miRNA identification, therefore has the potential to be an exciting cancer indicator for preliminary diagnosis. The MoS_2 QDs–MXene nanocomposite possessed an efficient capability to inject electrons, excellent luminescence efficiency, electrochemical characteristics, and a 2D-nanosheet structure, making it a self-luminous Faraday cage nanomaterial. A system for miRNA collection and a detecting surface were provided by the Au NPs@biomimetic lipid layer in the meantime. Clinically detecting miRNA-135b in exosomes in patients with stomach tumor effusion using the ECL biosensor has yielded promising results. The synthesized

MXene-based ECL sensor had LRD and LOD values for miRNA-135b of 30 fM to 20 nM and 10 fM, respectively.

Amara *et al.*[190] utilized a simple mixing technique to mix the MAX phase precursor and copper chloride to synthesize $Ti_3C_2Cl_2$ MXene. After the synthesis of MXene, it can be uniformly deposited on the surface of the conductive graphitic pencil electrode (GPE). The deposition of MXene on the surface of the GPE is responsible for enhancing the SSA of electrodes to enhance their sensing performance. The selective ionic liquid (IL) 1-methyl imidazolium acetate is employed on the interface of MXene *via* π–π interactions. The employed IL provides a practical and robust binding site for biomolecules. The employment of MXene and the IL on the surface of the GPE is responsible for enhancing the stability and sensing power of the MXene-based IL-MXene/GPE ECL sensor. The synthesized MXene-based IL-MXene/GPE ECL sensor effectively senses dopamine (DA).

DA is a well-known neuromodulator that controls an extensive spectrum of neurological functions. Numerous neurological illnesses have been linked to DA impairment. The signature of continuing physiological circumstances and neuronal health is DA homeostasis. The synthesized IL-MXene/GPE ECL sensor possessed a modified sensitivity of up to 9.61 μA μM^{-1} cm^{-2}, and the LOD and LRD values of the synthesized IL-MXene/GPE ECL sensor were 702 nM and 10 μM–2000 μM, respectively. Researchers believe that this architecture will make it possible to create MXene-based sensors that are robust and commercially feasible without sacrificing any fundamental characteristics.

The synthesis procedure for the MXene-based ECL sensor and its sensing mechanism to detect DA are shown in Fig. 18a. CV was employed to investigate the behaviour of the response and surface activity at the interface between the surfaces when 80 μM of DA was present in the experiment. It was possible to change the scan rate from 25 to 425 mV s^{-1}. Following an increase in the scan rate, the CV curves demonstrated that the potential moved more favourably. Fig. 18b illustrates this situation. As illustrated in Fig. 18c, DA is successfully detected by the generating interface at a voltage of 0.25 V. Especially at extremely high concentrations, it exhibits an insignificant reaction to other chemicals but a substantial response to DA. The intense contact between the nitrogen of imidazolium and DA causes this selectivity. The reliability and repeatability of the upgraded sensor's functionality were evaluated. With 2.3% variance, it demonstrated good reproducibility when the same electrode was employed repeatedly. The reproducibility of the

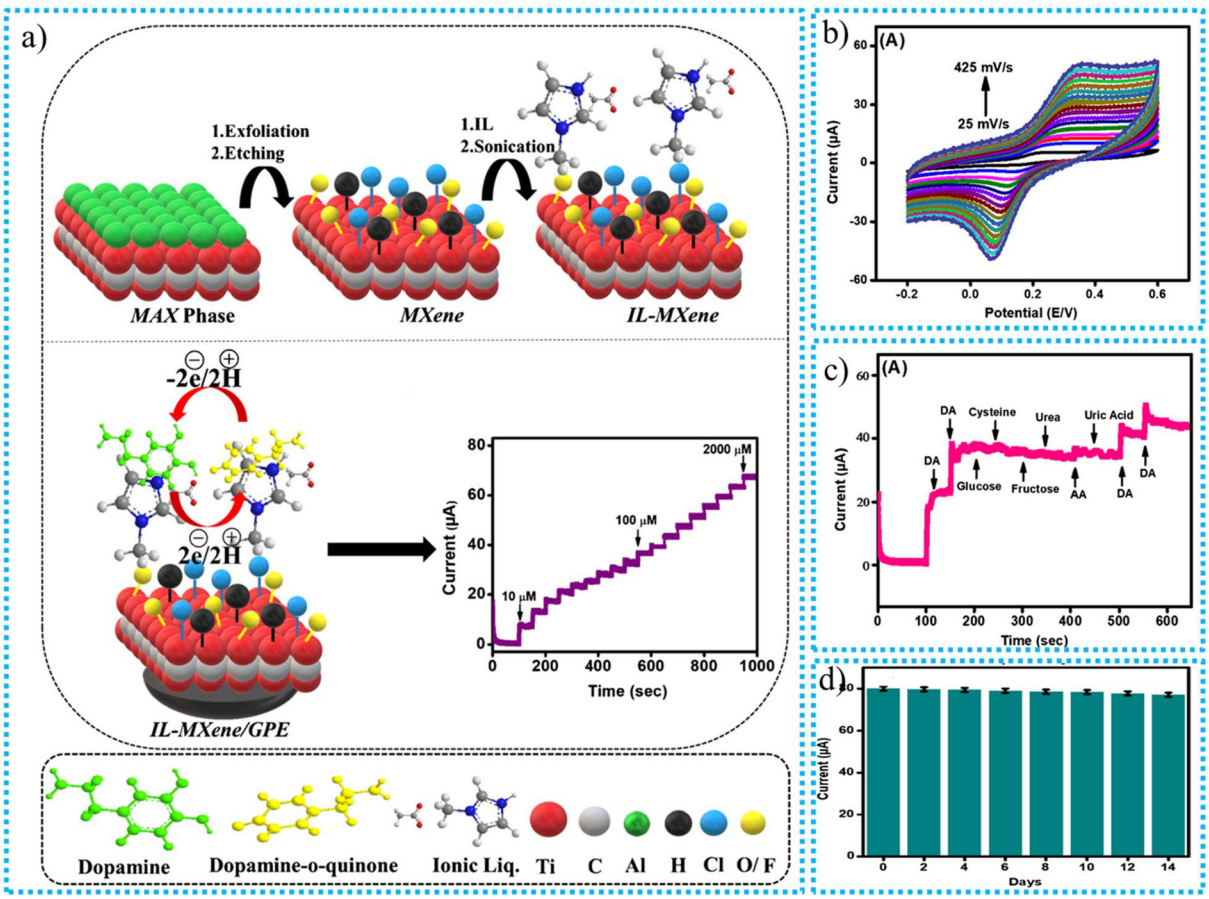

Fig. 18 The MXene-based ECL sensor: (a) synthesis procedure and the sensing mechanism to detect DA, (b) CV response, (c) 40 μM DA (first 2 spikes), 20 μM DA (last 2 spikes), and 500 μM interfering molecules, (d) stability.[190]

sensor was likewise good, varying only 1.9% between electrodes manufactured under identical circumstances. The sensor demonstrated a long shelf life of 14 days at room temperature, with 1.3% fluctuation, despite MXene's usual stability problems, as shown in Fig. 18d. When the sensor was tested on actual samples, it performed effectively despite the existence of different biological materials. With recovery rates ranging from 98.3% to 100%, the sensor accurately identifies DA in serum and phosphate buffer saline specimens. Employing the conventional addition approach, the precision of the sensor in complicated biological settings was proved. The MXene layer and the multipurpose IL make this type of sensor stable and reasonably priced. It reduces the sensitivity of the sensor as well as its capacity to detect limits. The sensor also showed good performance in human serum, indicating that clinical application is a viable alternative.

Nei *et al.*[191] utilized a cost-effective technique to synthesize the MXene-based ECL sensor by adding Au_{SA} and MXene to form the Au_{SA}/MXene nanocomposite for effectively sensing miRNA-187. Introducing the Au_{SA} nanostructure into MXene is responsible for modifying the stability and sensing performance of the MXene-based ECL sensor. Single gold atoms were bound by $Ti_3C_2T_x$ MXene vacancies, avoiding the visualization of active catalytic sites. Titanium dioxide found on the nanosheets made from MXene might also accelerate the movement of electrons. The high electrochemical and catalytic performance of the AuSA/MXene nanocomposites promotes the generation of free radicals from hydrogen peroxide (H_2O_2), resulting in a great-efficiency ECL sensor. The heterogeneous structures of functional substances can improve MXene's ability to detect the desired material through sensing. The AuSA/MXene hybrid was used to construct a Faraday cage-style ECL sensor with fluid nano-islands to detect miRNA-187 in triple-negative tumors in breast cells. The LRD and LOD values of the synthesized MXene-based ECL sensor were 15.6 fM and 40 fM–20 nM, respectively.

Huang *et al.*[192] utilized a cost-effective synthesis technique to prepare the MXene-based ECL sensor by combining Zr-TCBPE-MO and MXene to form Zr-TCBPE-MOL/MXene nanomaterial for the sensing of miRNA-141. Because of its abnor-

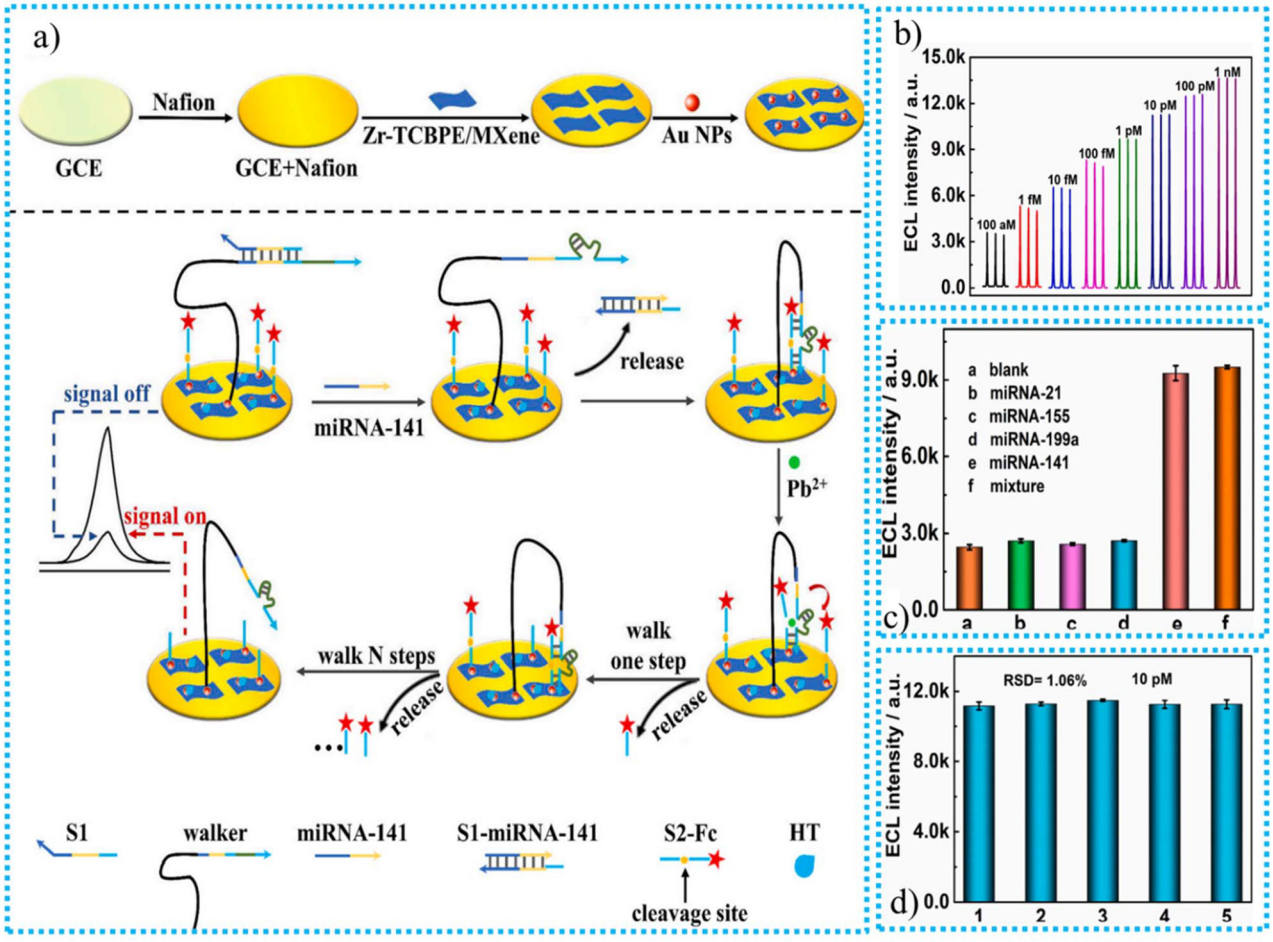

Fig. 19 (a) The hairpin-free and nuclease-free amplification methods with DNAzyme assistance and MXene-based Zr-TCBPE/MXene ECL sensor, (b) ECL responses of the sensing platform toward several concentrations of miRNA-141 (100 aM–1 nM), MXene-based Zr-TCBPE/MXene ECL, (c) selectivity, (d) reproducibility.[192]

mal prostate and breast cancer activity, miRNA-141 is a crucial biomarker. Introducing MXene onto the Zr-TCBPE-MOL interface is responsible for enhancing the conductivity and migration of electrons between respective electrodes. Pristine Zr-TCBPEMOL possesses a 4.1 times lower performance than Zr-TCBPEMOL/MXene nanomaterials. The MXene-based ECL sensor possessed LOD and LRD values of 16.2 aM and 100 aM–1 nM, respectively. According to the Zr-TCBPE-MOL/MXene nanomaterial's strong ECL output, as well as the successful DNAzyme-assisted hairpin-free and nuclease-free amplification technique, miRNA-141 could be easily and sensitively detected using the newly developed ECL biosensor. This demonstration of concept research is valuable motivation for creating robust and suitable ECL materials, paving the way for developing hypersensitive biosensing systems. The synthesis procedure for the MXene-based Zr-TCBPE/MXene ECL sensor and the DNAzyme-assisted hairpin-free and nuclease-free amplification techniques are shown in Fig. 19a. The selectivity, stability, and repeatability of the ECL sensor were evaluated. Because of its excellent selectivity, it only identified the target miRNA-141 and disregarded other similar compounds, as shown in Fig. 19b and c. Throughout 12 cycles (0.63% RSD), the sensor's ECL signals showed very little change, indicating stability, as shown in Fig. 19d.

Additionally, it showed good consistency, with variations of only 1.06% when utilizing different electrodes. The sensor did well in all three categories. The findings demonstrated that an increase in miRNA-141 concentration was accompanied by an increase in the sensor's ECL signals. With an acceptable detection limit of 16.2 aM, the sensor showed a strong positive correlation between ECL signals and the logarithm of miRNA-141 levels. This ECL sensor demonstrated improved analytical performance for miRNA-141 detection compared to earlier research.

8. Challenges and future work

The synthesis method for any material will likely have an impact on the properties of the resulting nanomaterial. Every synthesis process produces a different type of nanomaterial with a different structure. The classic or often employed way to create MXenes is to use the HF-etching procedure. The main drawbacks of this approach are that it yields MXenes with subpar quality features and pollutes the environment through massive atmospheric discharge. For instance, the F functionality on the top layer of MXenes is vulnerable to the release of HF during hydrolysis operations due to the excess consumption of HF acid. The detrimental impacts of HF would drastically limit the rate of enzyme synthesis. The dependability and efficiency of HF-etched MXenes in the biological sensing process are severely compromised by their susceptibility to oxidation at room temperature or during the OER procedure. The HF-etching procedure constrains the biomedical applications of MXenes. As a result, dependable, robust, and fluorine-free production procedures are needed to create stable, biodegradable MXene nanocomposites.[170]

Numerous applications that promise to quantify significant biomarkers depend on continued optimization of the ECL enhancement mechanism. The placement of ECL luminophores, radical strength, and the kinetics of the heterogeneous transmission of electron mechanisms in the reactant all affect the rate of the whole reaction. These factors greatly impact the ECL mechanism and the final signaling result.

MXene-based materials have many applications in research and technology. The possibility of employing them as next-generation detectors has attracted a lot of attention. Given this unique 2D material's extraordinary sensing abilities, there is currently a need for further scientific study to apply these materials in sensing devices. However, additional research is

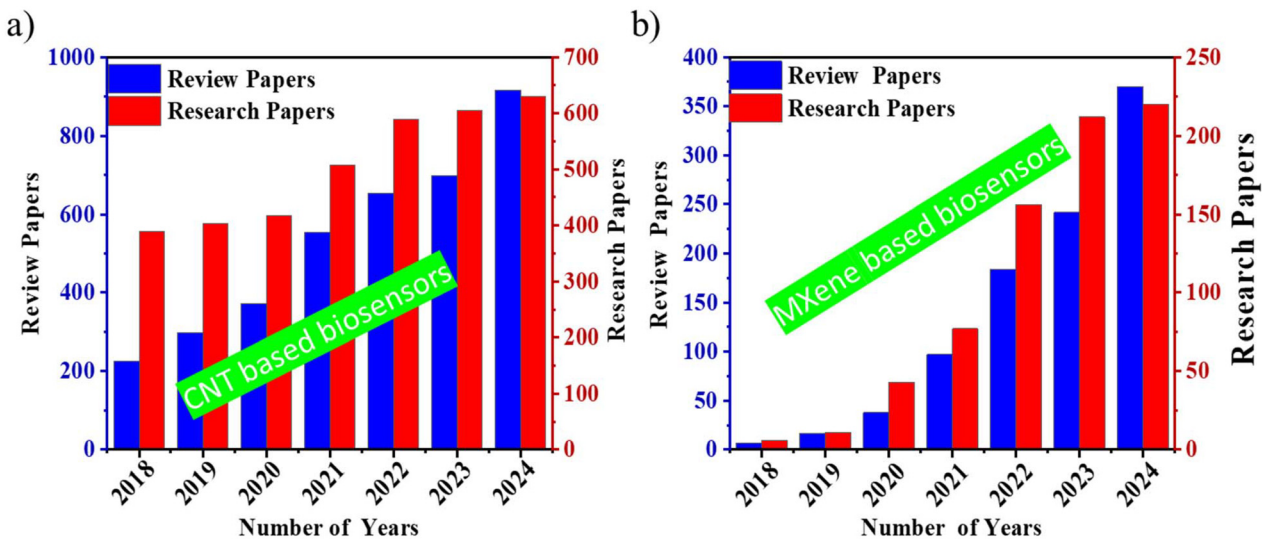

Fig. 20 The number of publications on (a) CNTs and (b) MXene-based biosensors. Data were collected from Sciencedirect using the keywords "biosensor" + "CNTs" or "MXene" for the period Jan 2018 to Aug 2024.

needed on their enhanced functionality, commercial uses, environmental impact, and life cycle analysis.

Despite extensive research on CNTs, CNT-based biosensors continue to have issues. The selectivity and sensitivity of enzymatic sensors for detecting glucose are good. Still, the expensive cost of an enzyme is a limiting factor. Additionally, the chemical characteristics of the enzyme are unstable and susceptible to many influences. The emergence of nonenzymatic sensors enhances electrocatalytic activity and stability. The nonenzymatic sensor has better commercial value and development potential due to its ease of use and financial advantages; this justifies further study. Controlling and fixing the composite material of CNTs and different particles is challenging. Despite various theories and trials, there are still some obstacles to applications and commercialization. More research is still being done on biosensors' properties, such as sensitivity, detection limits, and response times.

Additionally, more technologies ought to be used. This review focuses primarily on electrochemically based biosensors, but their high cost and complex preparation equally constrain them. More affordable materials with comparable or superior performance, like paper- and cloth-based substances, will be preferred to cut production costs. The procedures and processes must be standardized and more straightforward for production applications. The production of biosensors will be automated and on a massive scale thanks to 3D printing and printed circuits. Biosensors can be converted into wearable devices that provide real-time physiological data thanks to the miniaturization of their size, which is enabled by integrated technology and nanotechnology. Additionally, computational models can predict and simulate CNT-based materials and biosensors' mechanical and electrical characteristics, increasing productivity and conserving resources. Interest from scientists increases day by day for creating more promising biosensors composed of CNT- and MXene-based nanomaterials. So, the number of publications increases yearly for synthesizing biosensors by altering the inherent properties of CNTs and MXenes, as shown in Fig. 20a and b.

Biosensors will become more portable, multipurpose, and miniaturized in the future. *In vitro* devices and devices will also be worn on and implanted into the body. CNT-based biosensors will significantly contribute to disease prevention and medical treatments to protect human health and life.

9. Conclusions

Biosensors are crucial in various fields, such as drug development, biomedicine, food safety, and environmental research. Conventional biosensors have limited performance, prompting scientists to develop enhanced biosensors with improved selectivity, sensitivity, stability, and reusability. Carbon nanotubes and MXenes are up-and-coming materials for improved biosensors due to their excellent chemical and physical characteristics and minimal toxicity. MXene is often considered superior for biosensing due to its substantial surface area, exceptional electrical conductivity, and compatibility with moist settings, making it highly efficient for detecting biological targets. MXene exhibits more versatility and stability across a range of temperatures. Although carbon nanotubes possess strength and durability, the chemical flexibility of MXenes makes them more suitable for biosensors designed to operate in water-based conditions. Both materials are highly beneficial for detecting contaminants in food, the environment, and the human body.

Author contributions

Nadeem Hussain Solangi: data curation, formal analysis, investigation, methodology, visualization; writing – original draft. Nabisab Mujawar Mubarak, Rama Rao Karri: conceptualization, methodology, project guidance, supervision, writing – review & editing. Shaukat Ali Mazari, Bharat Prasad Sharma: writing – review & editing.

Data availability

No data were used for the research described in the article.

Conflicts of interest

The authors declare that they have no known competing financial interests or personal relationships that could have appeared to influence the work reported in this paper.

References

1 L. C. Clark, Monitor and control of blood and tissue oxygen tensions, *Trans. – Am. Soc. Artif. Intern. Organs*, 1956, **2**, 41–48.
2 N. H. Solangi, N. M. Mubarak, R. R. Karri, S. A. Mazari and A. S. Jatoi, Advanced growth of 2D MXene for electrochemical sensors, *Environ. Res.*, 2023, **222**, 115279.
3 M. Mathew and C. S. Rout, Electrochemical biosensors based on Ti3C2Tx MXene: future perspectives for on-site analysis, *Curr. Opin. Electrochem.*, 2021, **30**, 100782.
4 W. Ismail, G. Ibrahim, H. Atta, B. Sun, A. El-Shaer and M. Abdelfatah, Improvement of physical and photoelectrochemical properties of TiO_2 nanorods toward biosensor and optoelectronic applications, *Ceram. Int.*, 2024, **50**(10), 17968–17976.
5 S. Chauhan and A. Thakur, Chitosan-based biosensors-A comprehensive Review, *Mater. Today: Proc.*, 2023, DOI: 10.1016/j.matpr.2023.01.123.
6 T. Arakawa, D. V. Dao and K. Mitsubayashi, Biosensors and chemical sensors for healthcare monitoring: a review, *IEEJ Trans. Electr. Electron. Eng.*, 2022, **17**(5), 626–636.
7 F. Cui, Y. Yue, Y. Zhang, Z. Zhang and H. S. Zhou, Advancing biosensors with machine learning, *ACS Sens.*, 2020, **5**(11), 3346–3364.

8 V. Naresh and N. Lee, A review on biosensors and recent development of nanostructured materials-enabled biosensors, *Sensors*, 2021, **21**(4), 1109.
9 M. B. Kulkarni, N. H. Ayachit and T. M. Aminabhavi, Biosensors and microfluidic biosensors: from fabrication to application, *Biosensors*, 2022, **12**(7), 543.
10 M. A. Morales and J. M. Halpern, Guide to selecting a biorecognition element for biosensors, *Bioconjugate Chem.*, 2018, **29**(10), 3231–3239.
11 U. Amara, I. Hussain, M. Ahmad, K. Mahmood and K. Zhang, 2D MXene–based biosensing: a review, *Small*, 2023, **19**(2), 2205249.
12 K. Youssef, A. Ullah, P. Rezai, A. Hasan and A. Amirfazli, Recent advances in biosensors for real-time monitoring of pH, temperature, and oxygen in chronic wounds, *Mater. Today Bio*, 2023, **22**, 100764.
13 A. Wiorek, M. Parrilla, M. Cuartero and G. A. Crespo, Epidermal patch with glucose biosensor: pH and temperature correction toward more accurate sweat analysis during sports practice, *Anal. Chem.*, 2020, **92**(14), 10153–10161.
14 Y. Dong, A. Laaksonen, Q. Gao and X. Ji, Molecular mechanistic insights into the ionic-strength-controlled interfacial behavior of proteins on a TiO2 surface, *Langmuir*, 2021, **37**(39), 11499–11507.
15 S. Panda, S. Hajra, K. Mistewicz, P. In-na, M. Sahu, P. M. Rajaitha and H. J. Kim, Piezoelectric energy harvesting systems for biomedical applications, *Nano Energy*, 2022, **100**, 107514.
16 U. Chadha, P. Bhardwaj, R. Agarwal, P. Rawat, R. Agarwal, I. Gupta, M. Panjwani, S. Singh, C. Ahuja, S. K. Selvaraj, M. Banavoth, P. Sonar, B. Badoni and A. Chakravorty, Recent progress and growth in biosensors technology: A critical review, *J. Ind. Eng. Chem.*, 2022, **109**, 21–51.
17 L. Mei, S. Zhu, Y. Liu, W. Yin, Z. Gu and Y. Zhao, An overview of the use of nanozymes in antibacterial applications, *Chem. Eng. J.*, 2021, **418**, 129431.
18 Y. Liu, Y. Deng, S. Li, F. W. N. Chow, M. Liu and N. He, Monitoring and detection of antibiotic residues in animal derived foods: Solutions using aptamers, *Trends Food Sci. Technol.*, 2022, **125**, 200–235.
19 C. Deepa, L. Rajeshkumar and M. Ramesh, Preparation, synthesis, properties and characterization of graphene-based 2D nano-materials for biosensors and bioelectronics, *J. Mater. Res. Technol.*, 2022, **19**, 2657–2694.
20 A. Hashem, M. M. Hossain, A. R. Marlinda, M. A. Mamun, S. Sagadevan, Z. Shahnavaz, K. Simarani and M. R. Johan, Nucleic acid-based electrochemical biosensors for rapid clinical diagnosis: Advances, challenges, and opportunities, *Crit. Rev. Clin. Lab. Sci.*, 2022, **59**(3), 156–177.
21 T. Dong, N. M. Matos Pires, Z. Yang and Z. Jiang, Advances in electrochemical biosensors based on nanomaterials for protein biomarker detection in saliva, *Adv. Sci.*, 2023, **10**(6), 2205429.
22 M. A. Islam, A. Karim, B. Ethiraj, T. Raihan and A. Kadier, Antimicrobial peptides: Promising alternatives over conventional capture ligands for biosensor-based detection of pathogenic bacteria, *Biotechnol. Adv.*, 2022, **55**, 107901.
23 G. Hu, S. Cui, H. Wang, Y. Shi and Z. Li, Mechanism of high sensitivity proton acids doped polypyrrole molecularly imprinted electrochemical sensor and its application in urea detection, *Talanta*, 2024, **278**, 126514.
24 M. V. Sullivan, C. Fletcher, R. Armitage, C. Blackburn and N. W. Turner, A rapid synthesis of molecularly imprinted polymer nanoparticles for the extraction of performance-enhancing drugs (PIEDs), *Nanoscale Adv.*, 2023, **5**(19), 5352–5360.
25 J. Min, J. Tu, C. Xu, H. Lukas, S. Shin, Y. Yang, S. A. Solomon, D. Mukasa and W. Gao, Skin-interfaced wearable sweat sensors for precision medicine, *Chem. Rev.*, 2023, **123**(8), 5049–5138.
26 Z. Meng and K. A. Mirica, Covalent organic frameworks as multifunctional materials for chemical detection, *Chem. Soc. Rev.*, 2021, **50**(24), 13498–13558.
27 C. Dincer, R. Bruch, E. Costa-Rama, M. T. Fernández–Abedul, A. Merkoçi, A. Manz, G. A. Urban and F. Güder, Disposable sensors in diagnostics, food, and environmental monitoring, *Adv. Mater.*, 2019, **31**(30), 1806739.
28 S. A. Ozkan and E. Zor, Recent trends in sensors and diagnostics, *TrAC, Trends Anal. Chem.*, 2024, **172**, 117575.
29 M. Pirzada and Z. Altintas, Historical development of sensing technology, in *Fundamentals of Sensor Technology*, Woodhead Publishing, 2023, pp. 3–16.
30 R. Kashyap, A. Chauhan, A. Negi, G. R. Chaudhary and R. K. Sharma, Biosensors, in *Advanced Materials for Biomedical Applications: Development and Processing*, Springer Nature Singapore, Singapore, 2023, pp. 167–183.
31 A. Williams, M. R. Aguilar, K. G. Pattiya Arachchillage, S. Chandra, S. Rangan, S. Ghosal Gupta and J. M. Artes Vivancos, Biosensors for Public Health and Environmental Monitoring: The Case for Sustainable Biosensing, *ACS Sustainable Chem. Eng.*, 2024, **12**(28), 10296–10312.
32 C. Zhu, Z. Feng, H. Qin, L. Chen, M. Yan, L. Li and F. Qu, Recent progress of SELEX methods for screening nucleic acid aptamers, *Talanta*, 2024, **266**, 124998.
33 A. Brown, J. Brill, R. Amini, C. Nurmi and Y. Li, Development of better aptamers: structured library approaches, selection methods, and chemical modifications, *Angew. Chem., Int. Ed.*, 2024, **63**(16), e202318665.
34 M. Wolfe, A. Cramer, S. Webb, E. Goorskey, Y. Chushak, P. Mirau, N. Arroyo-Currás and J. L. Chávez, Rational Approach to Optimizing Conformation-Switching Aptamers for Biosensing Applications, *ACS Sens.*, 2024, **9**(2), 717–725.
35 E. E. Ferapontova, DNA electrochemistry and electrochemical sensors for nucleic acids, *Annu. Rev. Anal. Chem.*, 2018, **11**(1), 197–218.
36 Z. Yang, J. Guo, L. Wang, J. Zhang, L. Ding, H. Liu and X. Yu, Nanozyme–Enhanced Electrochemical Biosensors: Mechanisms and Applications, *Small*, 2024, **20**(14), 2307815.

37 Y. Zhou, B. Liu, R. Yang and J. Liu, Filling in the gaps between nanozymes and enzymes: challenges and opportunities, *Bioconjugate Chem.*, 2017, **28**(12), 2903–2909.
38 M. Aghaee, M. Salehipour, S. Rezaei and M. Mogharabi-Manzari, Bioremediation of organic pollutants by laccase-metal–organic framework composites: A review of current knowledge and future perspective, *Bioresour. Technol.*, 2024, 131072.
39 J. Song, H. Liu, Z. Zhao, P. Lin and F. Yan, Flexible organic transistors for biosensing: devices and applications, *Adv. Mater.*, 2024, **36**(20), 2300034.
40 J. Zou, H. Bai, L. Zhang, Y. Shen, C. Yang, W. Zhuang, J. Hu, Y. Yao and W. Hu, Ion-sensitive field effect transistor biosensors for biomarker detection: current progress and challenges, *J. Mater. Chem. B*, 2024, 8523–8542.
41 D. Bhatia, S. Paul, T. Acharjee and S. S. Ramachairy, Biosensors and their widespread impact on human health, *Sens. Int.*, 2024, **5**, 100257.
42 K. Kant, R. Beeram, L. G. Cabaleiro, Y. Cao, D. Quesada-González, H. Guo, S. Gomez-Grana, Y. Joung, S. Kothadiya, D. García-Lojo and M. Lafuente, Roadmap for Plasmonic Nanoparticle Sensors: Current Progress, Challenges and Future Prospects, *Nanoscale Horiz.*, 2024, DOI: **10.1039/D4NH00226A**.
43 H. Chen, S. Cai, J. Luo, X. Liu, L. Ou, Q. Zhang, B. Liedberg and Y. Wang, Colorimetric biosensing assays based on gold nanoparticles functionalized/combined with non-antibody recognition elements, *TrAC, Trends Anal. Chem.*, 2024, 117654.
44 M. Pourmadadi, A. Ghaemi, A. Khanizadeh, F. Yazdian, Y. Mollajavadi, R. Arshad and A. Rahdar, Breast Cancer Detection based on Cancer Antigen 15–3; emphasis on Optical and Electrochemical methods: a review, *Biosens. Bioelectron.*, 2024, 116425.
45 R. I. Boysen, L. J. Schwarz, D. V. Nicolau and M. T. Hearn, Molecularly imprinted polymer membranes and thin films for the separation and sensing of biomacromolecules, *J. Sep. Sci.*, 2017, **40**(1), 314–335.
46 H. Nasrollahpour, A. Mirzaie, M. Sharifi, A. Rezabakhsh, B. Khalilzadeh, R. Rahbarghazi, H. Yousefi and D. J. Klionsky, Biosensors; a novel concept in real-time detection of autophagy, *Biosens. Bioelectron.*, 2024, 116204.
47 A. Kłos-Witkowska and V. Martsenyuk, Investigation of biosensor potential component stability caused by influence of external condition, *Ecol. Chem. Eng. S*, 2019, **26**(4), 665–674.
48 P. Bhattarai and S. Hameed, Basics of biosensors and nanobiosensors, in *Nanobiosensors: From Design to Applications*, 2020, pp. 1–22.
49 P. S. Chary, R. Bhawale, R. Vasave, N. Rajana, P. K. Singh, J. Madan, S. B. Singh and N. K. Mehra, A review on emerging role of multifunctional carbon nanotubes as an armament in cancer therapy, imaging and biosensing, *J. Drug Delivery Sci. Technol.*, 2023, **85**, 104588.
50 U. Degirmenci and M. Kirca, Carbon-based nano lattice hybrid structures: Mechanical and thermal properties, *Phys. E*, 2022, **144**, 115392.
51 A. M. Musa, J. Kiely, R. Luxton and K. C. Honeychurch, An Electrochemical screen-printed Sensor based on gold-nanoparticle-decorated reduced Graphene Oxide–Carbon nanotubes composites for the determination of 17-β estradiol, *Biosensors*, 2023, **13**(4), 491.
52 R. R. Karri, N. H. Solangi, N. M. Mubarak, A. S. Jatoi, L. P. Lingamdinne, J. R. Koduru, M. H. Dehghani and N. A. Khan, Carbon nanotubes for sustainable renewable energy applications, in *Water treatment using engineered carbon nanotubes*, Elsevier, 2024, pp. 433–456.
53 N. Anzar, R. Hasan, M. Tyagi, N. Yadav and J. Narang, Carbon nanotube-A review on Synthesis, Properties and plethora of applications in the field of biomedical science, *Sens. Int.*, 2020, **1**, 100003.
54 A. Eatemadi, H. Daraee, H. Karimkhanloo, M. Kouhi, N. Zarghami, A. Akbarzadeh, M. Abasi, Y. Hanifehpour and S. W. Joo, Carbon nanotubes: properties, synthesis, purification, and medical applications, *Nanoscale Res. Lett.*, 2014, **9**, 1–13.
55 Y. Zeng, Z. Zhu, D. Du and Y. Lin, Nanomaterial-based electrochemical biosensors for food safety, *J. Electroanal. Chem.*, 2016, **781**, 147–154.
56 N. H. Solangi, R. R. Karri, N. M. Mubarak, A. S. Jatoi, R. Petra, S. A. Lim, L. P. Lingamdinne and J. R. Koduru, Applications of carbon nanotubes-based biosensors: a comprehensive review, in *Water treatment using engineered carbon nanotubes*, 2024, pp. 457–477.
57 H. Meskher, T. Ragdi, A. K. Thakur, S. Ha, I. Khelfaoui, R. Sathyamurthy, S. W. Sharshir, A. K. Pandey, R. Saidur, P. Singh and F. Sharifian Jazi, A review on CNTs-based electrochemical sensors and biosensors: unique properties and potential applications, *Crit. Rev. Anal. Chem.*, 2023, 1–24.
58 M. Sireesha, V. Jagadeesh Babu, A. S. Kranthi Kiran and S. Ramakrishna, A review on carbon nanotubes in biosensor devices and their applications in medicine, *Nanocomposites*, 2018, **4**(2), 36–57.
59 N. H. Solangi, S. A. Mazari, N. M. Mubarak, R. R. Karri, N. Rajamohan and D. V. N. Vo, Recent trends in MXene-based material for biomedical applications, *Environ. Res.*, 2023, **222**, 115337.
60 N. H. Solangi, N. M. Mubarak, R. R. Karri, S. A. Mazari and A. S. Jatoi, Advanced growth of 2D MXene for electrochemical sensors, *Environ. Res.*, 2023, **222**, 115279.
61 N. H. Solangi, N. M. Mubarak, R. R. Karri, S. A. Mazari, S. K. Kailasa and A. Alfantazi, Applications of advanced MXene-based composite membranes for sustainable water desalination, *Chemosphere*, 2023, **314**, 137643.
62 N. H. Solangi, R. R. Karri, N. M. Mubarak, S. A. Mazari and A. K. Azad, Emerging 2D MXenes as next-generation materials for energy storage applications, *J. Energy Storage*, 2023, **70**, 108004.
63 N. H. Solangi, N. M. Mubarak, R. R. Karri, S. A. Mazari and J. R. Koduru, Recent development of graphene and

MXene-based nanomaterials for proton exchange membrane fuel cells, *Int. J. Hydrogen Energy*, 2024, **73**, 905–931.
64 N. H. Solangi, A. Abbas, N. M. Mubarak, R. R. Karri, S. H. Aleithan, J. Kazmi, W. Ahmad and K. Khan, Insight Mechanism of MXene for Future Generation Highly Efficient Energy Storage Device, *Mater. Today Sustainability*, 2024, 100896.
65 J. Yoon, M. Shin, J. Lim, J. Y. Lee and J. W. Choi, Recent advances in MXene nanocomposite-based biosensors, *Biosensors*, 2020, **10**(11), 185.
66 N. H. Solangi, R. R. Karri, N. M. Mubarak, S. A. Mazari, A. S. Jatoi and J. R. Koduru, Emerging 2D MXene-based adsorbents for hazardous pollutants removal, *Desalination*, 2023, **549**, 116314.
67 N. H. Solangi, R. R. Karri, S. A. Mazari, N. M. Mubarak, A. S. Jatoi, G. Malafaia and A. K. Azad, MXene as emerging material for photocatalytic degradation of environmental pollutants, *Coord. Chem. Rev.*, 2023, **477**, 214965.
68 N. H. Solangi, N. M. Mubarak, R. R. Karri, S. A. Mazari, S. K. Kailasa and A. Alfantazi, Applications of advanced MXene-based composite membranes for sustainable water desalination, *Chemosphere*, 2023, **314**, 137643.
69 Q. Xu, S. Chen, J. Xu, X. Duan, L. Lu, Q. Tian, X. Zhang, Y. Cai, X. Lu, L. Rao and Y. Yu, Facile synthesis of hierarchical MXene/ZIF-67/CNTs composite for electrochemical sensing of luteolin, *J. Electroanal. Chem.*, 2021, **880**, 114765.
70 L. M. Esteves, H. A. Oliveira and F. B. Passos, Carbon nanotubes as catalyst support in chemical vapor deposition reaction: A review, *J. Ind. Eng. Chem.*, 2018, **65**, 1–12.
71 N. Arora and N. N. Sharma, Arc discharge synthesis of carbon nanotubes: Comprehensive review, *Diamond Relat. Mater.*, 2014, **50**, 135–150.
72 N. Liu, N. Lu, Y. Su, P. Wang and X. Quan, Fabrication of g-C3N4/Ti3C2 composite and its visible-light photocatalytic capability for ciprofloxacin degradation, *Sep. Purif. Technol.*, 2019, **211**, 782–789.
73 F. Qiu, Z. Wang, M. Liu, Z. Wang and S. Ding, Synthesis, characterization and microwave absorption of MXene/$NiFe_2O_4$ composites, *Ceram. Int.*, 2021, **47**(17), 24713–24720.
74 J. Mei, G. A. Ayoko, C. Hu and Z. Sun, Thermal reduction of sulfur-containing MAX phase for MXene production, *Chem. Eng. J.*, 2020, **395**, 125111.
75 S. Iijima, Helical microtubules of graphitic carbon, *Nature*, 1991, **354**(6348), 56–58.
76 U. Kumar and B. C. Yadav, State of art: an approach to the synthesis of pure and doped graphene, *Adv. Sci., Eng. Med.*, 2018, **10**(7–8), 638–644.
77 C. J. Lee, D. W. Kim, T. J. Lee, Y. C. Choi, Y. S. Park, Y. H. Lee, W. B. Choi, N. S. Lee, G. S. Park and J. M. Kim, Synthesis of aligned carbon nanotubes using thermal chemical vapor deposition, *Chem. Phys. Lett.*, 1999, **312**(5–6), 461–468.
78 R. J. Nemanich, J. A. Carlisle, A. Hirata and K. Haenen, CVD diamond—Research, applications, and challenges, *MRS Bull.*, 2014, **39**(6), 490–494.
79 I. S. Merenkov, H. Katsui, M. N. Khomyakov, V. S. Sulyaeva, R. V. Pushkarev, R. Tu, T. Goto and M. L. Kosinova, Extraordinary synergetic effect of precursors in laser CVD deposition of SiBCN films, *J. Eur. Ceram. Soc.*, 2019, **39**(16), 5123–5131.
80 T. Guo, P. Nikolaev, A. Thess, D. T. Colbert and R. E. Smalley, Catalytic growth of single-walled manotubes by laser vaporization, *Chem. Phys. Lett.*, 1995, **243**(1–2), 49–54.
81 J. Prasek, J. Drbohlavova, J. Chomoucka, J. Hubalek, O. Jasek, V. Adam and R. Kizek, Methods for carbon nanotubes synthesis, *J. Mater. Chem.*, 2011, **21**(40), 15872–15884.
82 J. Benjamin, G. Jency, G. Vijila, J. Benjamin, G. Jency and G. Vijila, A review of different etching methodologies and impact of various etchants in wet etching in micro fabrication, *Int. J. Innovative Res. Sci. Eng. Technol.*, 2014, **3**, 558–564.
83 C. Prasad, X. Yang, Q. Liu, H. Tang, A. Rammohan, S. Zulfiqar, G. V. Zyryanov and S. Shah, Recent advances in MXenes supported semiconductors based photocatalysts: Properties, synthesis and photocatalytic applications, *J. Ind. Eng. Chem.*, 2020, **85**, 1–33.
84 C. O. Ujah, D. V. V. Kallon and V. S. Aigbodion, Tribological properties of CNTs-reinforced nanocomposite materials, *Lubricants*, 2023, **11**(3), 95.
85 C. A. Dyke and J. M. Tour, Covalent functionalization of single-walled carbon nanotubes for materials applications, *J. Phys. Chem. A*, 2004, **108**(51), 11151–11159.
86 L. Meng, C. Fu and Q. Lu, Advanced technology for functionalization of carbon nanotubes, *Prog. Nat. Sci.*, 2009, **19**(7), 801–810.
87 Y. L. Zhao and J. F. Stoddart, Noncovalent functionalization of single-walled carbon nanotubes, *Acc. Chem. Res.*, 2009, **42**(8), 1161–1171.
88 G. Li, X. Wan, Q. Zheng, M. Yang, Y. Xia, X. Qi, T. Wang and Z. Wu, Deep eutectic solvent-mediated synthesis of $ZnCo_2O_4$/MWCNT-COOH: Investigation of electrocatalytic activity for gatifloxacin detection, *Colloids Surf., A*, 2024, **699**, 134713.
89 C. K. Thakur, C. Karthikeyan, M. S. Abou-Dahech, M. M. A. Altabakha, M. J. S. Al Shahwan, C. R. Ashby Jr, A. K. Tiwari, R. J. Babu and N. S. H. N. Moorthy, Microwave-assisted functionalization of multi-walled carbon nanotubes for biosensor and drug delivery applications, *Pharmaceutics*, 2023, **15**(2), 335.
90 Y. Zhou, Y. Fang and R. P. Ramasamy, Non-covalent functionalization of carbon nanotubes for electrochemical biosensor development, *Sensors*, 2019, **19**(2), 392.
91 Y. T. Liu, W. Zhao, Z. Y. Huang, Y. F. Gao, X. M. Xie, X. H. Wang and X. Y. Ye, Noncovalent surface modification of carbon nanotubes for solubility in organic solvents, *Carbon*, 2006, **44**(8), 1613–1616.
92 Y. P. Bernal, J. Alvarado, R. L. Juárez, E. A. de Vasconcelos, W. M. de Azevedo and B. S. Soto-Cruz, Synthesis and characterization of carbon nanotubes/silica composites using gum Arabic, *Mater. Res. Express*, 2018, **5**(7), 075028.

93 N. A. Zulkifli, N. H. Ismail, M. Jaafar and A. R. Othman, Effect of carbon nanotubes on the flexural properties and flammability of carbon fiber/epoxy multi–scale composites, *Materialwiss. Werkstofftech.*, 2022, **53**(12), 1544–1550.
94 M. Matiyani, M. Pathak, B. S. Bohra and N. G. Sahoo, Noncovalent functionalization of carbon nanotubes, in *Handbook of Carbon Nanotubes*, Springer International Publishing, Cham, 2022, pp. 421–448.
95 N. Mohd Nurazzi, M. M. Asyraf, A. Khalina, N. Abdullah, F. A. Sabaruddin, S. H. Kamarudin, S. B. Ahmad, A. M. Mahat, C. L. Lee, H. A. Aisyah and M. N. F. Norrrahim, Fabrication, functionalization, and application of carbon nanotube-reinforced polymer composite: An overview, *Polymers*, 2021, **13**(7), 1047.
96 E. Blasco, M. B. Sims, A. S. Goldmann, B. S. Sumerlin and C. Barner-Kowollik, 50th anniversary perspective: polymer functionalization, *Macromolecules*, 2017, **50**(14), 5215–5252.
97 Y. Liu, X. Wang, K. Qi and J. H. Xin, Functionalization of cotton with carbon nanotubes, *J. Mater. Chem.*, 2008, **18**(29), 3454–3460.
98 S. Mallakpour and S. Soltanian, Surface functionalization of carbon nanotubes: fabrication and applications, *RSC Adv.*, 2016, **6**(111), 109916–109935.
99 R. Ibragimova, P. Erhart, P. Rinke and H. P. Komsa, Surface functionalization of 2D MXenes: trends in distribution, composition, and electronic properties, *J. Phys. Chem. Lett.*, 2021, **12**(9), 2377–2384.
100 A. S. Jatoi, N. M. Mubarak, Z. Hashmi, N. H. Solangi, R. R. Karri, Y. H. Tan, S. A. Mazari, J. R. Koduru and A. Alfantazi, New insights into MXene applications for sustainable environmental remediation, *Chemosphere*, 2023, **313**, 137497.
101 I. Raheem, N. M. Mubarak, R. R. Karri, N. H. Solangi, A. S. Jatoi, S. A. Mazari, M. Khalid, Y. H. Tan, J. R. Koduru and G. Malafaia, Rapid growth of MXene-based membranes for sustainable environmental pollution remediation, *Chemosphere*, 2023, **311**, 137056.
102 N. H. Solangi, N. M. Mubarak, R. R. Karri, S. A. Mazari, A. S. Jatoi, J. R. Koduru and M. H. Dehghani, MXene-based phase change materials for solar thermal energy storage, *Energy Convers. Manage.*, 2022, **273**, 116432.
103 J. Chen, Q. Huang, H. Huang, L. Mao, M. Liu, X. Zhang and Y. Wei, Recent progress and advances in the environmental applications of MXene related materials, *Nanoscale*, 2020, **12**(6), 3574–3592.
104 N. H. Solangi, R. R. Karri, N. M. Mubarak and S. A. Mazari, Mechanism of polymer composite-based nanomaterial for biomedical applications, *Adv. Ind. Eng. Polym. Res.*, 2024, **7**(1), 1–19.
105 Y. Xia, T. S. Mathis, M. Q. Zhao, B. Anasori, A. Dang, Z. Zhou, H. Cho, Y. Gogotsi and S. Yang, Thickness-independent capacitance of vertically aligned liquid-crystalline MXenes, *Nature*, 2018, **557**(7705), 409–412.
106 X. He, S. Koo, E. Obeng, A. Sharma, J. Shen and J. S. Kim, Emerging 2D MXenes for antibacterial applications: Current status, challenges, and prospects, *Coord. Chem. Rev.*, 2023, **492**, 215275.
107 X. Tao, Y. Zhao, S. Wang, C. Li and R. Li, Recent advances and perspectives for solar-driven water splitting using particulate photocatalysts, *Chem. Soc. Rev.*, 2022, **51**(9), 3561–3608.
108 M. Mozafari and M. Soroush, Surface functionalization of MXenes, *Mater. Adv.*, 2021, **2**(22), 7277–7307.
109 I. A. Vasyukova, O. V. Zakharova, D. V. Kuznetsov and A. A. Gusev, Synthesis, toxicity assessment, environmental and biomedical applications of MXenes: A review, *Nanomaterials*, 2022, **12**(11), 1797.
110 B. Earp, D. Dunn, J. Phillips, R. Agrawal, T. Ansell, P. Aceves, I. De Rosa, W. Xin and C. Luhrs, Enhancement of electrical conductivity of carbon nanotube sheets through copper addition using reduction expansion synthesis, *Mater. Res. Bull.*, 2020, **131**, 110969.
111 F. Shahzad, A. Iqbal, H. Kim and C. M. Koo, 2D transition metal carbides (MXenes): applications as an electrically conducting material, *Adv. Mater.*, 2020, **32**(51), 2002159.
112 L. Deng, S. J. Eichhorn, C. C. Kao and R. J. Young, The effective Young's modulus of carbon nanotubes in composites, *ACS Appl. Mater. Interfaces*, 2011, **3**(2), 433–440.
113 M. Chen, B. B. Murphy, Y. Wang, F. Vitale and S. Yang, SMART Silly Putty: Stretchable, Malleable, Adherable, Reusable, and Tear–Resistible Hydrogels, *Small*, 2023, **19**(6), 2205854.
114 K. L. Firestein, J. E. von Treifeldt, D. G. Kvashnin, J. F. Fernando, C. Zhang, A. G. Kvashnin, E. V. Podryabinkin, A. V. Shapeev, D. P. Siriwardena, P. B. Sorokin and D. Golberg, Young's modulus and tensile strength of Ti_3C_2 MXene nanosheets as revealed by in situ TEM probing, AFM nanomechanical mapping, and theoretical calculations, *Nano Lett.*, 2020, **20**(8), 5900–5908.
115 Y. Jin, J. Geng, Y. Wang, Z. Zhao, Z. Chen, Z. Guo, L. Pei, F. Ren, Z. Sun and P. G. Ren, Flexible all-solid-state asymmetric supercapacitor based on Ti_3C_2Tx MXene/graphene/carbon nanotubes, *Surf. Interfaces*, 2024, **53**, 104999.
116 B. Song, F. Liu, H. Wang, J. Miao, Y. Chen, P. Kumar, H. Zhang, X. Liu, H. Gu, E. A. Stach and X. Liang, Giant gate-tunability of complex refractive index in semiconducting carbon nanotubes, *ACS Photonics*, 2020, **7**(10), 2896–2905.
117 J. Ji, L. Zhao, Y. Shen, S. Liu and Y. Zhang, Covalent stabilization and functionalization of MXene via silylation reactions with improved surface properties, *FlatChem*, 2019, **17**, 100128.
118 T. Zhang, X. Guo, B. Solomon, M. Sharifpur and L. Z. Zhang, A hydrophobic-hydrophilic MXene/PVDF composite hollow fiber membrane with enhanced antifouling properties for seawater desalination, *J. Membr. Sci.*, 2022, **644**, 120146.
119 Y. Xu, Y. S. Ang, L. Wu and L. K. Ang, High sensitivity surface plasmon resonance sensor based on two-dimensional MXene and transition metal dichalcogenide: a theoretical study, *Nanomaterials*, 2019, **9**(2), 165.

120 M. A. A. M. Abdah, H. T. A. Awan, M. Mehar, M. N. Mustafa, R. Walvekar, M. W. Alam, M. Khalid, R. Umapathi and V. Chaudhary, Advancements in MXene-polymer composites for high-performance supercapacitor applications, *J. Energy Storage*, 2023, **63**, 106942.
121 G. Zhang, T. Wang, Z. Xu, M. Liu, C. Shen and Q. Meng, Synthesis of amino-functionalized Ti 3 C 2 T x MXene by alkalization-grafting modification for efficient lead adsorption, *Chem. Commun.*, 2020, **56**(76), 11283–11286.
122 N. H. Solangi, R. R. Karri, S. A. Mazari, N. M. Mubarak, A. S. Jatoi, G. Malafaia and A. K. Azad, MXene is an emerging material for photocatalytic degradation of environmental pollutants, *Coord. Chem. Rev.*, 2023, **477**, 214965.
123 W. Zhang, X. X. Ji and M. G. Ma, Emerging MXene/cellulose composites: Design strategies and diverse applications, *Chem. Eng. J.*, 2023, **458**, 141402.
124 R. Verma, P. Thakur, A. Chauhan, R. Jasrotia and A. Thakur, A review on MXene and its' composites for electromagnetic interference (EMI) shielding applications, *Carbon*, 2023, **208**, 170–190.
125 N. M. Mubarak, N. H. Solangi, R. R. Karri, Y. H. Tan, S. Shams, K. N. Ruslan, S. A. Mazari and M. Khalid, Holistic Mechanism of Nanomaterials for Removal of Cd2+ from the Wastewater, *Water, Air, Soil Pollut.*, 2024, **235**(4), 1–27.
126 N. H. Solangi, R. R. Karri, N. M. Mubarak and S. A. Mazari, Comparative analysis of the Carbon Nanotubes and Emerging MXene for CO_2 capture and storage, *Process Saf. Environ. Prot.*, 2024, 1012–1037.
127 Z. Li, Z. Zhuang, F. Lv, H. Zhu, L. Zhou, M. Luo, J. Zhu, Z. Lang, S. Feng, W. Chen and L. Mai, The marriage of the FeN4 moiety and MXene boosts oxygen reduction catalysis: Fe 3d electron delocalization matters, *Adv. Mater.*, 2018, **30**(43), 1803220.
128 K. Conley and A. J. Karttunen, Bridging the junction: Electrical conductivity of carbon nanotube networks, *J. Phys. Chem. C*, 2022, **126**(40), 17266–17274.
129 N. H. Solangi, R. R. Karri, N. M. Mubarak, S. A. Mazari and A. K. Azad, Emerging 2D MXenes as next-generation materials for energy storage applications, *J. Energy Storage*, 2023, **70**, 108004.
130 N. H. Solangi, N. M. Mubarak, R. R. Karri, S. A. Mazari and J. R. Koduru, Holistic mechanism of graphene oxide and MXene-based membrane for the desalination processes, *Desalination*, 2023, 117035.
131 F. Q. Liu, X. Liu, L. Sun, R. Li, C. X. Yin and B. Wu, MXene-supported stable adsorbents for superior CO2 capture, *J. Mater. Chem. A*, 2021, **9**(21), 12763–12771.
132 K. Farhana, K. Kadirgama, A. S. F. Mahamude and R. Jose, Review of MXenes as a component in smart textiles and an adsorbent for textile wastewater remediation, *Chin. Chem. Lett.*, 2024, **35**(2), 108533.
133 N. H. Solangi, N. M. Mubarak, R. R. Karri, S. A. Mazari, A. S. Jatoi, J. R. Koduru and M. H. Dehghani, MXene-based phase change materials for solar thermal energy storage, *Energy Convers. Manage.*, 2022, **273**, 116432.
134 S. Li, R. Xu, J. Wang, Y. Yang, Q. Fu and C. Pan, Ultra-stretchable, super-hydrophobic and high-conductive composite for wearable strain sensors with high sensitivity, *J. Colloid Interface Sci.*, 2022, **617**, 372–382.
135 D. Maiti, X. Tong, X. Mou and K. Yang, Carbon-based nanomaterials for biomedical applications: a recent study, *Front. Pharmacol.*, 2019, **9**, 1401.
136 E. Ahmadian, D. Janas, A. Eftekhari and N. Zare, Application of carbon nanotubes in sensing/monitoring of pancreas and liver cancer, *Chemosphere*, 2022, **302**, 134826.
137 M. Gaur, C. Misra, A. B. Yadav, S. Swaroop, F. Ó Maolmhuaidh, M. Bechelany and A. Barhoum, Biomedical applications of carbon nanomaterials: fullerenes, quantum dots, nanotubes, nanofibers, and graphene, *Materials*, 2021, **14**(20), 5978.
138 S. Yu, H. Tang, D. Zhang, S. Wang, M. Qiu, G. Song, D. Fu, B. Hu and X. Wang, MXenes as emerging nanomaterials in water purification and environmental remediation, *Sci. Total Environ.*, 2022, **811**, 152280.
139 B. Patrick, T. Akhtar, R. Kousar, C. C. Huang and X. G. Li, Carbon nanomaterials: emerging roles in Immuno-Oncology, *Int. J. Mol. Sci.*, 2023, **24**(7), 6600.
140 F. S. A. Khan, N. M. Mubarak, Y. H. Tan, M. Khalid, R. R. Karri, R. Walvekar, E. C. Abdullah, S. Nizamuddin and S. A. Mazari, A comprehensive review on magnetic carbon nanotubes and carbon nanotube-based buckypaper for removal of heavy metals and dyes, *J. Hazard. Mater.*, 2021, **413**, 125375.
141 S. Muniandy, S. J. Teh, K. L. Thong, A. Thiha, I. J. Dinshaw, C. W. Lai, F. Ibrahim and B. F. Leo, Carbon nanomaterial-based electrochemical biosensors for foodborne bacterial detection, *Crit. Rev. Anal. Chem.*, 2019, **49**(6), 510–533.
142 E. Kosri, F. Ibrahim, A. Thiha and M. Madou, Micro and nano interdigitated electrode array (IDEA)-based MEMS/NEMS as electrochemical transducers: a review, *Nanomaterials*, 2022, **12**(23), 4171.
143 X. Ji, Z. Liu, Y. Xiao, Y. Xi, W. Wang, W. Lyu, T. Wang, Z. Qi and H. Yang, Combining nanoflares biosensor and mathematical resolution technique for multi-class mycotoxin analysis in complex food matrices, *Food Chem.*, 2023, **402**, 134487.
144 S. Azimi, A. Farahani and H. Sereshti, Plasma-functionalized highly aligned CNT–based biosensor for point of care determination of glucose in human blood plasma, *Electroanalysis*, 2020, **32**(2), 394–403.
145 M. Bolourinezhad, M. Rezayi, Z. Meshkat, S. Soleimanpour, M. Mojarrad, S. H. Aghaee-Bakhtiari and S. M. Taghdisi, Design of a rapid electrochemical biosensor based on MXene/Pt/C nanocomposite and DNA/RNA hybridization for the detection of COVID-19, *Talanta*, 2023, **265**, 124804.
146 V. Osuna, A. Vega-Rios, E. A. Zaragoza-Contreras, I. A. Estrada-Moreno and R. B. Dominguez, Progress of polyaniline glucose sensors for diabetes mellitus manage-

ment utilizing enzymatic and non-enzymatic detection, *Biosensors*, 2022, **12**(3), 137.

147 M. F. Hossain and G. Slaughter, PtNPs decorated chemically derived graphene and carbon nanotubes for sensitive and selective glucose biosensing, *J. Electroanal. Chem.*, 2020, **861**, 113990.

148 Z. Sun, H. Liu and X. Wang, Thermal self-regulatory intelligent biosensor based on carbon-nanotubes-decorated phase-change microcapsules for enhancement of glucose detection, *Biosens. Bioelectron.*, 2022, **195**, 113586.

149 M. Yang, H. Wang, P. Liu and J. Cheng, A 3D electrochemical biosensor based on Super-Aligned Carbon NanoTube array for point-of-care uric acid monitoring, *Biosens. Bioelectron.*, 2021, **179**, 113082.

150 C. Yuan, Z. He, Q. Chen, X. Wang, C. Zhai and M. Zhu, Selective and efficacious photoelectrochemical detection of ciprofloxacin based on the self-assembly of 2D/2D g-C_3N_4/Ti_3C_2 composites, *Appl. Surf. Sci.*, 2021, **539**, 148241.

151 N. B. Messaoud, M. E. Ghica, C. Dridi, M. B. Ali and C. M. Brett, Electrochemical sensor based on multiwalled carbon nanotube and gold nanoparticle modified electrode for the sensitive detection of bisphenol A, *Sens. Actuators, B*, 2017, **253**, 513–522.

152 S. Guo, Y. Lin, Z. Lian, T. Zeng, L. Wang, R. Ye, B. Hong, Q. Liang, Q. Wu, J. Hu and A. Li, A label-free ultrasensitive microRNA-21 electrochemical biosensor based on MXene (Ti_3C_2)-reduced graphene oxide-Au nanocomposites, *Microchem. J.*, 2023, **190**, 108656.

153 Y. Lu, C. Ding, J. Guo, W. Gan, P. Chen, R. Chen, Q. Ling, M. Zhang, P. Wang and Z. Sun, Cobalt-doped ZnAl-LDH nanosheet arrays as recyclable piezo-catalysts for effective activation of peroxymonosulfate to degrade norfloxacin: non-radical pathways and theoretical calculation studies, *Nano Energy*, 2023, **112**, 108515.

154 R. Devaraj and L. A. Kumar, Circulating microRNA as a potential biomarker and its nanotechnology based detection methods: A literature review, *Nanomed. J.*, 2023, **10**(3), 171–179.

155 P. R. de Oliveira, C. Kalinke, J. A. Bonacin, L. H. Marcolino-Junior, M. F. Bergamini and B. C. Janegitz, Carbon-Based Materials for Electrochemical Sensing of SARS-CoV-2, in *COVID-19 Metabolomics and Diagnosis: Chemical Science for Prevention and Understanding Outbreaks of Infectious Diseases*, Springer International Publishing, Cham, 2023, pp. 41–62.

156 K. Ahmad, W. Raza, A. Alsulmi and H. Kim, Design and fabrication of MnO_2@ ZIF-8 composite for electrochemical sensing of environment pollutant hydrogen peroxide, *Colloids Surf., A*, 2023, **674**, 131937.

157 N. Ebrahimi, J. B. Raoof, R. Ojani and M. Ebrahimi, Designing a novel DNA-based electrochemical biosensor to determine of Ba^{2+} ions both selectively and sensitively, *Anal. Biochem.*, 2022, **642**, 114563.

158 J. Chung, H. Yin, R. Wang, Y. Wang, J. Zhang, Y. Peng, J. W. Han, S. Ryu and J. Li, Applying heteroatom co-doped carbon nanotube for manifesting high performance in the electrochemical reduction of aqueous nitrogen oxide by gold nanoparticles, *Nano Res.*, 2024, **17**(3), 1151–1164.

159 M. J. Kang, Y. W. Cho and T. H. Kim, Progress in nanobiosensors for non-invasive monitoring of stem cell differentiation, *Biosensors*, 2023, **13**(5), 501.

160 F. Ghorbanizamani, H. Moulahoum, E. Guler Celik and S. Timur, Material Design in Implantable Biosensors toward Future Personalized Diagnostics and Treatments, *Appl. Sci.*, 2023, **13**(7), 4630.

161 X. Su, Q. You, L. Zhuang, Z. Chang, M. Ge, L. Yang and W. F. Dong, Bifunctional electrochemical biosensor based on PB-MXene films for the real-time analysis and detection of living cancer cells, *J. Pharm. Biomed. Anal.*, 2023, **234**, 115479.

162 X. Sun, J. Sun, Y. Ye, J. Ji, L. Sheng, D. Yang and X. Sun, Metabolic pathway-based self-assembled Au@ MXene liver microsome electrochemical biosensor for rapid screening of aflatoxin B1, *Bioelectrochemistry*, 2023, **151**, 108378.

163 M. A. Zamzami, G. Rabbani, A. Ahmad, A. A. Basalah, W. H, Al-Sabban, S. N. Ahn and H. Choudhry, Carbon nanotube field-effect transistor (CNT-FET)-based biosensor for rapid detection of SARS-CoV-2 (COVID-19) surface spike protein S1, *Bioelectrochemistry*, 2022, **143**, 107982.

164 X. Li, Y. Zhao, J. Chen, Y. Mi, Z. He and F. Gao, Ultra-sensitive acetylcholinesterase biosensor based on leaching $Al_{42}Cu_{40}Fe_{16}$ quasicrystal modified by MWCNTs-COOH for the determination of organophosphorus pesticide, *Microchem. J.*, 2022, **176**, 107214.

165 S. Veeralingam and S. Badhulika, Enzyme immobilized multi-walled carbon nanotubes on paper-based biosensor fabricated via mask-less hydrophilic and hydrophobic microchannels for cholesterol detection, *J. Ind. Eng. Chem.*, 2022, **113**, 401–410.

166 M. Song, S. Y. Pang, F. Guo, M. C. Wong and J. Hao, Fluoride–free 2D niobium carbide MXenes as stable and biocompatible nanoplatforms for electrochemical biosensors with ultrahigh sensitivity, *Adv. Sci.*, 2020, **7**(24), 2001546.

167 J. Wei, Z. Liu, Z. Zhang, K. Lan, Y. Wang, R. Chen and G. Qin, Suspended CNTs/MoS_2 heterostructure field effect transistor for high performance biosensor and its application for serum PSA detection, *Sens. Actuators, B*, 2023, **381**, 133417.

168 G. Wang, J. Sun, Y. Yao, X. An, H. Zhang, G. Chu, S. Jiang, Y. Guo, X. Sun and Y. Liu, Detection of Inosine Monophosphate (IMP) in meat using double-enzyme sensor, *Food Anal. Methods*, 2020, **13**, 420–432.

169 M. Wu, Q. Zhang, Y. Fang, C. Deng, F. Zhou, Y. Zhang, X. Wang, Y. Tang and Y. Wang, Polylysine-modified MXene nanosheets with highly loaded glucose oxidase as cascade nanoreactor for glucose decomposition and electrochemical sensing, *J. Colloid Interface Sci.*, 2021, **586**, 20–29.

170 A. Shafaat, S. Jankovskaja, V. G. Gomes and T. Ruzgas, Franz cells for facile biosensor evaluation: A case of HRP/

SWCNT-based hydrogen peroxide detection via amperometric and wireless modes, *Biosens. Bioelectron.*, 2021, **191**, 113420.

171 T. Xia, G. Liu, J. Wang, S. Hou and S. Hou, MXene-based enzymatic sensor for highly sensitive and selective detection of cholesterol, *Biosens. Bioelectron.*, 2021, **183**, 113243.

172 M. Chandran, E. Aswathy, I. Shamna, M. Vinoba, R. Kottappara and M. Bhagiyalakshmi, Laccase immobilized on Au confined MXene based electrode for electrochemical detection of catechol, *Mater. Today: Proc.*, 2021, **46**, 3136–3143.

173 M. Song, S. Y. Pang, F. Guo, M. C. Wong and J. Hao, Fluoride–free 2D niobium carbide MXenes as stable and biocompatible nanoplatforms for electrochemical biosensors with ultrahigh sensitivity, *Adv. Sci.*, 2020, 7(24), 2001546.

174 G. Rabbani, M. E. Khan, E. Ahmad, M. V. Khan, A. Ahmad, A. U. Khan, W. Ali, M. A. Zamzami, A. H. Bashiri and W. Zakri, Serum CRP biomarker detection by using carbon nanotube field-effect transistor (CNT-FET) immunosensor, *Bioelectrochemistry*, 2023, **153**, 108493.

175 V. S. Kumar, S. Kummari, G. Catanante, K. V. Gobi, J. L. Marty and K. Y. Goud, A label-free impedimetric immunosensor for zearalenone based on CS-CNT-Pd nanocomposite modified screen-printed disposable electrodes, *Sens. Actuators, B*, 2023, **377**, 133077.

176 T. C. Lu, Y. M. Sun, Y. Zhong, X. H. Lin, Y. Lei and A. L. Liu, Electrochemical immunosensor based on AuNPs/ERGO@ CNT nanocomposites by one-step electrochemical co-reduction for sensitive detection of P-glycoprotein in serum, *Biosens. Bioelectron.*, 2023, **222**, 115001.

177 G. Rabbani, M. E. Khan, E. Ahmad, M. V. Khan, A. Ahmad, A. U. Khan, W. Ali, M. A. Zamzami, A. H. Bashiri and W. Zakri, Serum CRP biomarker detection by using carbon nanotube field-effect transistor (CNT-FET) immunosensor, *Bioelectrochemistry*, 2023, **153**, 108493.

178 Y. Li, J. Tan, M. Wang, Q. Jia, S. Zhang, M. Wang and Z. Zhang, A dual-photoelectrode fuel cell-driven self-powered aptasensor based on the 1D/2D In_2S_3/MoS_2@ Fe-CNTs heterojunction for the ultrasensitive detection of Staphylococcus aureus, *Anal. Chim. Acta*, 2023, **1272**, 341473.

179 T. Su, Z. Mi, Y. Xia, D. Jin, Q. Xu, X. Hu and Y. Shu, A wearable sweat electrochemical aptasensor based on the Ni–Co MOF nanosheet-decorated CNTs/PU film for monitoring of stress biomarker, *Talanta*, 2023, **260**, 124620.

180 T. Laochai, J. Yukird, N. Promphet, J. Qin, O. Chailapakul and N. Rodthongkum, Non-invasive electrochemical immunosensor for sweat cortisol based on L-cys/AuNPs/MXene modified thread electrode, *Biosens. Bioelectron.*, 2022, **203**, 114039.

181 A. Kalkal, S. Kadian, S. Kumar, G. Manik, P. Sen, S. Kumar and G. Packirisamy, Ti3C2-MXene decorated with nanostructured silver as a dual-energy acceptor for the fluorometric neuron specific enolase detection, *Biosens. Bioelectron.*, 2022, **195**, 113620.

182 Q. Zhou, Y. Liu, L. Wang, K. Wang, H. Chen, H. Zheng, Y. Zhou, Z. Hu, Z. Peng, J. Wan and B. Wang, A visible and near-infrared light dual-responsive PEC immunosensor for archaeological silk microtrace detection based on in situ growth of Ag_2S on ZnO-MXene nanocomposites, *Chem. Eng. J.*, 2023, **469**, 143926.

183 T. Zhu, Q. Tang, Y. Zeng, S. Chen, Y. Yang, H. Wang, J. Chen, L. Guo and L. Li, Sensitive determination of prostate-specific antigen with graphene quantum dot-based fluorescence aptasensor using few-layer V_2CTx MXene as quencher, *Spectrochim. Acta, Part A*, 2023, **293**, 122474.

184 D. Jiang, M. Wei, X. Du, M. Qin, X. Shan, W. Wang and Z. Chen, Ultrasensitive near-infrared aptasensor for enrofloxacin detection based on wavelength tunable AgBr nanocrystals electrochemiluminescence emission triggered by O-terminated Ti_3C_2 MXene, *Biosens. Bioelectron.*, 2022, **200**, 113917.

185 D. Wang, Y. Liang, Y. Su, Q. Shang and C. Zhang, Sensitivity enhancement of cloth-based closed bipolar electrochemiluminescence glucose sensor via electrode decoration with chitosan/multi-walled carbon nanotubes/graphene quantum dots-gold nanoparticles, *Biosens. Bioelectron.*, 2019, **130**, 55–64.

186 W. Huang, S. Gao, W. B. Liang, Y. Li, R. Yuan and D. R. Xiao, In situ growth of metal-organic layer on ultrathin Ti3C2Tx MXene nanosheet boosting fast electron/ion transport for electrochemiluminescence enhancement, *Biosens. Bioelectron.*, 2023, **220**, 114886.

187 R. F. Huang, L. T. Wang, Q. Q. Gai, D. M. Wang and L. Qian, DNA-mediated assembly of carbon nanotubes for enhancing electrochemiluminescence and its application, *Sens. Actuators, B*, 2018, **256**, 953–961.

188 Y. Wu, X. Li, X. Tan, D. Feng, J. Yan, H. Zhang, X. Chen, Z. Huang and H. Han, A cyclic catalysis enhanced electrochemiluminescence aptasensor based 3D graphene/photocatalysts Cu_2O-MWCNTs, *Electrochim. Acta*, 2018, **282**, 672–679.

189 F. Du, Z. Dong, F. Liu, S. Anjum, M. Hosseini and G. Xu, Single-electrode electrochemical system based on tris (1, 10-phenanthroline) ruthenium modified carbon nanotube/graphene film electrode for visual electrochemiluminescence analysis, *Electrochim. Acta*, 2022, **420**, 140431.

190 Y. Guo, Y. Nie, P. Wang, Z. Li and Q. Ma, MoS_2 QDs-MXene heterostructure-based ECL sensor for the detection of miRNA-135b in gastric cancer exosomes, *Talanta*, 2023, **259**, 124559.

191 U. Amara, B. Sarfraz, K. Mahmood, M. T. Mehran, N. Muhammad, A. Hayat and M. H. Nawaz, Fabrication of ionic liquid stabilized MXene interface for electrochemical dopamine detection, *Microchim. Acta*, 2022, **189**(2), 64.

192 Y. Nie, P. Wang, Q. Ma and X. Su, Confined gold single atoms–MXene heterostructure-based electro-

chemiluminescence functional material and its sensing application, *Anal. Chem.*, 2022, **94**(31), 11016–11022.

193 C. Miao, A. Zhang, Y. Xu, S. Chen, F. Ma, C. Huang and N. Jia, An ultrasensitive electrochemiluminescence sensor for detecting diphenhydramine hydrochloride based on l-cysteine-functionalized multiwalled carbon nanotubes/gold nanoparticles nanocomposites, *Sens. Actuators, B*, 2015, **213**, 5–11.

194 M. Jiao, X. Fan, Z. Wang, K. Wu, A. Deng and J. Li, Electrochemiluminescence resonance energy transfer system based on ox-MWCNTs-IGQDs and PdAg nanosheets for the detection of 5-fluorouracil in serum, *Microchem. J.*, 2022, **183**, 108066.